CRANFIELD UNIVERSITY

Tony Lusiola

Synthesis and Processing of KNN Powders and Thick Films for MEMS Devices

School of Applied Science

PhD
Academic Year: 2009 - 2012

Supervisor: Prof. Rob Dorey and Dr. Qi Zhang
October 2012

CRANFIELD UNIVERSITY

School of Applied Science

PhD

Academic Year 2009 - 2012

Tony Lusiola

Synthesis and Processing of KNN Powders and Thick Films for MEMS Devices

Supervisor: Prof. Rob Dorey and Dr. Qi Zhang
October 2012

© Cranfield University 2012. All rights reserved. No part of this publication may be reproduced without the written permission of the copyright owner.

ABSTRACT

Pb-free piezoelectric materials have grown in importance through increased environmental concern related to the presence of Pb and the subsequent legislation that has arisen including directives such as Waste Electrical and Electronic Equipment (WEEE) and the Restriction of Hazardous Substances Directive (RoHS). While much progress has been made on producing Pb-free bulk materials, the need to integrate these next generation Pb-free piezoelectric materials with substrates to form functional micro devices has received less attention and raises a number of challenges. With respect to the high temperature mixed oxide synthesis method, a simple, cost effective and robust low temperature molten hydroxide synthesis (MHS) method derived from the molten salt synthesis (MSS) method, has been developed to produce $K_{0.5}Na_{0.5}NbO_3$ (KNN) small grain powders and is a method that lends itself easily to industrial scale up. A powder/sol gel composite ink film forming technique has been used to produce KNN thick films on silicon substrates. Characterisation of the produced films has shown the films to exhibit piezoelectric coefficients for un-doped material in the region of 30pC/N. The work will report on the Na ion favouring mechanism of the MSS and the related mechanism of the MHS. The work will also report on the dielectric and piezoelectric characteristics of initial KNN thick films produced and an investigation into use of dopants and process modification to improve the KNN thick film's characteristics.

Keywords:

Potassium sodium niobate; Pb-free; Si wafers; Piezoelectric coefficient; Dielectric loss.

ACKNOWLEDGEMENTS

I acknowledge the immense help and support received from my supervisors Prof. Robert Dorey and Dr. Qi Zhang, their endless support, patience and expertise was something to behold and I shall always treasure this. I also wish to thank the members of the department of Nanosystems and Microtechnology for the training, discussion and direction offered on numerous occasions throughout my experimental work in the labs at Cranfield, namely Dr. Christopher Shaw, Mr. Andrew Stallard and Mr. Matthew Taunt. I would also like to thank the teaching staff for the insightful discussions and their helpful support during my research namely Dr. Paul Jones, Dr. Glenn Leighton, Dr. Michele Pozzi, Dr. Zhaorong Huang and Dr. Meiling Zhu. I would also like to thank my friends in the group for the morale and academic support throughout this work; Dr. Joe Briscoe, Dr. Matt Hockley, Dr. Andy Pickwell, Dr. Matt Stock, Mr. Ashley James and the initial work of Dr. Francesca Bortolani and Mr. Nitin Chelwani.

Special thanks go to my special wife Beverly and adorable son Cadima-Mukasa for the support and love that always brings joy to my life. I would like to thank my parents Betty and Lawrence, my brother Trevor and sister Michelle for the love, support and friendship through the years. My thanks also go to my enormously large extended family around the world, thank you grandmas and grandpas, uncles and aunties, cousins, nieces and nephews for making me feel a part of a larger being.

Finally, I would like to thank the financial support from the EPSRC and Cranfield University.

PUBLICATIONS

Papers

T. Lusiola, N. Chelwani, F. Bortolani, Q. Zhang and R.A. Dorey, **Low temperature production of lead-free piezoelectric thick films,** Ferroelectrics, 422, 50–54; 2011.

Tony Lusiola, Francesca Bortolani, Qi Zhang, Robert Dorey, **Analysis of Molten Salt Synthesis Method of Potassium $K_{0.5}Na_{0.5}NbO_3$ Production and Introduction of Molten Hydroxide Synthesis of $K_{0.5}Na_{0.5}NbO_3$,** Journal of Materials Sciences, 47, 4, 1938–1942; 2012.

Presentations

R.A. Dorey, Tony Lusiola, F. Bortolani, N. Chelwani and Q. Zhang, **Low temperature production of lead-free piezoelectric thick films,** presentation at Electroceramics XII - 13th-16th June, 2010 Conference: Trondheim, Norway.

T. Lusiola, N. Chelwani, F. Bortolani, Q. Zhang and R.A. Dorey, **Low temperature production of $K_{0.5}Na_{0.5}NbO_3$,** presentation at Piezo - 28th Feb – 2nd Mar, 2011 Conference: Electroceramics for End users VI; Sestriere, Italy.

Poster

R.A. Dorey, Tony Lusiola, F. Bortolani, N. Chelwani and Q. Zhang, **Low temperature production of lead-free piezoelectric thick films,** poster presentation at 19th IEEE International Symposium on the Applications of Ferroelectrics (ISAF) & 10th European Conference on the Applications of Polar Dielectrics - 9th - 12th August 2010: Edinburgh, Scotland.

Contents

ABSTRACT i
ACKNOWLEDGEMENTS iii
PUBLICATIONS v
LIST OF FIGURES viii
LIST OF TABLES xi
LIST OF EQUATIONS xii
LIST OF ABBREVIATIONS xiii
Chapter 1 1
1.1. Introduction 2
1.2. Aims and Objectives 4
1.3. Thesis structure 5
Chapter 2 6
2. Literature Review 7
2.1. History of piezoelectric materials 7
2.2. Piezoelectric effect 13
2.3. Electrical impedance 22
2.4. Relative permittivity 26
2.5. Dielectric loss 29
2.6. Lead zirconate titanate 32
2.7. Pb-free candidates 39
2.8. Potassium sodium niobate 43
2.9. Thick films 49
2.10. Powder preparation 54
2.11. Doping powders 58
2.12. Thick film deposition 64
2.13. Summary 69
Chapter 3 71
3. Experimental 72
3.1. Introduction 72
3.2. Powder production 72
3.3. Sol production 76
3.4. Slurry production 76
3.5. Deposition 78
3.6. Preparation of bulk disc compacts 80
3.7. Physical characterisation 80
3.8. Electrical characterisation 81
Chapter 4 84
4. KNN powder production 85
4.1. Molten salt synthesis 85

4.2. Molten hydroxide synthesis 95
4.3. Single salt molten salt synthesis 106
4.4. Comparison of powder synthesis methods 107
4.5. Doped KNN powders 113
4.5. Summary 121
Chapter 5 123
5. Thick films 124
5.1. Introduction 124
5.2. Bulk KNN 124
5.3. Standard KNN thick films 125
5.4. Processing and constituents of KNN thick films 127
5.5. Sol infiltration treatments 141
5.6. Sol base-layer 146
5.7. Impedance analysis of KNN thick films 153
5.8. Summary 156
Chapter 6 158
6. Doped KNN thick films 159
6.1. Introduction 159
6.2. A-site doping 160
6.3. Transition metal doping 163
6.4. Summary 169
Chapter 7 171
7. Effect of heat treatment & sol base-layers on KNN thick films 172
7.1. Introduction 172
7.2. Effect of heat treatment and sol base-layers on the dielectric properties prior to electrical poling 173
7.3. Effect of heat treatment temperatures and sol base-layers on dielectric properties after electrical poling 182
7.4. Effect of heat treatment and sol base-layers on d_{33} 189
7.5. Summary 191
Chapter 8 193
8.1. Conclusion 194
8.2. Further work 196

LIST OF FIGURES

Figure 1 15
Figure 2 17
Figure 3 18
Figure 4 22
Figure 5 24
Figure 6 31
Figure 7 35
Figure 8 45
Figure 9 79
Figure 10 86
Figure 11 87
Figure 12 88
Figure 13 90
Figure 14 91
Figure 15 93
Figure 16 94
Figure 17 96
Figure 18 97
Figure 19 99
Figure 20 102
Figure 21 103
Figure 22 104
Figure 23 105
Figure 24 107
Figure 25 108
Figure 26 109
Figure 27 110
Figure 28 114

Figure 29. 114
Figure 30 117
Figure 31 118
Figure 32 120
Figure 33 129
Figure 34 131
Figure 35 131
Figure 36 133
Figure 37 134
Figure 38 136
Figure 39 137
Figure 40 138
Figure 41 141
Figure 42 142
Figure *43* 143
Figure 44 144
Figure 45 146
Figure 46 147
Figure 47 148
Figure 48 150
Figure 49 152
Figure 50 154
Figure 51. 161
Figure 52 165
Figure 53 174
Figure 54 175
Figure 55 177
Figure 56 178
Figure 57 180

Figure 58. 181
Figure 59 184
Figure 60 188
Figure 61 190

LIST OF TABLES

Table 1 various applications of piezoelectric materials in industry 12

Table 2 effects of various parameters on particle size, shape and the effect on reaction rates..... 58

Table 3 classification of heating ramp rates 73

Table 4 showing dopants used..... 74

Table 5 showing molar mass of reactants..... 75

Table 6 ESEM-EDX analysis of powder made using MSS showing atomic percentages of constituent parts 86

Table 7 molar ratios of starting reagents in MSS synthesis 88

Table 8 elemental analysis of different KNN powder processing routes 111

Table 9 analysis of powder yields made using different synthesis methods. 112

Table 10 ionic radii (nm) (Atomistic Simulation Group, 2012) (Shannon, 1976) 116

Table 11 elemental analysis of KNN thick films 127

Table 12 elemental analysis of a KNN thick films..... 130

Table 13 elemental ESEM-EDX analysis of film 132

Table 14 piezoelectric and dielectric characteristics of various inter-mixed KNN and PZT based thick films..... 145

Table 15 showing inter-relationship between dielectric loss & impedance at 1kHz for KNN and PZT thick films 155

Table 16 the sol base-layers deposited and the heat treatment temperatures utilised for each sample 173

LIST OF EQUATIONS

Equation 2-1 19
Equation 2-2 20
Equation 2-3 21
Equation 2-4 23
Equation 2-5 23
Equation 2-6 23
Equation 2-7 24
Equation 2-8 28
Equation 2-9 28
Equation 2-10 32
Equation 2-11 32
Equation 3-1 83
Equation 4-1 91
Equation 4-2 91
Equation 4-3 91
Equation 4-4 92
Equation 4-5 (Wang, et al., 2010) 119
Equation 4-6 (Wang, et al., 2010) 119

LIST OF ABBREVIATIONS

1, 2, 3	Directional Vectors
2θ	Angle between the transmitted and Bragg diffracted beams
4, 5, 6	Spin vectors
A	Area of plate capacitors
AC	Alternative Current
C	Capacitance
CSD	Chemical Solution Deposition
d	Thickness of film
d_{xy}	Piezoelectric coefficient relating to the mechanical strain of a material with an applied electric field
D	Electric Displacement
DC	Direct Current
DF	Dissipation factor
E	Applied Electric Field
ε	Permittivity
ε_0	Permittivity of free space
E_c	Coercive Field
EDX	Energy Dispersive X-ray Spectroscopy
EHDA	Electrohydrodynamic atomisation
ε^T_{33}	Relative permittivity after electrical poling in direction parallel to applied field
ε_r	Relative permittivity
ESEM	Environmental Scanning Electron Microscope
ESR	Equivalent Series Resistance
g	Piezoelectric Voltage Constant
GPa	Gigapascals
HS	Hydrothermal Synthesis
Hz	Hertz
ijk	Matrix notations
j	Imaginary unit ($\sqrt{-1}$)
k	Kilo-
M	Mega
MEMS	Micro Electro Mechanical Systems
MHS	Molten Hydroxide Synthesis
MOS	Mixed Oxide Synthesis
MPB	Morphotropic Phase Boundary
MSS	Molten Salt Synthesis
P	polarisation

pC/N	pico-Coulombs per Newton
PPT	Polymorphic Phase Transition
P_r	Remnant Polarisation
P_s	Saturation Polarisation
QF	Quality factor
R	Resistive element of resistance
RoHS	Restriction of the use of certain Hazardous Substances in electrical and electronic equipment
s	Elastic Compliance
SFEG	Schottky Field Emission Gun
SEM	Scanning Electron Microscope
T	State of Stress
$tan\delta$	Dielectric loss
T_c	Temperature at which spontaneous polarisation is lost on heating
THz	Tera-Hertz
T_{O-T}	Orthogonal to tetragonal phase transition temperature
μ	Micro-
V	Volts
WEEE	Waste Electrical and Electronic Equipment
X	Reactive element of impedance
XRD	X-ray diffraction
$\|Z\|$	Magnitude of impedance
$\|Z\|cos\theta$	Real part of impedance
$\|Z\|sin\theta$	Imaginary part of impedance
$\angle\theta$	Impedance phase angle

Chapter 1

1.1. Introduction

Piezoelectricity is the ability some materials have to convert mechanical energy into electrical energy and vice versa. Compared to other electromechanical technologies, piezoelectric materials offer a high pressure per density ratio for actuator devices, high environmental and chemical stability and capabilities of operating at high temperatures and frequencies (Aksel & Jones, 2010). Piezoelectric systems are also smaller and simpler with respect to alternative systems used to perform similar tasks which may include permanent magnets, high voltage transformers and capacitors within their structure (APC International Ltd., 2012). The broad application range, cost and reliability of piezoelectric materials has resulted in their use in a large variety of products from common household products to novel and highly specialized devices. The global demand for piezoelectric devices was valued at approximately US$14.8 billion in 2010 (Acmite Market Intelligence, 2011).

Lead zirconate titanate (PZT) is the most widely used piezoelectric material, but is a hazardous material due to its lead content. The European Union directed, through the Waste Electrical and Electronic Equipment (WEEE) and the Restriction of the use of certain Hazardous Substances in electrical and electronic equipment (RoHS) directives, for industry to substitute various hazardous materials (including lead) for safer less environmentally hazardous materials as soon as is technologically possible, a process that is being adopted increasingly worldwide (Rodel, et al., 2009). Due to these government led directives, there is a large research effort to minimise the use of Pb-based piezoelectric materials and hence the focus on developing Pb-free piezoelectric materials.

Research of Pb-free piezoelectric ceramics is at an early stage and the excellent wide ranging piezoelectric properties of PZT remain unmatched. Potassium Sodium Niobate (KNN) is one of the most promising Pb-free piezoelectric candidates, though various obstacles present themselves with this material. $K_{0.5}Na_{0.5}NbO_3$ (KNN) a piezoelectric material discovered in the 1950's was ignored through the years due to the success of PZT, the inferiority of KNN's properties to those of PZT and difficulties encountered with KNN processing. Work done by Yasuyoshi Saito (Saito, et al., 2004), which reported that doped and highly textured KNN was found to have piezoelectric constants comparable to typical actuator grade PZT at room temperature, led to increased interest in KNN. While much research into KNN derived piezoelectric materials has involved its use in bulk ceramics and later thin film ceramics, a gap exists in the integration of thick film KNN onto silicon wafers which can be fabricated and create functional micro-devices. Research into thin and thick films is driven by the desire for cost effective, small devices, with more power, higher sensitivity and more system integration.

In order to successfully produce KNN powders, its notorious processing difficulties would have to be tackled. The main difficulty faced with the use of high temperature calcined KNN powders involves the precursor volatility that leads to compositional in-homogeneity (Rodel, et al., 2009), leading to a ceramic product with varied grain sizes and poor piezoelectric activity (Li, et al., 2010). The Molten Salt Synthesis (MSS) powder processing method offers a lower temperature alternative to the high temperature Mixed Oxide synthesis of KNN powders. This technique has been used successfully to prepare ceramic particles in the sub-micron range. In addition novel techniques in thick film processing such as composite sol-gel technology, spin coating help to overcome the limitations of the standard deposition methods.

1.2. Aims and Objectives

The aim of the project is to develop a process of making Pb-free thick films that can be used in micro-systems for medical applications and a range of Micro-Electro-Mechanical Systems (MEMS) devices.

To achieve this aim the following objectives were set. The first objective involved the synthesis of KNN powders that are compatible with the composite sol-gel and spin coating processes utilised in developing thick films. From the processing of PZT through the MSS process smaller, uniform grains that are ideally suited to thick film processing have been produced (Bortolani, 2010).

The second objective involves the production and characterisation of basic KNN piezoelectric thick films focussing on the piezoelectric coefficient, relative permittivity and dielectric losses. Two other related objectives involve doping the KNN powder, a common process utilised to control the film properties and the final objective entailed the control and improvement of the properties of the KNN thick films through processing by carrying out an investigation into a range of processing temperatures and composite sol-gel deposition modifications. The research in this report is of an interdisciplinary nature and utilises engineering and manufacturing expertise from a wide and diverse range of technical areas including chemical engineering as well as materials science and electronics.

1.3. Thesis structure

This thesis is structured as eight chapters, of which this, the *Introduction*, is the first.

In Chapter two the *Literature review* is presented. This chapter covers the history of piezoelectricity, an introduction to the piezoelectric effect and the piezoelectric coefficient as well as the material characterisation techniques used and a section on the most popular piezoelectric ceramic today i.e. PZT. Pb-free piezoelectric ceramic candidates are introduced and KNN is discussed. Powder synthesis techniques used in this work are considered as well as the processing and technological application of the material as a thick film.

Chapter three, (*Experimental*) contains a description of the methodologies adopted for this work.

Chapter four entitled *KNN Powder Production,* considers powder synthesis techniques used in this study namely mixed oxide synthesis and the molten salt synthesis, as well as the introduction of the molten hydroxide synthesis and the single salt molten salt synthesis.

The development of the KNN thick film technology is discussed in chapter five to seven with initial studies given in chapter five, improvements in properties through doping discussed in chapter six and process modification considered in chapter seven.

The thesis ends with the *Conclusion and further work* section in Chapter eight which summarizes the key conclusions of this work and suggests actions for the future.

Chapter 2

2. Literature Review

2.1. History of piezoelectric materials

Jacques and Pierre Curie discovered an unusual characteristic in crystals such as quartz (SiO_2), tourmaline and Rochelle salt (Seignette's salt/sodium potassium tartrate; $KNaCH_4O_6 \cdot 4H_2O$) during their study of how pressure generates electrical charge in these minerals. When a force was applied to the materials, an electric polarisation of the crystals occurred which led to the publication of this discovery in 1880. A year later, Gabriel Lippmann deduced mathematically from fundamental thermodynamic principles the converse effect, i.e. that these materials could be deformed by an applied electric field. Further work by the Curie's provided qualitative proof of this effect and further provided proof of the linear and reversible nature of the as yet un-named effect (UK Centre for Materials Education, 2008-2010) (Piezo Systems Incorporated, 2012). This behaviour was labelled the piezoelectric effect, from the Greek word 'piezein', meaning to press or squeeze. Thomas Alva Edison is thought to be the first to commercially utilise the piezoelectric effect in 1899 when he developed the phonograph (Lüker, 2011).

Following this discovery more scientific interest was committed to better understand the piezoelectric effect and shortly after, the core of piezoelectric science was established whereby the asymmetry associated with piezoelectric crystal structures was established, the reversibility of the piezoelectric effect that includes the relationship between electrical and mechanical energy and the importance of thermodynamics to quantify the various energies involved in the process. In 1910 Woldemar Voigt published a book, 'Lerbuch der

Kristallphysik', which acted as a standard reference of piezoelectricity at this point whereby thermodynamic treatment of crystal structures using tensorial analysis led to a complete definition of the 20 natural occurring crystal classes in which the piezoelectric effect occurred and described all 18 possible macroscopic piezoelectric coefficients (Piezo Systems Incorporated, 2012) (Jordan & Ounaies, 2001).

Piezoelectricity had been regarded as a scientific curiosity with no practical applications until its first major application during World War I where an ultrasonic submarine transducer was developed to detect submarines in 1917 by Paul Langevin and his co-workers (Jordan & Ounaies, 2001). Thin quartz crystals glued between two steel plates acted as a transducer mounted in a housing suitable for submersion under water and by applying a voltage a high frequency 'chirp' was emitted, which enabled them to measure the depth by timing the return echo and was the basis for sonar (UK Centre for Materials Education, 2008-2010). This led to further research in France and Britain and by 1918 both nations had produced prototypes. In the inter-war period numerous applications of the piezoelectric effect were discovered and most of the common devices used today were developed, such as microphones, phonograph pick-ups, accelerometers, signal filters etc. all developed during this period (Piezo Systems Incorporated, 2012).

Ferroelectricity (dielectric materials that exhibit reversible spontaneous electrical polarisation with the application of an electric field), a phenomenon displayed by particular types of piezoelectric materials was discovered in 1920 in Rochelle salt by Joseph Valasek during a study of the analogy between the magnetic properties of ferro-magnetics and the dielectric properties of Rochelle salt (Lüker, 2011) (Cross & Newham, 1987). However the piezoelectric materials used at this time had quite a limited application range, mainly due to the instability of Rochelle salt which was susceptible to dehydration in both a vacuum or dry

air, making the application of electrodes difficult (Cross & Newham, 1987) and with quartz displaying a limited degree of material properties (Murata Manufacturing Company, 1997). Valasek also discovered the temperature dependence of the piezoelectric effect (Lüker, 2011) and in his studies of the charge and discharge in Rochelle salt crystals, the hysteretic nature of electrical polarization was demonstrated for the first time (Cross & Newham, 1987). In 1935, Paul Scherrer and his student Georg Busch discovered piezoelectricity and the related phenomenon of ferroelectricity in potassium dihydrogen phosphate (KH_2PO_4) which was the first major family of piezoelectrics to be discovered (Jordan & Ounaies, 2001), but limited performance of these materials, hindered wider use of piezoelectric based devices, though they found use as higher power sonar transducers.

During World War II mica was used in most capacitors, but owing to the threat to supplies of raw material, due to submarine (U-boat) attacks, research into alternatives was accelerated (Lüker, 2011). Various research groups working on improved capacitor materials discovered that certain materials that were prepared by sintering metallic oxide powders exhibited dielectric constants far in excess of common single crystal piezoelectric ceramics in use at the time and also showed similarly positive improvements in piezoelectric characteristics. These materials were also found to gain mechanical strength through the sintering process and were considered to be chemically inert (APC International, 2002). Due to the ease in production of these materials, research interest in the piezoelectric materials increased (Piezo Systems Incorporated, 2012) and augmented the use of inorganic non-metallic ceramics in this field. Barium titanate and the most popular piezoelectric material to date, lead titanate zirconate ($PbZrO_3$-$PbTiO_3$; PZT) were discovered in the 1940's and 1950's respectively, as well as about 100 other piezoelectric materials such as potassium sodium niobate (KNN), in the following years due to competition between Ray Pepinsky and his group at the Pennsylvania

State University and Berndt Matthias and his co-workers at Bell Telephone (Cross & Newham, 1987). Initial reports in the 1940's were based on doping studies of TiO_2 with BaO, which produced ceramic materials with enhanced dielectric permittivities. The discovery of ferroelectricity in $BaTiO_3$ piezoelectric ceramics demonstrated that ferroelectricity could exist in simple oxide materials and it was not always associated with hydrogen bonding as seen with KH_2PO_4. Due to the simplicity of $BaTiO_3$'s structure, X-ray diffraction studies of the structural changes that occur at its phase transitions were carried out and this enabled further investigation of the theoretical backgrounds of perovskite materials (Lüker, 2011). B. Jaffe and his co-workers established PZT as a material that was suitable for the formulation of piezoelectrics and highlighted the importance of the composition-dependent rhombohedral-tetragonal ferroelectric-ferroelectric phase change near the 52:48 Zr to Ti mole fraction composition (Cross & Newham, 1987). The group recognised that the temperature-independent morphotropic phase boundary [MPB (i.e. a phase boundary, where a change in the elemental composition only changes the phase and thus maximizes the materials dielectric permittivity and piezoelectric coefficient (Rodel, et al., 2009))] in PZT allowed one to stay close to the phase change with increasing temperature during the poling process as PZT has a vertical MPB. R.B. Gray is credited with producing the first working piezoelectric transducer in 1945. He understood the importance of electrical poling in establishing a remnant polar domain configuration in piezoelectric ceramics that consequently leads to a strong piezoelectric-response (Cross & Newham, 1987).

In the 1960s the proliferation of many new ferroelectric materials occurred, leading to an age of wider and deeper research into ferroelectric and piezoelectric materials. In this period the number of piezoelectric materials grew to encompass 25 families of ferroelectrics, more than twenty perovskite compounds and an innumerable amount of solid solutions (Cross &

Newham, 1987). The development of an understanding of the link between the perovskite crystal structure and electromechanical activity also occurred with the study of these new materials during this period (Piezo Systems Incorporated, 2012). The 1970's was the age of diversification and led to the development of ferroics, electro-optics and thermistors (Cross & Newham, 1987); as a consequence a vast array of piezoelectric devices had been developed though only a few high volume commercial applications had resulted (e.g. phono-cartridges and filter elements). The piezoelectric ceramics showed vastly improved dielectric and piezoelectric qualities and with the addition of metallic dopants, allowed tailoring of these materials to a wide variety of applications rather than vice versa as happened before with the single crystal based materials (Piezo Systems Incorporated, 2012) (Jordan & Ounaies, 2001).

The 1980's has been described as the age of integration whereby piezoelectric materials were incorporated into electric circuits such as thick and thin film circuits as well as multi-layered packages. PZT has emerged as the main family of materials used for electromechanical devices such as sensors, actuators, transducers etc, dominating the market. There are numerous advantages PZT possesses over other piezoelectric materials which include superior stability, easier machinability and superior piezoelectric properties and these characteristics led to its emergence as the dominant material in piezoelectric ceramic applications. Most modern piezoelectric materials are ceramics, although polymer-based materials and single crystal piezoelectric materials also exist and are used commercially in many applications. The 1990's have been described as the age of miniaturization in which three-dimensional ceramic circuitry was developed using techniques from the semi-conductor industry. Multi-layered structures on a micro-scale that incorporate resistors, capacitors, dielectrics, metal interconnects and piezoelectric transducers were developed during this period (Cross & Newham, 1987).

Table 1 various applications of piezoelectric materials in industry

Industry	Applications
Automotive	Air bag sensor, air flow sensor, fuel atomiser, keyless door entry, seat belt buzzers (UK Centre for Materials Education, 2008-2010), parking sensors, alarm systems, accelerometers, wheel balancing, engine knock sensors, fuel level sensors, ignition systems and emission monitoring (Morgan Technical Ceramics, 2009), etc.
Power Generation & Distribution	Circuit breaker switch gear, piezoelectric bimorphs for energy harvesters, high performance ultrasonic meters, data link isolators (Morgan Technical Ceramics, 2009), etc.
Industrial Equipment	Ultrasonic welding, ultrasonic level meters, ultrasonic inspection, guitar pick-ups, textile machine needles, braille readers, viscosity meters, coin validation systems, non-destructive testing, gas and liquid flow detectors (Morgan Technical Ceramics, 2009), etc.
Aerospace	Ultrasonic level sensing, guidance sensors, vibration sensors (Morgan Technical Ceramics, 2009), etc.
Commercial Sonar	Fish finders, oil exploration sonar, surveying, sea-bed mapping, underwater pipe-laying, oil well monitoring/drilling, depth sounders (Morgan Technical Ceramics, 2009), etc.
Computer	Disc drives, inkjet printers (UK Centre for Materials Education, 2008-2010), etc.
Consumer	Cigarette lighters, quartz clocks (Tech-FAQ, 2012), depth finders, humidifiers, jewellery cleaners, musical instruments, speakers, telephones, ultrasonic toothbrushes (Morgan Technical Ceramics, 2009), gas-powered appliances like ovens, grillers, room heaters, and hot water heaters, etc.
Medical	Disposable patient monitors, foetal heart monitors, ultrasonic imaging (UK Centre for Materials Education, 2008-2010), micro-pumps (Gonzalez & Moussa, 2002), ultrasonic air-in-line sensors, ultrasonic dental de-scalers and ultrasonic scalpels (Morgan Technical Ceramics, 2009), etc.
Military	Depth sounders, guidance systems, sonar, hydrophones, torpedo guidance systems, sono-buoy, gyroscopes, mine detection systems (Morgan Technical Ceramics, 2009), etc.
Toys	Piezo-popper (Educational Innovations, Inc., 2012), piezo-buzzers in toys, tennis racquet piezoelectric shock absorber (UK Centre for Materials Education, 2008-2010), etc.

Since the year 2000 piezoelectric ceramics have witnessed a tremendous growth rate in use. This is in part connected to the successful transfer of multilayer capacitor technology to the manufacture of multilayer actuators. With faster response, large displacements and actuators able to withstand much larger stresses, application opportunities now abound in the areas of piezoelectric motors, printing machines, fuel injection, piezo-electrically controlled thread guides, micro-positioning systems, etc (Rodel, et al., 2009). Currently the requirements and uses for piezoelectric materials extend from medical applications, to the communications

field, to military applications, consumer products and the automotive field (Jordan & Ounaies, 2001). *Table 1* above shows applications of some typical piezoelectric devices.

2.2. Piezoelectric effect

There are 7 crystal systems, namely triclinic, monoclinic, orthorhombic, tetragonal, rhombohedral, hexagonal and cubic. These can be further subdivided into 32 classes or point groups; 21 of these classes do not possess a centre of symmetry and 20 of these are piezoelectric (one class, that is expected to be piezoelectric due to the absence of a centre of symmetry, is not because of a combination of other symmetry elements) (Jordan & Ounaies, 2001). For a material to display the piezoelectric effect the single crystallographic requirement is that it should be non-centro-symmetric (Aksel & Jones, 2010) (Aurelienr.com, 2001).

Smart materials are materials that undergo transformations through physical interactions and can be further defined as materials that sense alteration in their environment and through the use of a response system, adjust to correct or eradicate the change. Magneto-strictive materials, electro-rheological fluids, shape-memory alloys, electro-strictive materials, ferro-fluids, thermo-electric materials are some examples of smart materials (Jordan & Ounaies, 2001). The direct piezoelectric effect is the internal generation of electrical charge (a voltage proportional to the pressure as the grains within the material are electrically polarized) resulting from an applied mechanical force (tension or compression) on a piezoelectric material while the reverse piezoelectric effect is the internal generation of a mechanical force (lengthening or shortening) by a piezoelectric material resulting from an applied electric field (APC International, 2002) (NEC-Tokin, 2010) (Murata Manufacturing Company, 1997).

With that description, piezoelectric materials are considered to be part of the class of materials referred to as smart materials. Piezoelectric properties occur naturally in some crystalline materials (e.g. mica, quartz, Rochelle salt, sugar, etc.) (Tech-FAQ, 2012), in biological matter (e.g. bone, proteins, DNA, tendon, teeth, wood, hair, etc.) (Kalinin, et al., 2007) (Fukada, 1983), and can be induced in man-made crystals (e.g. gallium orthophosphate (Kistler, 2007), langasite (Rodel, et al., 2009)), as well as other polycrystalline materials such as certain ceramics (PZT, KNN etc.) and in polymers such as nylon, polyvinylidene fluoride, PVC etc. (Measurement Specialities Inc., 1999).

The most commercially available and extensively used piezoelectric materials today are ceramics and are based on the perovskite structure which describes a group of materials and takes its name from the mineral $CaTiO_3$ and are denoted ABX_3 (sometimes ABO_3) (Lüker, 2011) (Jordan & Ounaies, 2001). This mineral lends its name to a class of materials that have a similar crystal structure where A and B are cations of two different sizes where A (Ca, Pb, Ba, Na, K etc) is larger than B (Ti, Zr, Nb etc) and X for oxygen (in most cases) that bonds to both cations. The oxygen atoms form an octahedron and are linked in a regular cubic array with the B-site cations that occupy a central octahedron and A-site cations fill the space between octahedra. The perovskite structure allows for multiple substitutions at the A and B-sites resulting in a number of useful and more complex compounds which allows for numerous characteristics to be exploited and applied as well as the addition of chemical dopants. Crystals with the perovskite structure may ideally be visualized as cubes, though in reality they are pseudo-cubic and crystallize in the orthorhombic system (Jordan & Ounaies, 2001) as shown in *Figure 1*.

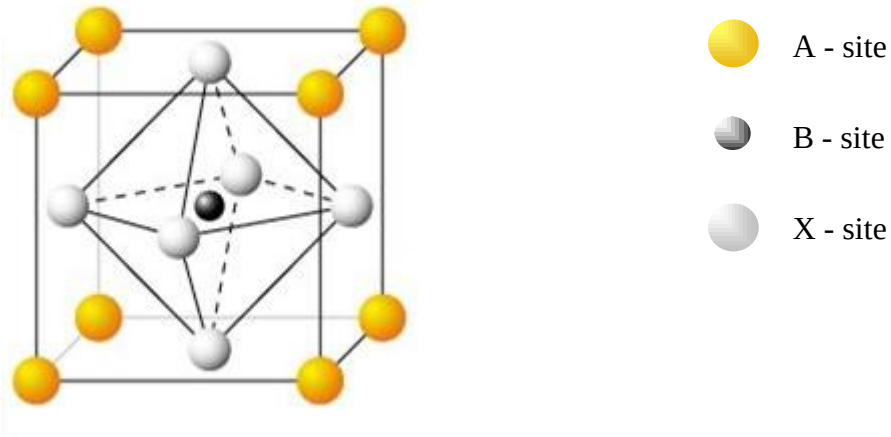

Image courtesy of http://mrc.iisc.ernet.in/Research_Areas/01_Perovskite.htm

Figure 1 ABX_3 perovskite crystal unit cell

Within the perovskite structure the rules that govern the position and coordination numbers of each ionic atom are extremely stringent and any deviation and distortions from the rule result in lowering the ionic atoms coordination numbers and as a result reduced symmetry within the crystal lattice. Due to the wide variety of atoms that are able to combine to form the perovskite structure instability within this structure is the norm in many cases and this is remedied by either tilting the BX_6 octahedron or the B-site cation settling in an off-centre position within the octahedron; as a consequence allowing for bonding stability. Ferroelectricity, a sub-group of piezoelectric materials is a resultant phenomenon of this distortion that creates a permanent dipole within the crystal lattice allowing it to change its direction of spontaneous polarization in response to the application of an electric field (Jordan & Ounaies, 2001). The occurrence of an electric dipole moment within the perovskite structure that is induced by the perovskite crystal structure is the source of the piezoelectric effect in these structures. In many piezoelectric materials the spontaneous polarization of the material exists due to the separation of the positive and negative charge centres in the crystallographic unit cell. As the perovskite structured material is cooled from the high temperature cubic phase (which is centro-symmetric), it undergoes several different phase

transitions that may include transformations to tetragonal, rhombohedral, orthorhombic or monoclinic structures at the various phase transitions (Aksel & Jones, 2010). The piezoelectric effect may also be caused in other materials (e.g. biological materials) containing asymmetric electrical charges by their molecular groups.

Above the T_c (the temperature above which polarisation disappears and the piezoelectric qualities are lost and is also the temperature at which the value of the relative permittivity is at a peak) each perovskite crystal in a ceramic material exhibits a simple cubic symmetry with no dipole moment. At temperatures below the T_c, each crystal has tetragonal, orthorhombic or rhombohedral symmetry and so a dipole moment due to the off-centre position of the B-site cation. Adjacent dipoles form regions of local alignment called domains with each domain displaying a net dipole moment and as a result a net polarisation. The direction of polarisation among neighbouring domains is random and hence the bulk ceramic material has no overall polarisation initially. Since the materials contain many domains all oriented in different directions, the local areas of spontaneous polarization cancel each other and the material does not exhibit a net overall polarization. For a polycrystalline ferroelectric material to exhibit piezoelectricity at the macroscopic level, the domains in the ceramic material may be aligned by applying a strong electric field (poling), usually at elevated temperatures (Jordan & Ounaies, 2001) (APC International, 2002). During poling domains aligned or closely aligned with the electric field expand at the expense of domains that are not aligned with the field, and the element lengthens in the direction of the field; a process which describes the reverse piezoelectric effect. After poling, the material will have a net overall polarization parallel to the direction of the poling field and will exhibit piezoelectricity on a macroscopic level (*Figure 2*) (Aksel & Jones, 2010) (APC International, 2002).

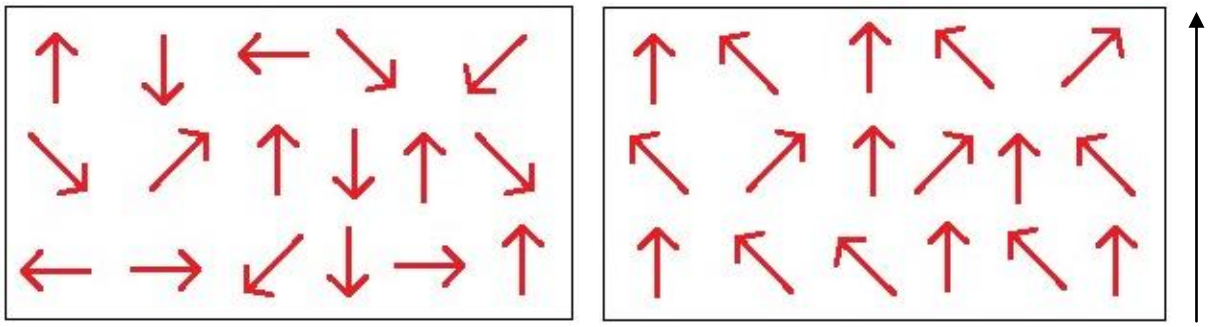

a) random polar domains prior to polarisation

b) remnant polarisation of domains after DC poling

Figure 2 electrical poling leading to polarisation of a piezoelectric ceramic

The processing of bulk piezoelectric ceramics involves the baking of polycrystalline ceramics at elevated temperatures. Electrodes are mounted on the hard baked ceramic and an electric field applied in order to polarize the ceramic material; once polarized, the material exhibits piezoelectric properties, allowing measurement of its properties (NEC-Tokin, 2010).

There are several piezoelectric characteristics that can be measured using different features of a material. Some include the piezoelectric voltage constant (*g*), elastic compliance (*s*), the piezoelectric charge constant (*d*) etc. The piezoelectric charge constant (*d*), is the polarisation generated per unit of mechanical stress applied to a piezoelectric material or, alternatively, is the mechanical strain experienced by a piezoelectric material per unit of electric field applied. Due to the anisotropy of piezoelectric materials, the piezoelectric constants relate to the direction of applied electric or mechanical force and thus each piezoelectric constant has two subscripts (Jordan & Ounaies, 2001). These relate to two linked quantities such as stress and strain. As illustrated in *Figure 3* the polarisation is made to coincide with the Z-axis. The Cartesian directions *X, Y, Z* are represented by the subscripts *1, 2* and *3*. The shear planes are indicated by the subscripts *4, 5* and *6* and are perpendicular to *1, 2* and *3*. The first subscript of the *d* constant indicates the electrical field (or dielectric displacement) direction and the second gives the component of mechanical stress or deformation (APC International, 2002).

Because the strain induced in a piezoelectric material by an applied electric field is the product of the value for the electric field as a consequence the value for the piezoelectric charge constant, is an important indicator of a material's suitability for strain-dependent applications. High *d*-coefficients in piezoelectric ceramics are highly prized for applications as actuators (Jordan & Ounaies, 2001). In this study d_{33} was used to characterise the piezoelectric characteristics of the materials.

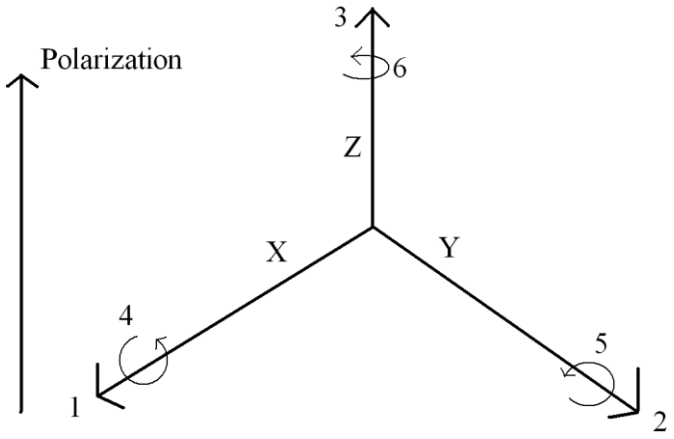

Figure 3 direction of forces affecting a piezoelectric material

$\boldsymbol{d_{33}}$ – is the induced polarisation in the direction 3 (parallel to direction in which ceramic material is polarized) per unit stress applied in direction 3 or may also be described as the induced strain in direction 3 per unit of electric field applied in direction 3 (APC International, 2002).

To test the piezoelectric characteristics of ceramic materials, they may be sintered into bulk discs, rods or plates etc. samples and electrodes applied to the ceramic. Electrical poling is used to orient the domains by polarizing the ceramic through the application of a static electric field. A sufficiently high electric field is applied to enable the domains to rotate and switch, in the direction of the applied electric field. Normally a full orientation of all domains is never achieved but, the polycrystalline ceramic will exhibit a large piezoelectric effect. As

the materials are piezoelectric, during the poling process a lengthening of the material along the poling axis and a contraction in the directions that are perpendicular to it occurs (Jordan & Ounaies, 2001).

A direct method of measurement may be employed to measure the piezoelectric coefficients. The various techniques used enable thermal behaviour, aging, non-linearity, hysteresis, frequency response and other characteristics to be established. In general a known input to the piezoelectric ceramic is applied such as an electric field or a force and the consequent output namely a deformation or an electric charge is recorded and these tests can be done under varying condition e.g. varying temperature, frequency etc (Jordan & Ounaies, 2001).

Using a constitutive equation (a relation between two physical quantities e.g. response of a piezoelectric crystal to an applied electric field) for piezoelectric materials care is taken to account for the change in electrical displacement and strain in three orthogonal directions caused by cross-coupling effects due to the applied electrical field and mechanical stresses. As piezoelectric materials are anisotropic, the response to an applied electric field or the mechanical force in different directions can vary to a great extent and hence the piezoelectric coefficient is a tensor (Huidong, 2008). The tensor notation (i.e. subscripts) are utilised, and the reference axes are shown in *Figure 3*. The piezoelectric equation that relates to the piezoelectric charge constant is written as -

$$D_i = \varepsilon_{ij}^{T} E_j + d_{ijk} T_{jk} \qquad \textit{Equation 2-1}$$

Where D is the electric displacement, ε is permittivity, E is the electric field, d is the piezoelectric charge constant and T describes the state of the stress. The subscripts ijk are matrix notations that are simplified tensor notations that are used to describe a set of equations that relate the crystal symmetry and the choice of reference axes properties in

different orientations of the material which is orientation-dependent. If E_i is zero (i.e. short circuit), ***Equation 2-1*** then reduces to –

$$D_i = d_{ij} T_j \qquad \textit{Equation 2-2}$$

Knowing the applied stress and measuring the electric displacement, the appropriate d_{ij} coefficient can be found and the case of this research and equipment used the d_{33} is the coefficient measured. It is important to note that the most commonly used SI units of d_{33} are pico-Coulombs per Newton (pC/N).

Although the magnitude of piezoelectric voltages and forces are minute, often requiring amplification, in the 20th century the piezoelectric effect has been utilized in a large number of new applications (APC International, 2002). Piezoelectric devices fit into 4 general categories, depending on what effect of piezoelectricity is used. The grouping includes generators, sensors, actuators, and transducers. Generators and sensors utilise the direct piezoelectric effect, i.e. mechanical energy is altered into a dielectric displacement, which is measurable as a charge or voltage signal between the metallised electrodes of the sensor and generators. Actuators use the inverse piezoelectric effect when they transform electrical energy into mechanical energy. Transducers utilize both the direct and inverse piezoelectric effects within one and the same device (Nuffer & Bein, 2006).

The origin of the high dielectric constant in perovskite based piezoelectric materials is due to a permanent internal dipole moment. The existence of the internal dipole moment allowed the development and application of ABO_3 structure as ferroelectrics. Ferroelectricity is a property of certain materials to be spontaneously electrically polarized and this process can be reversed by the application of an electric field upon the material over a temperature range. The importance of ferroelectric materials is due to the high relative permittivity that is displayed by these materials allowing for controllable capacitance and small size compared to

other non-ferroelectric piezoelectric ceramics (Jordan & Ounaies, 2001) (APC International, 2002). By applying a large electric AC to an electroded piezoelectric ceramic that has been polarised causes the polarisation to be reversed and this gives rise to the ferroelectric hysteresis loop. This relates the polarization (P) to the applied electric field (E). These characteristics are exploited through the development of a wide array of multi-layered capacitors (Jordan & Ounaies, 2001) and with the desire for integration and miniaturization in the 1980's and 1990's; ferroelectric materials became extremely popular (Cross & Newham, 1987).

Ferroelectricity is directly measured by the aforementioned ferroelectric hysteresis loop. At large electric signals, both the electric displacement (D_i) and the polarisation (P_i) are non-linear functions of the electric field (E_i) and are related to each other through the linear equation - ***Equation 2-3***.

$$D_i = P_i + \varepsilon_0 E_i \qquad \textit{Equation 2-3}$$

Where ε_0 is the permittivity of free space (8.85 x 10^{-12} F/m). Generally for ferroelectric ceramics, the P term in ***Equation 2-3*** is negligible, and as a result a D-E loop and a P-E loop become interchangeable. The point at which the polarisation is zero is the coercive field (E_c) and remnant polarisation (P_r) is the value of the polarization when the electric field is zero. Once the electric field is switched off the material will have a polarization equal to P_r. In most cases, the existence of a saturated P-E loop is considered as evidence towards establishing that a material is ferroelectric. The loop is considered to be saturated when E_c and P_r no longer fluctuate (Jordan & Ounaies, 2001).

The P-E hysteresis loops of ferroelectric single crystals and polycrystalline ceramics are different (*Figure 4*).

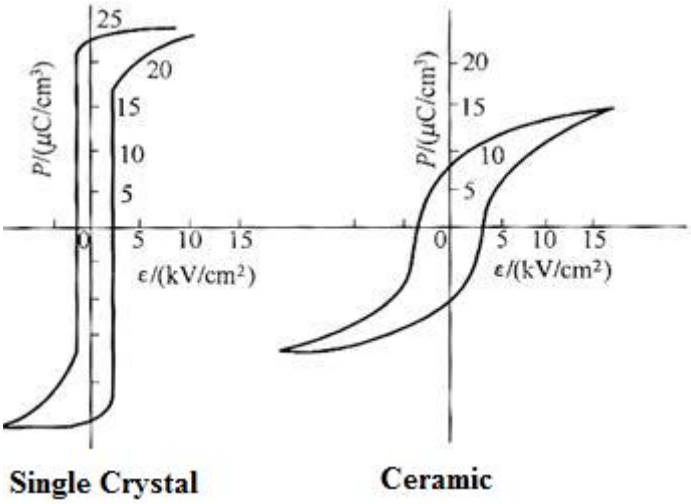

Figure 4 showing the difference between the P-E loops of single crystals and polycrystalline ceramics (Yancheng Institute of Materials Engineering, 2005-2006)

The hysteresis loops of single crystal materials tend to be rectangular, with the P_s (saturation polarisation) and P_r values being very close; while in the case of polycrystalline ceramics, the P_s and P_r values vary more widely, indicating the difficulty faced by these materials to form a single domain as is the case with the single crystals (Yancheng Institute of Materials Engineering, 2005-2006).

2.3. Electrical impedance

Ceramics are usually characterized by fixed frequency measurements, typically at 1 kHz which is appropriate for measuring the key properties of dielectric loss and relative permittivity as it is quick and simple. However such measurements place severe limitations on the amount of information that is readily obtainable, especially with materials that may be electrically heterogeneous. Impedance measurements offer the ability for a comprehensive characterization of electro-ceramics and in particular, characterization of their electrical microstructure (West, et al., 1997).

Impedance is an important property that materials posses and is used to create a better understanding of the characteristics of electronic circuits, components, and the materials used to make components. Impedance may be described as generalized resistance and can be defined as the resistance to flow of an alternating current as it passes through a material (Don Whitley Scientific Limited, 1999). Piezoelectric ceramics act as capacitors when an AC electrical field is applied to them. Circuits that contain capacitors and inductors have a much more complicated response to electric energy when compared to simple resistive circuits as they are non-ideal and thus dielectric spectroscopy/impedance spectroscopy is a useful technique to better understand the properties of capacitors (piezoelectric materials) and inductors. Capacitors and inductors are linear devices and therefore the output of electrical energy in a linear circuit increases exactly in proportion to the input energy. Capacitors and inductors are described to have reactance [are reactive (X)] while resistors are described to have resistance [are resistive (R)].

Impedance describes the relative amplitudes of the current and voltage and also the relative phases of each and can be expressed using the Cartesian form $R + jX$, where j is the imaginary unit ($\sqrt{-1}$), (R = resistance and X = reactance) or in the polar form as the magnitude of impedance and phase angle: $|Z|\angle\theta$. Impedance is especially useful for representing a series connection of resistance and reactance, because it can be expressed simply as a sum of R and X (Okada & Sekino, 2003).

Resistance + Reactance = Impedance $\quad Z = R + jX = |Z|\angle\theta$ ***Equation 2-4***

Therefore

$R = |Z|cos\theta$ = real part of impedance ***Equation 2-5***

$X = |Z|sin\theta$ = imaginary part of impedance ***Equation 2-6***

Circuits containing only capacitors and inductors always have purely imaginary impedance which means the voltage and current are always 90° out of phase and hence the circuit is said

to be purely reactive. In the case of a circuit containing only resistors the impedance is considered to be the real part and the term reactance would refer to the imaginary part and will not exhibit a phase shift between the voltage and the current. Passive components do not generate electronic signals by themselves (capacitors, inductors, resistors) while active components such as transistors and semiconductors do. A passive complex electrical system may comprise both an energy dissipater (resistor) element and an energy storage (capacitor) element. Resistance and reactance together determine the magnitude and phase of the impedance as shown in *Figure 5*.

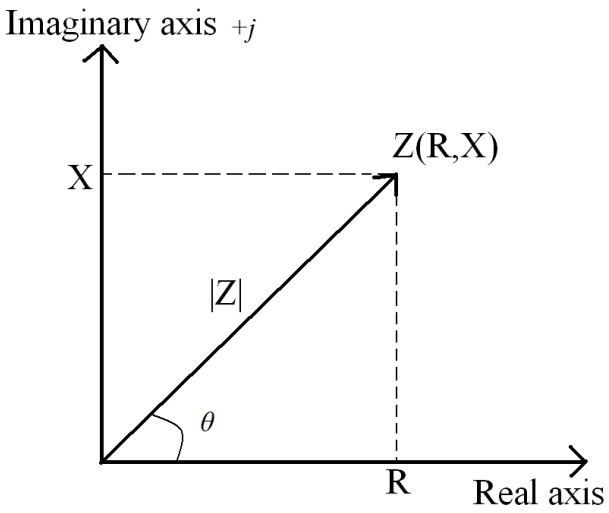

Figure 5 impedance (*Z*) consists of a real part (*R*) and an imaginary part (*X*) as shown on a Cartesian plane

When the phase angle ($\angle\theta$) of impedance for capacitors is measured at low frequencies it is found to be around -90°, in the case of resistors the measured phase angle of impedance is around 0° while it is around +90° when inductors are involved. The ratio of the reactance of the tuned circuit to its resistance is called the Quality Factor (Q or Q-factor). The Q-factor of a complex impedance can be calculated from a division of imaginary and real parts of the impedance.

$$Q = \frac{X}{R} \qquad \text{Equation 2-7}$$

The Q-factor has no unit, and the value is always positive (or zero, in case of a pure resistor). The Q-factor is the ratio of the energy stored to the energy dissipated in the circuit per cycle.

Impedance spectroscopy is an important material characterization tool in laboratories that is slowly making its way into the service environment as units are decreased in size and become portable. Impedance spectroscopy is functional due to the capacity to differentiate the dielectric and electric properties of individual contributions of the components under investigation (ETH Zurich, 2003). There are two main categories of impedance spectroscopy; these are electrochemical impedance spectroscopy (EIS) and dielectric impedance spectroscopy (Macdonald, 1992). EIS involves measurements and analysis of materials in which ionic conduction strongly predominates. Examples of such materials are solid and liquid electrolytes, fused salts, ionic conducting glasses and polymers and non-stoichiometric ionic bonded single crystals, where conduction can involve motion of ion vacancies and interstitials. Dielectric impedance spectroscopy may be utilized to measure the dielectric properties of materials as a function of frequency and temperature (Frubing, 2001) where solid or liquid non-conductors whose electrical characteristics involve dipole moment rotation may be characterised. Impedance spectroscopy may also be utilised in biology e.g. studies of polarization across cell membranes and studies of plant and animal tissues (Macdonald, 1992).

The frequency range of measurement is very large with impedance spectroscopy, extending over nearly 18 orders in magnitude from the visible light end of the electromagnetic spectrum (μHz) to close to the infrared region (THz). Dielectric impedance spectroscopy can be used to characterise dipolar species and localised charges in materials by determining their strength, kinetics and interactions. This makes dielectric impedance spectroscopy a powerful tool for the electrical characterisation of piezoelectric ceramic materials in relation to their structure

(Frubing, 2001), their frequency response, energy storage capabilities and dissipation properties.

A complete impedance spectrum analysis, normally involves more than a single set of measurements and thus a full characterization requires that these measurements are carried out over a wide range of temperatures and/or other externally controlled experimental variables. Impedance spectroscopy measurements are simple in principle, but are often complicated in practice. Due to the fact that the impedance spectroscopy response of materials, vary greatly over huge ranges because of the differences in the resistive and capacitive components when considering different materials, electrodes and temperatures; difficulty arises in attempting to measure accurately. As a consequence measurements require comparison with standard values of these components and are thus only as accurate as the standards. Further complexity arises due to the huge frequency range involved in impedance spectroscopy measurements (Macdonald, 1992).

Impedance data is often represented graphically using Bode plots, Cole-Cole plots or Nyquist plots. The Bode plot of impedance is plotted with log frequency on the *x*-axis and both the magnitude of impedance and phase-shift on the *y*-axis. The Nyquist plot is achieved when the real part of impedance is plotted on the *x*-axis and the imaginary part on the *y*-axis of a graphical chart. The Cole-Cole plot is a plot with the imaginary part of permittivity on the *y*-axis against real part of permittivity on the *x*-axis (ETH Zurich, 2003) (Macdonald, 1992).

2.4. Relative permittivity

A dielectric material may be defined as an insulator that on the application of an electric field would be polarized; as unlike conductors where electrical charge carriers flow through the

materials, due to loosely bound or free electrons, in dielectric materials the electric field pulls the bound electrons and pushes the positively charged nuclei and thus causes dielectric polarization (Kim, 2000) (Encyclopædia Britannica, 2012). There are two types of dielectrics i.e. polar (e.g. water) and non-polar dielectrics (do not possess natural permanent electrical dipole moment, it must be induced). On the application of an external electric field to a non-polar dielectric an electrical dipole moment may be induced (Massachusetts Institute of Technology, 2005). Piezoelectric ceramics are considered to be non-polar dielectric materials. An ideal dielectric would have a high dielectric constant, low dielectric loss, high breakdown voltage; have a low cost in terms of raw materials and production costs, allowing for simple fabrication into capacitors and would not be affected by changes in voltage and temperature. All dielectrics are non-ideal, thus material characteristics define the application of the dielectric to particular tasks (Johnson, 2001).

A capacitor is a device which stores electric charge and the basic configuration is two parallel conductors carrying equal but opposite charges. In many capacitors there is normally insulating material between the conducting plates. The material (the dielectric) can be used to maintain a physical separation of the plates, though since dielectrics break down less readily than air, electrical charge leakage can be reduced, especially when high voltages are applied and therefore describe the primary function of dielectric materials use as capacitors. Capacitors are used for a wide variety of purposes in electronics such as forming resonant circuits, delaying voltage changes when coupled with resistors, making frequency-dependent and independent voltage dividers when combined with resistors, filtering out unwanted frequency signals and as occurs with dielectric materials, the storage of electric potential energy (Massachusetts Institute of Technology, 2005) and they come from a myriad of materials and in many different forms e.g. parallel plate capacitors, cylindrical capacitors,

spherical capacitors etc. (Johnson, 2001). Experimentally it was found that capacitance increases when the space between the conductors is packed with dielectric materials (Massachusetts Institute of Technology, 2005). Capacitance is a measure of the ability of a body to store electric charge for a given electrical potential difference and the SI unit of capacitance is the farad (1 farad = 1 coulomb/volt).

Permittivity is a constant of proportionality that was formulated in 1865 by James Clerk Maxwell in his paper where he derived equations on electromagnetism, specifically those describing electric fields. Permittivity (ε) is an expression of how much electrical charge/energy a material can store when subjected to an electric field. Relative permittivity or the dielectric constant (ε_r, κ or K) is a ratio of the amount of electrical energy stored in a material, relative to that stored in a vacuum; or it may also be described as the ratio of a dielectric material's capacitance with respect to a capacitor with a vacuum in place of any other material and since it is a ratio ε_r has no dimensions. Once a material has been electrically polarised the relative permittivity in this work is denoted by the symbol $\varepsilon^T_{33.}$ The main engineering application of relative permittivity is in capacitors. Relative permittivity can be derived from permittivity and the permittivity of free space as shown in ***Equation 2-8*** –

$$\varepsilon_r = \frac{\varepsilon}{\varepsilon_0} \qquad \textit{Equation 2-8}$$

Capacitance of a material is first measured and then using the formula –

$$\varepsilon_r = \frac{Cd}{\varepsilon_0 A} \qquad \textit{Equation 2-9}$$

Where, C = capacitance, d = thickness of film, ε_0 = permittivity of free space (8.85 x 10^{-12} F/m), A = area of electrode, the relative permittivity of a material can be calculated. Capacitance measurements to determine material properties are usually carried out at 1 kHz

and at low excitation voltages (i.e. at the milli-volt level), though research has shown capacitance and loss to vary with excitation voltage and frequency (Jordan & Ounaies, 2001). Use of this measure enables comparisons between different materials.

When subjected to an increasingly strong electrical field, matter ionises and conducts current e.g. spark observed between two points with strong electrical voltage difference. Dielectrics are materials with strong resistance to ionisation, allowing for higher voltage application to a capacitor without sparking and eventual breakdown, enabling greater capacity for electrical charge storage. Piezoelectric metal oxides, in general, have high relative permittivities when compared to other materials. The desire to manufacture integrated circuits and for miniaturization causes materials with high relative permittivities to be highly sought. The drawback to these materials is the inability to withstand electric fields that materials with low relative permittivity properties, such as air are able to endure. When an applied AC electric field becomes increasingly strong for these materials, they increasingly loose energy due to loss mechanisms as heat and when the applied current reaches a certain tipping point, they tend to conduct current a phenomenon known as dielectric breakdown (Jordan & Ounaies, 2001).

2.5. Dielectric loss

An essential property of dielectric materials is their capacity to support electrostatic fields while dissipating minimal energy mostly in the form of heat. The lower the proportion of electrical energy lost the more effective the dielectric is considered to be. The energy loss that occurs has many descriptions such as the dielectric dissipation factor, dielectric loss factor, dielectric loss tangent, dielectric loss or simply *tanδ*. In this work it shall be referred to as

either the dielectric loss or *tanδ*. It is a parameter that measures the energy losses in dielectric materials and thus also a measure of the heat generation capacity of dielectrics when exposed to an applied oscillating electric field. The importance of measuring the dielectric loss is that materials with high dielectric loss may induce overheating during high frequency operation (Robert, et al., 2001). When measuring the dielectric loss a direct measurement is carried out and is usually measured at the same conditions as that of capacitance (Jordan & Ounaies, 2001). The direct measurement taken is the dielectric dissipation factor (*DF*). The tangent of the angle between a capacitor's impedance vector (*tanδ*) and the negative reactive axis is equal to the capacitor's dissipation factor, when expressing the electrical circuit parameters as vectors in a complex plane, known as phasors and therefore the two parameters are interchangeable. The dissipation factor is defined as the ratio of the Equivalent Series Resistance (ESR - the sum of the ohmic losses of the dielectric, materials and connections used in the construction of the capacitor) and capacitive reactance (Illinois Capacitor Inc., 2012). *DF* is normally expressed as a percentage and values for dielectric loss typically are determined at 1 kHz (APC International, 2002).

There are two types of losses dielectric materials face. One is conduction loss which involves actual flow of charge through the dielectric material which happens in all dielectrics, but to a very low degree as to be rendered negligible. The other is dielectric loss which is due to the movement or rotation of the atoms or molecules in an alternating electric field where energy is lost as heat when molecules collide and tends to be the main contributor to energy loss in dielectrics. Dielectric loss/heating in water (as energy is dissipated in the form of heat) is the reason for food and drink getting hot in a microwave oven (Johnson, 2001).

On application of a sinusoidal current, ionic and dipolar relaxation occurs and with increasing frequency atomic and electronic resonance occur. Increasing the frequency of an AC field has

an effect on the piezoelectric ceramic leading to the excitation of the molecular dipoles and atoms. As the frequency is further increased the material's responses i.e. rotation/oscillation begins lagging the applied electrical field energy and this extra energy is lost as heat. In a perfect capacitor, the voltage and current are out of phase, shifted by 90° with the current leading the voltage as shown in *Figure 6*. If there are impurities in the material, such as atomic vacancies, low particle density, moisture, impurities etc, the reactance of the material decreases, resulting in an increase in resistive current through the material. The current and voltage will be shifted by less than 90°, and the extent to which the phase shift is less than 90° is indicative of the level of dielectric loss of the material. The dielectric loss is the tangent of the angle between a capacitor's impedance vector (resistive/lossy) and the reactive (reactance/lossless) axis in a complex plane (High Voltage Incorporated, 2007).

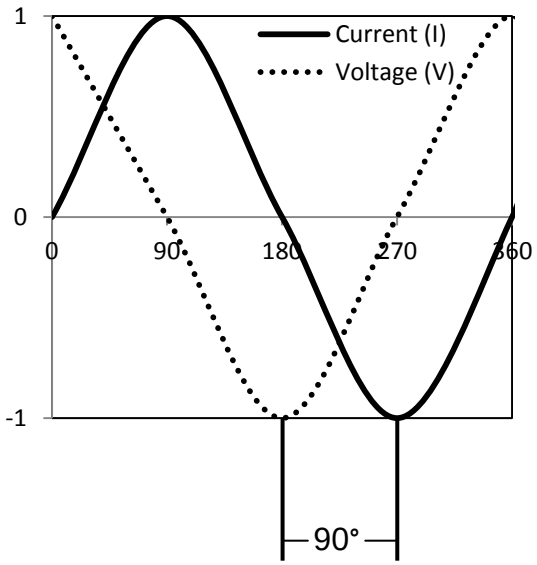

Figure 6 sinusoidal wave showing capacitive voltage lagging current by 90°

When an AC field is applied, the relative permittivity has both a real and an imaginary part and the dielectric loss is defined as the ratio of the imaginary part of the relative permittivity to the real part of the relative permittivity (Jordan & Ounaies, 2001). In general the dielectric constant may be written as a complex number –

$$\varepsilon_r = \varepsilon_r' - j\varepsilon_r'' \qquad \textit{Equation 2-10}$$

Where ε_r' is the real part and ε_r'' is the imaginary part. The real part (ε_r') represents the relative permittivity (static dielectric contribution) in the capacitance calculation and the imaginary part (ε_r'') represents the energy loss in a dielectric material (Li, et al., 2009) (Nobre & Lanfredi, 2003). Taking as an example the effect an alternating electric field has on a dipole within a dielectric material when the field first strikes the dipole, the dipole will rotate to align itself with the applied electric field. As the electric field reverses its direction, the dipole rotates in order to remain aligned with the field. As the dipole rotates, energy is lost through the generation of heat/friction, as well as the acceleration and deceleration of the rotational motion of the dipole. The degree to which the dipole is out of phase with the applied electric field and the dielectric losses that result, determine how large the imaginary part of the permittivity is as a function of the dielectric material and frequency. The larger the imaginary part of the permittivity, the more energy dissipated through dipole motion reducing the amount of energy able to propagate past the dipole. Therefore the imaginary part of the relative permittivity directly relates to dielectric loss in a system (Bishop, 2001). For a good dielectric $\varepsilon_r' >> \varepsilon_r''$ (Johnson, 2001) and therefore dielectric loss may be defined as –

$$tan\delta = \frac{\varepsilon_r''}{\varepsilon_r'} \qquad \textit{Equation 2-11}$$

2.6. Lead zirconate titanate

Lead titanate zirconate [$Pb(Zr_xTi_{x-1})O_3$ (where $0 \leq x \leq 1$)] describes a wide family of inorganic lead-based materials that grew to become the most significant piezoelectric ceramics. The Pb-based family of piezoelectric and ferroelectric ceramic materials includes $PbTiO_3$, $PbMg_{1/3}Nb_{2/3}O_3$–$PbTiO_3$, $PbZn_{1/3}Nb_{2/3}O_3$–$PbTiO_3$ (PZNT), $BiScO_3$–$PbTiO_3$

(BSPT), $Pb_{1.1}(Zr_{0.3}Ti_{0.7})O_3$ (PZT-30/70), $Pb_{0.83}La_{0.17}(Zr_{0.3}Ti_{0.7})_{0.9575}O_3$ - (PLZT), $PbZr_{0.52}Ti_{0.48}O_3$ (PZT) etc. (Guo, et al., 2004) with PZT being the most popular piezoelectric formulation within this family of materials due to the increased piezoelectric response and poling efficiency near to Zr = 0.52. PZT consists of a disordered mixture of $PbTiO_3$ and $PbZrO_3$ which in combination give rise to PZT's excellent piezoelectric response. The macroscopic phase of PZT depends on the zirconium/titanium ratio and temperature. Six phases of PZT exists and these are a low temperature anti-ferroelectric phase, two rhombohedral phases that exist at different temperatures, a tetragonal phase, a paraelectric high-temperature cubic phase and a recently discovered low-temperature monoclinic phase that exists around the 50/50 Zr to Ti composition (Cooper, et al., 2002).

Under usual operating conditions such as standard temperature and pressure (STP), sub-coercive driving fields and pressures, the best performing piezoelectric materials are those that contain the lead atom (Damjanovic, et al., 2010). Besides its favourable dielectric and piezoelectric characteristics other advantages of PZT are that it is cheap, the raw materials are abundant, has high machinability allowing low cost device production, high stability, allows for a broad range of electrical and mechanical applications by altering the material compositions and PZT lends itself as a suitable material for mass production (Murata Manufacturing Company, 1997). PZT piezoelectric ceramics exhibit greater sensitivity and higher operating temperatures, when compared to similar characteristics of other piezoelectric materials (APC International, 2002). A great advantage for continued use of PZT today is that there is an extensive hinterland of knowledge built up through continued research and development for over half a century.

Despite the end members of PZT namely $PbTiO_3$ (displays moderate piezoelectricity) and $PbZrO_3$ (non-piezoelectric) displaying average to poor piezoelectric properties, two reasons

why the bulk material displays excellent piezoelectric characteristics are that there is a high contribution to the electromechanical properties from the motion of ferroelectric domain walls and second the presence of the MPB near Zr : Ti = 52:48, which separates the rhombohedral and tetragonal phases (Damjanovic, et al., 2010). PZT undergoes a compositionally induced phase transition in the MPB region that changes the crystallographic direction from the rhombohedral (Zr-rich compositions) to the tetragonal (Ti-rich compositions) via an intermediary monoclinic phase due to the ferroelectric polarization (*Figure 7*). This condition makes PZT extremely susceptible to polarization rotations such as transverse permittivity (ε_{11}) and the shear piezoelectric coefficients (d_{15}) and to a smaller extent, to polarization extensions, that is, the permittivity along polar axis (ε_{33}) and the longitudinal piezoelectric coefficient (d_{33}), so maximizing PZT's properties such as piezoelectric coefficients, dielectric permittivity and coupling factors. The domain walls are thought to account for as much as 70% of the dielectric and piezoelectric properties in PZT. The reason for the high domain walls contributions at the MPB is said to be related to the general anisotropic flattening of the free energy profile in the transition region between the tetragonal and rhombohedral phases. This leads to the possible conclusion after considering research of other piezoelectric materials that the Pb cation is an essential addition, in order to achieve the special enhancements to the piezoelectric properties (Damjanovic, et al., 2010).

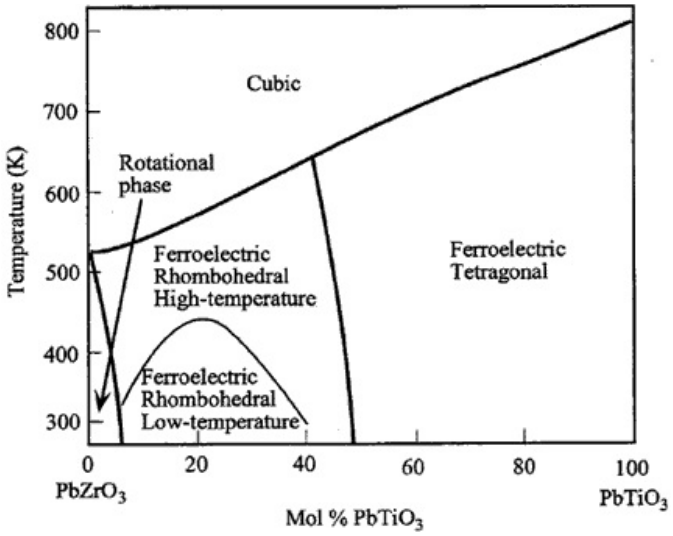

Figure 7 Schematic phase diagram of PZT (University of Cambridge, 2004-2012)

The high vapour pressure of PbO at the forming temperature, originally considered a disadvantage was later found to provide PZT with a measure of auto-compensation in the semiconductor properties due to the nature of the PbO. Owing to this, high resistivity samples can be made with a much wider range of alio-valent dopant ions than would be possible in the $BaTiO_3$ family of piezoelectric materials. This flexibility for chemical manipulation in PZT allowed manufacturers to easily modify ferroelectric properties to tailor the original advantageous properties for specific application areas (Cross & Newham, 1987). Another advantage to the use of PZT is that with favourable coercive field and remnant polarisation properties, the poling field is much lower than the dielectric breakdown strength therefore poling PZT at elevated temperatures give the materials directional properties and transfers them into the piezoelectric state. Due to the temperature stability displayed by PZT materials, some large-volume applications that require strain over an extended temperature range are easily achieved with the use of PZT, which can provide stable application up to about 175°C with little temperature dependence. Finally, doping PZT with acceptors and donors allows manufacture of hard PZT (where domain wall motion is restricted by the dopants thus

reducing dielectric losses at the expense of the piezoelectric constant) and soft PZT (where a higher piezoelectric constant achieved, but larger dielectric losses) as a result increasing the amount of applications that are accessible due to the wide range of material properties (Rodel, et al., 2009).

Most commercially available piezoelectric ceramic materials are comprised of more than 50-60% weight of Pb (Aksel & Jones, 2010) (Ichiki, et al., 2004). A growing disadvantage to the use of PZT is related to the fact that Pb is a heavy metal that is highly toxic to humans, flora and fauna. Pb enters the environment by evaporation during calcination and sintering of the Pb-based piezoelectric materials due to high processing temperatures coupled with the volatility of PbO. Pb also finds its way into the environment at the end of a commercial device's life, when it has to be disposed of or recycled. With current technology it is almost impossible to recover all the Pb from discarded electronic devices (Ichiki, et al., 2004) leading to Pb contamination of soil and ground water from its disposal in landfill sites. The increasing success of PZT releases an increasing amount of Pb to the environment. Since the 1950's there has been focussed research on Pb-free or low-Pb-containing piezoelectrics to counter the negative effects from the use of Pb, though no significant shift away from PZT had come about through that period (Rodel, et al., 2009).

The toxicity and environmental hazard of Pb is due to the fact that it takes a long time to degrade in the environment and it accumulates in biological organisms, causing damage to the brain and nervous systems (Demartin Maeder, et al., 2004). Due to these factors, Pb and other hazardous materials such as mercury, cadmium, hexavalent chromium, polybrominated biphenyls, polybrominated diphenyl ether and acrylamide, have been legislated against by the European Union, which directed through the Waste Electrical and Electronic Equipment (WEEE) and the Restriction of the use of certain Hazardous Substances in electrical and

electronic equipment (RoHS) directives, adopted in 2003 and became law in 2006, for industry to substitute the named hazardous materials for safer less environmentally hazardous materials as soon as is technologically possible, a process that is being adopted worldwide (Rodel, et al., 2009). The WEEE directive was introduced in response to the rapid growth of electrical and electronic equipment waste generation in the EU, and during this period there were insufficient rates of electrical and electronic equipment waste recycling and as well as negative environmental impacts that arose from electrical waste disposal in landfill sites. When set up the WEEE directive set collection, recycling, and recovery targets for all types of electrical goods directing that electrical and electronic equipment was re-used, recycled and recovered (the 3 R's). The WEEE directive also aims to improve the environmental performance of businesses that manufacture, supply, use, recycle and recover electrical and electronic equipment (Environment and Heritage Service, 2005) (Environment Agency, 2012). The RoHS regulations limit the use of hazardous substances in the manufacture of new electrical and electronic equipment placed on the market anywhere in the European Union in order to contribute to the protection of human health and the environmentally sound recovery and disposal of waste electrical and electronic equipment (European Parliament and of the Council, 2007). For the devices not excluded from the directives, the maximum allowed concentration is set to 0.1 wt% in homogeneous materials for lead, mercury, hexavalent chromium, polybrominated biphenyls, and polybrominated diphenyl ethers, and to 0.01% for cadmium (Rodel, et al., 2009).

The use of Pb in piezoelectric ceramics is currently exempt from the directive, but is subject to review every four years; whereby alternatives will be compared to PZT devices and at the point where new materials are technologically similar or better than the standard, directives will be instituted for the elimination of PZT. Around the world measures are being taken to

duplicate the EU directives (Ichiki, et al., 2004) and thus greater importance and emphasis placed into developing piezoelectric materials that are bio-compatible and environmentally friendlier (Demartin Maeder, et al., 2004).

A further drawback to PZT is human *in vitro* use of Pb-based piezoelectric materials which is severely limited due to the nature of the material therefore limiting much needed piezoelectric biological applications (Aksel & Jones, 2010). For example bio-sensing applications utilized inside the human body, require the piezoelectric materials to be biocompatible with the human body (Huidong, 2008). Besides the toxicity of Pb, another drawback is the low elastic modulus of PZT when compared to other piezoelectric ceramics; PZT's elastic modulus closely matches that of ordinary window glass. When poled, multilayered PZT actuators which have electrically active layers and inactive layers, face strain beyond their elastic modulus which leads to easier crack initiation and propagation due to strain incompatibility between active and inactive regions (Rodel, et al., 2009) (Ichiki, et al., 2004). There is also a strong interest in high temperature application of piezoelectric technology which the PZT family of materials cannot fulfil (Demartin Maeder, et al., 2004) due to lower T_c.

The PZT family of materials appears in a dozen varieties and covers a wide range of applications and current research into Pb-free replacements indicates that none shows the wide range of applications of PZT; the most likely result being application specific materials being developed (Rodel, et al., 2009).

2.7. Pb-free candidates

The selection criteria for Pb-free piezoelectric ceramic materials for use in piezoelectric devices are numerous and varied due to the versatility of the PZT family of materials. The first overriding criterion is non-toxicity of precursors and resulting product from the precursors as the aim is a replacement for the toxic Pb. The application requirements that the material may be used for are a joint primary consideration i.e. actuators (require high strain with high force), sensors (require a high piezoelectric coefficient, low temperature dependence of the material, a high electric resistivity and a low permittivity) and transducers (sets similar conditions as actuators and sensors, but includes observing the coupling coefficient, dielectric permittivity, acoustic velocity and acoustic impedance) (Rodel, et al., 2009).

Other pre-conditions of the selection criteria include suitable perovskite crystal structure, high elastic moduli, a highly anisotropic favouring nature of the electronic structure and thus allowing for increasing polarizability. In terms of the crystal structure of the 20 non-centrosymmetric crystallographic point groups with the potential to display piezoelectricity only 10 require closer scrutiny as they are ferroelectric making them easier to polarise when compared to non-ferroelectric piezoelectric materials. Within the perovskite crystal structure there are materials that bear variations on that structure such as $LiNbO_3$ – were the Li ion is too small therefore affecting the polarizability of the domain walls, the Bismuth Layer Structure (BLS) that has perovskite bismuth based crystal structure separated by $(Bi_2O_2)^{2+}$ layers which limits the number of domain orientations that may occur during the phase transition into the low temperature ferroelectric phase (Rodel, et al., 2009). Therefore in

terms of the crystal structure a clear understanding of the sort of perovskite structure a material has is essential to maximise its piezoelectric characteristics.

As PZT is known to have one of the lowest elastic moduli (Young's elastic modulus of 70 GPa), alternative Pb-free ceramics would add additional applicability to piezoelectric ceramics if they come with better elasticity when compared to that of PZT. The electronic structure is crucial where the polarizability of the ions and their tendency to form chemical bonds by hybridization of electronic orbitals is examined. As a result, a highly anisotropic polarizability of the ion leads to changes in the crystal lattice that favour large ionic vibrations and in turn leads to high piezoelectric coefficients. Pb^{2+} contains a lone pair of electrons which form a dumbbell-like extrusion of the electron density on one side of the ion, increasing the polarizability and the distortion of the unit cell and in addition to this characteristic the lone pair electrons lend themselves very easily to hybridization with the orbitals of other ions allowing the bonding distance between the Pb ion and the oxygen ion to be much shorter. This situation of hybridised orbitals with the Pb ion is in contrast to the situation with the Ba ion in $BaTiO_3$ which does not have this characteristic and thus the Ba and oxygen ions are quite distant from each other. Thus $BaTiO_3$ lacks the ability to enhance the distortion of the unit cell. The replacement Pb-free ceramic requires an A-site atom that has high polarizability similar to the Pb ion and posses a lone pair of electrons in an outer shell. The Bi^{3+} ions best fulfils these conditions as well as being the cheapest and least toxic substitute (Rodel, et al., 2009).

Another critical requirement is for materials that exhibit a MPB. It is understood that the MPB linking the rhombohedral and tetragonal phases of PZT, maximizes the piezoelectric coefficient, coupling factor and the dielectric permittivity. At the MPB, PZT exhibits anisotropic flattening enhancing domain wall mobility. PZT also contains a Polymorphic

Phase Transition (PPT) which is a temperature dependent phase change (in contrast to the MPB which is composition dependent) which further enhances its piezoelectric properties. Materials that exhibit an MPB are more essential as the desired properties are not restricted to a narrow temperature range. Application of theoretical knowledge of the chemical interactions of the precursor elements has been carried out by computational modelling and simulation. Pb-free materials were also selected based on an economic standpoint; the elements had to satisfy the requirement for low cost of the raw materials and production costs as the PZT family of materials are cheap and abundant and processing the material to create effective devices involves low cost technology from raw material to finished product (Rodel, et al., 2009). A desire for bio-compatible materials for devices that can be inserted directly into living tissue, including the human body is another factor that drives the candidature and research into Pb-free materials (Demartin Maeder, et al., 2004).

The search for Pb-free materials with high properties has focussed on solid solutions exhibiting MPB's due to the successful utilisation of the MPB in PZT (Damjanovic, et al., 2010). The low density of Pb-free based materials can also be an advantage i.e. when used in transducers for underwater and medical imaging due to expected lower acoustic impedance. Numerous devices have been created from Pb-free piezoelectric materials for operation at high temperatures as this is one of the few applications PZT is unable to perform (Demartin Maeder, et al., 2004).

There are several Pb-free piezoelectric perovskite structured ceramic candidates that have been reported that fulfil some of the mentioned criteria some of which have firmly established place in special applications; these include $LiTaO_3$, $BaTiO_3$, (Na, K)NbO_3 system, $BiTiO_3$ system, langasite system ($La_3Ga_5SiO_{14}$) (Shimamura, et al., 1996) etc. and there are very many others. Bi-based piezoelectric ceramics are of special interest because of

similarities between the Bi and Pb atoms (Damjanovic, et al., 2010). Bi-based materials were found to form MPB's with enhanced piezoelectric properties and layered structures are best known for their high T_c and temperature stability (Rodel, et al., 2009) and have also been successfully used as Pb-free alternatives with growing industrial applications. The problems faced with Bi-based materials are to do with Bi's slight toxicity, issues of the instability of Bi-based structures (Demartin Maeder, et al., 2004) and the piezoelectric properties are inferior to those of PZT so limiting use to high temperature applications (Rodel, et al., 2009). The main application of langasite piezoelectric materials is in their use as piezoelectric substrates for filters operating both at bulk waves (BAW) and surface waves (SAW) and is used as an intermediate material between quartz and lithium tantalate. The langasite system contains gallium which is considered an expensive precursor. As one of the first families (1940s) of piezoelectric ceramic materials to find commercial use, $BaTiO_3$ was replaced by PZT due to it having a low T_c (120°C), much lower than PZT and so a material that is considered to have a small range of use for most piezoelectric applications (Demartin Maeder, et al., 2004). $BaTiO_3$ is also known to be characterised with high dielectric losses that also reduce wider use of this material (Johnson, 2001). Despite the disadvantages this material is being revisited and research has revealed interesting piezoelectric properties from textured ceramics and ceramics derived from nano-powders. Barium strontium titanate ($(Ba,Sr)TiO_3$; BST) a perovskite solid solution where the A-site is doped with Sr, which alters the T_c. The problems faced with BST are the high dielectric loss properties that limit its use in thin film technology and high growth temperature that limits use on various substrates, which are not able to be exposed to BST's high growth temperatures i.e. 700°-1000°C (Lüker, 2011). Other examples of specialist piezoelectric materials include oxyborates for operation at high temperatures and aluminium nitride (AlN) for high frequencies. The historic

materials i.e. Rochelle salt and KDP exhibit equally high or even far superior piezoelectric properties to PZT, but are impractical due to chemical instability or limited temperature ranges necessary for operation. Due to their sometimes limited piezoelectric and coupling coefficients and considering the vast spectrum of applications of PZT, the many Pb-free material candidates cannot be considered as alternatives for the entire PZT family of piezoelectric ceramics, instead they may be considered as complementary to PZT and so far appear to be of interest only for specific applications (Damjanovic, et al., 2010).

2.8. Potassium sodium niobate

Work on piezoelectric alkaline niobates was first carried out in the 1950's and 1960's, but due to the success of PZT as well as the inferiority of $K_{0.5}Na_{0.5}NbO_3$'s (KNN) properties to those of PZT and difficulty faced with KNN processing; interest in KNN materials began to fade. Shirane *et al* first reported the existence of ferroelectricity in KNN in 1954. Over the past few years there has been an increase in the research of alkali niobates following a decline in interest, in these materials over the intervening period since the 1970's (Rodel, et al., 2009). $K_{1-x}Na_xNbO_3$ is a solid solution of ferroelectric $KNbO_3$ and anti-ferroelectric $NaNbO_3$ and form a solid solution across the whole compositional range. $KNbO_3$ exists in the non-piezoelectric cubic phase above 435°C, is tetragonal between 435° and 225°C, orthorhombic at room temperature and displays the rhombohedral phase below -12°C. Application of $KNbO_3$ is limited to exploiting its large surface acoustic waves coupling factors as its piezoelectric characteristics are low (Demartin Maeder, et al., 2004). $NaNbO_3$ is cubic above 630°C and is paraelectric; however, upon cooling it undergoes a sequence of phase transitions i.e. ferroelectric rhombohedral phase via intermediate paraelectric tetragonal and orthorhombic phases and finally the anti-ferroelectric orthorhombic phase at room

temperature. $NaNbO_3$ is used in high density optical storage, enhancing non-linear optical properties, as hologram recording materials etc. It has been suggested by Mishra *et al* from their experimental work that there is evidence of the coexistence of a ferroelectric and anti-ferroelectric phases over a wide range of temperatures (i.e. -258.15°C to 1.85°C) in $NaNbO_3$ (Mishra, et al., 2011).

Solid solutions of $KNbO_3$ and $NaNbO_3$ led to a system with several MPB's, displaying ferroelectricity up to about 90% $NaNbO_3$. From earlier studies conducted in the 1950's by L. Egerton and Dolores M. Dillon (Egerton, 1959), the stoichiometric ratios with the best piezoelectric characteristics were settled upon (50:50 of K-Na). At this ratio the composition is close to the MPB between two orthorhombic phases, similar to the PZT system (López-Juárez, et al., 2011) and MPBs can be observed in the solution up to 90% $NaNbO_3$ (Demartin Maeder, et al., 2004). The phase diagram of $K_{1-x}Na_xNbO_3$ is complex compared to that of PZT as it has numerous PPT's and MPB's having a mixed phase transition character, though the phase transition sequence is quite similar to that of $KNbO_3$. As a result of the mixed MPB and PPT characteristics present in KNN, there is major thermal instability of the properties when KNN samples are cooled or heated from room temperature. There has been limited research in this area to understand the mechanism of the thermal instability due to the mixed phase transition character (Damjanovic, et al., 2010). At room temperature, the KNN phase transitions lie at 17.5%, 32.5%, and 47.5% of $NaNbO_3$ content, the latter commonly rounded up to read 50:50 (Rodel, et al., 2009). *Figure 8* shows the phase diagram of the KNN binary system.

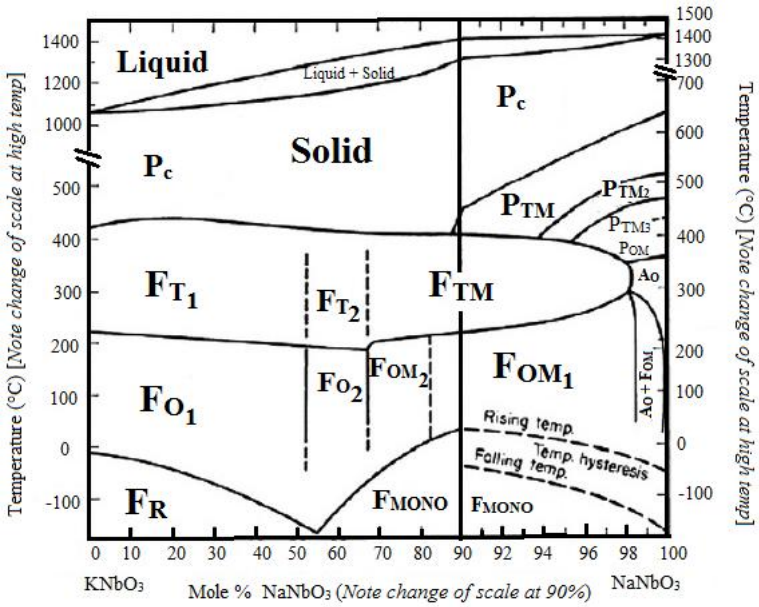

Figure 8 phase diagram of the binary $KNbO_3$–$NaNbO_3$ (KNN) system. **F**, **P**, and **A** refer to the ferroelectric, paraelectric, and anti-ferroelectric phases, respectively. **C**, **T**, **O**, **R**, and **MONO** denote cubic, tetragonal, orthorhombic, rhombohedral, and monoclinic structures (Springer Science+Business Media, LLC, 2012).

Work done by Yasuyoshi Saito and colleagues (Saito, et al., 2004) coupled with their 2004 Toyota Central Research Laboratory patent, which reported that doped and highly textured KNN was found to have piezoelectric constants comparable to typical actuator grade PZT at room temperature, led to an explosion in efforts placed into the study of KNN piezoelectric ceramics, making KNN the most researched Pb-free compound of the last few years (Rodel, et al., 2009). The major insight from the work of Saito *et al* was to show that the modification of the PPT with the use of dopants, led to superior piezoelectric properties at room temperature which appeared to be caused by the proximity of the temperature induced PPT between tetragonal and orthorhombic phases at room temperature (Damjanovic, et al., 2010) (López-Juárez, et al., 2011).

The advantages that KNN bears include low density, high relative permittivity and mechanical strength in general compared to PZT (Demartin Maeder, et al., 2004). KNN has a higher than PZT T_c (420°C) and an electro-mechanical coupling constant comparable to PZT

(Ichiki, et al., 2004). KNN films were shown to exhibit moderate losses (Kugler, et al., 2004) and high piezoelectric properties (Jarupoom, et al., 2008). KNN is a bio-compatible piezoelectric ceramic that is cheap with respect to other non-toxic bio-compatible Pb-free piezoelectric ceramics that basically consists of carbonates and oxide powders of the desired elements.

With the aforementioned advantages there are various obstacles inherent with the use of KNN. Initially the favoured method of KNN powder production involved high temperature mixed oxide calcination of KNN precursors with a long soak time, used by Shirane *et al*, Egerton *et al* etc (López-Juárez, et al., 2011). There are four issues raised with the conventional mixed oxide synthesis of KNN powders namely the compositional inhomogeneity, phase instability at high temperatures, volatility of alkali oxides and poor densification.

The main difficulty faced with the use of high temperature calcined KNN powders involved the precursor volatility that led to low purity which in turn led to a ceramic with varied grain sizes and poor piezoelectric activity (Li, et al., 2010). The precursor volatility and the related issues are due to the volatility of K_2O at calcination temperatures of 800°-950°C which lead to low density materials and the resultant production of extra phases of non-perovskite structures of potassium niobate (Zeng, et al., 2007) with poor piezoelectric characteristics. Methods employed to curtail alkaline volatility during the mixed oxide synthesis include introduction of excess alkali metal oxides and calcination and sintering in atmospheric powder in sealed crucibles which reduces the mass loss. High energy ball milling was also introduced to help with reducing particle size by creating larger surface area for reactions to take place (Rodel, et al., 2009). Other methods developed to deal with alkaline volatility were the introduction of low temperature synthesis routes and examples include the molten salt

synthesis (MSS) (Zeng, et al., 2007), sol-gel method (Lai & Li, 2007), Pechini/citrate method (Yang, et al., 2008) and the hydrothermal process (Zhang, et al., 2008) etc.

The compositional inhomogeneity that occurs with the introduction of Ta as a chemical dopant is controlled by forming precursors of predetermined compositions of materials with similar reactivity. High sintering temperatures lead to production of extra phases some of which are moisture sensitive and may lead to disintegration of samples on exposure to atmospheric moisture (Demartin Maeder, et al., 2004). The phase stability is limited to 1140°C limiting the level of sintering temperatures that may be attempted. The phase instability of the KNN perovskite phase at high temperatures is closely related to volatility of the alkali metal oxides and so may be controlled in a similar manner to that issue (Rodel, et al., 2009).

The KNN powders were widely used to produce bulk ceramic devices and later placed on substrates to create thin and thick films for MEMS technology [electronic devices composed of an active material (piezoelectric), mechanical elements, electrical connection and all deposited onto a solid substrate]. The most cited issue when processing bulk KNN ceramics is to do with densification, whereby difficulties were faced in getting dense ceramics using conventional methods (air sintering) due to the volatility of the alkali metals. Hot pressing has been used to improve the density of bulk KNN and thus improve the piezoelectric characteristics (Li & Sun, 2009). Spark plasma sintering is another method utilised to overcome these issues (Rodel, et al., 2009).

Other issues that exist with KNN include the fact that the MPB in KNN at the 50:50 ratio of sodium to potassium, separates two pseudo-orthorhombic phases resulting in a crystallographic distortion between the two phases that is much less pronounced than in PZT.

It has been established that the contribution to the enhancement of the piezoelectric property in KNN is not as great as is the case in PZT. PZT has an MPB at 52:48, Zr:Ti separating distinct rhombohedral and tetragonal phases with a possible monoclinic bridge between them and ends at a triply critical point where the rhombohedral and tetragonal ferroelectric phases and paraelectric cubic phase meet which is not the case with KNN. This suggests that the pseudo-orthorhombic structures by themselves do not, as is sometimes suggested, lead to remarkably large electromechanical characteristics (Damjanovic, et al., 2010). These differences in MPB characteristics between KNN and PZT indicate a difference in the mechanism at the electrical domain level that may result in each material displaying different piezoelectric responses.

Another factor with KNN and other Pb-free materials is the lack of research into domain wall activity/contributions to piezoelectric response which as stated before has been suggested to produce the bulk of the piezoelectric properties in PZT (specifically soft PZT). This raises the possibility that low piezoelectric response seen in Pb-free materials may be due to insufficient domain wall activity (Damjanovic, et al., 2010).

A lot of research has been carried out on general issues affecting PZT based piezoelectrics over the last 50 years and the knowledge gained has been successfully transferred with modifications into the KNN processing; such as the introduction of sintering aids to lower sintering temperatures and stabilize the stoichiometry. Other ideas transferred include the use of dopants to help with densification during bulk ceramic disc production, texture control, material specific calcination profiles etc. Processing techniques used to produce PZT devices have also been applied to Pb-free materials.

2.9. Thick films

The conventional method for actuating micro-engineered structures using PZT has been to use bulk PZT bonded to the structure in question (Harris, et al., 2006). Due to numerous obstacles encountered with this process novel solutions were sought to alleviate the problem and push the boundaries of piezoelectric materials capabilities even further. This resulted in the development of thin film and later thick film technologies, allowing for cost reductions and smaller devices that may operate at similar or beyond the capabilities of devices prepared through bulk processing routes (Pérez de la Cruz, 2012).

Thick film technology is traditionally an additive process whereby various components are produced on the substrate by applying inks, pastes or sol-gels. Thick films are considered to be films ranging in thickness between 10 μm and 100 μm (Dorey & Whatmore, 2004). Piezoelectric thick films have drawn significant interest in recent years with the development of MEMS due to the piezoelectric effect's provision of high forces with relatively low energy losses (Huang, et al., 2006). They are widely used in micro-pumps, ultrasonic motors, sensors, resonators, surface mount devices, high-frequency transducers, energy harvesters etc (Fu, et al., 2011). Ferroelectric films, a subset of piezoelectric materials are emerging as promising materials for integrated devices such as ferroelectric memories, micro-actuators, micro-sensors, and MEMS that conform to the aspiration for miniaturization (Lin, et al., 2007). As a consequence of the growing trend to miniaturize and integrate devices, the difficulties faced in processing bulk piezoelectrics into very thin elements and to dice very small elements in the fabrication of high frequency single element transducers and arrays, is a major issue to surmount and consequently led to the popularity in research of thick films (Dorey & Whatmore, 2004) (Zhou, et al., 2007).

The use of thick films in place of bulk ceramics offers numerous advantages from the production aspect and the application aspect. When used in various electronic devices e.g. conventional bulk ceramic processing involves distinct processes that include forming, machining and the bonding of components, a process which is time consuming, labour intensive, wasteful and as a result costly (Dorey & Whatmore, 2004) (Harris, et al., 2006). In contrast to the bulk ceramic processing route, with the use of thick film technology an active layer may be deposited straight onto the device component and as a result, reducing costs and simplifying the manufacturing process (Kuščer, et al., 2009). Another disadvantage to the use of bulk ceramic processing routes, involves the uneven grain size distribution prevalent in high temperature processed ceramics, making them difficult to cut to small dimensions (Smeltere, et al., 2011).

From an application aspect another disadvantage to the use of bonded bulk ceramics, is the detrimental effects introduced by the mechanical properties of the adhesives that bond bulk samples to the selected substrate therefore introducing further parameters to the equation. The fact that thick film technology has developed to the stage where whole wafers may have the active material deposited directly onto it and allowing for easy dicing of the wafer results in the production of large batches with increased conformity, unlike the situation with processing bulk ceramics (Harris, et al., 2006). Thick film fabrication routes allow for the prospect of directly integrating the films onto the selected substrate, so eliminating the complexity in the usage of thin fragile ceramic components (Dorey & Whatmore, 2004).

The advantages to thin film technology are that they lend themselves favourably to low temperature heat treatment processes and as a result are ideal materials for use with silicon substrates. With the use of sol-gel technology thin films have been deposited and activated at temperatures of between 500°-700°C hence reducing incidences of inter-diffusion of atomic

species between the substrate and thin film layers and reducing ionic vaporization, such as: lead in lead zirconate titanate oxide (PZT) films. PZT thin films have been largely deposited in order to produce several types of devices, such as: membrane sensors, accelerometers and micro-motors. However, devices that require larger actuation forces such as high frequency transducers, vibration control devices etc. require thicker piezoelectric films (Pérez de la Cruz, 2012). Another advantage to the use of thick films is that the thick films display larger surface displacements, tend to have broader working frequency ranges and higher voltage sensitivity for micro-sensor devices (Zhao, et al., 2003).

The main driver for the research into thin and thick films is the desire for smaller devices, with more power, higher sensitivity and increased system integration (Ryu, et al., 2007). A good example in terms of applications, comes from the medical field where there is a need for ultrasonic transducers that can work using thick film piezoelectric devices with operating frequencies greater than 100MHz with thicknesses less than 20μm (Lau, et al., 2011). Thick films offer many advantages over bulk ceramics as components in various electronic devices as stated, however initial low piezoelectric coefficients of thin and thick film Pb-free materials restricted their industrial applications (Fu, et al., 2011), but with Pb-based restrictive legislation and continuing improvements to piezoelectric characteristics and processing, Pb-free thick film materials are increasingly quite favourable materials (Rodel, et al., 2009).

Thick films occupy the technological region between the processing capabilities of thin film deposition techniques and machining of bulk ceramics (Dorey & Whatmore, 2004), thus new techniques have been developed and old techniques varied in order to process thick films. It is not convenient to produce thick films using standard thin film techniques; because of the increased risk of crack initiation due to shrinkage, also it is impractical to produce thick films

by a repetitive single layer deposition process as this is time consuming (Pérez de la Cruz, 2012). The preparation and characterisation of these integrated films are therefore becoming the most important tasks for MEMS applications (Park, et al., 2006). Use of Pb-based piezoelectric films has increased in the last few decades because ferroelectric thick films have the qualities of both bulk and thin film materials (Pérez de la Cruz, 2012) and have consequently been utilized in a wide range of applications such as detection devices, machinery tools, telecommunication tools, office automation tools, medical equipment and military armament (Park, et al., 2006) and Pb-free alternatives will be welcome (Zhihong, et al., 2005). Besides the capacity to work at low voltages and high frequency, as PZT thick film devices are compatible with semiconductor integrated circuits, they also possess good electric properties approaching near-bulk values (Pérez de la Cruz, 2012).

Piezoelectric thick films can be prepared by many techniques, such as tape casting, screen printing, electrophoretic deposition, aerosol deposition, ink-jet printing, and the method used in this study the deposition of a composite sol–gel (Fu, et al., 2011). The main issues affecting the processing of thick films include the materials compatibility with the substrate and constrained sintering which both occur due to the nature of the materials and the high calcination temperatures involved due to the need to densify films. This makes the selection and use of substrate an important issue to consider (Dorey & Whatmore, 2004).

The advantage to the use of alumina (96% Al_2O_3) and sapphire (Al_2O_3) substrates, is that they can withstand the high processing temperatures required for transition metal based piezoelectric ceramic processing routes. Alumina and sapphire substrates have been used in the past as substrates for piezoelectric thick films as they are both chemically and thermally stable. The problem with these materials is that they are very hard, chemically inactive and consequently posses poor machinability properties and in order to dice them, expensive lasers

need to be used. Sapphire and alumina are also very expensive materials. There was consequently a need for substrates that were cheaper, with easier machinability which would drastically reduce overall manufacturing costs. Examples of alternative materials used as substrates include silica (glass), iron, copper, chrome, nickel, cobalt, steel and the material used in this study silicon. The advantage to the use of these materials is that they are abundant in nature, low cost, easy to machine and in the case of metals, ductile. However, the limitations faced with the use of these materials, are the strengths that are identified with alumina and sapphire i.e. these materials are not thermally stable at the ceramic sintering temperatures and are not as chemically inert as the aluminium oxide based materials (Dorey & Whatmore, 2004).

Si wafers have been used as substrates due to the ease of fabrication of integrated circuits and micro-devices. An advantage of silicon wafers to metal based substrates is the lower thermal expansion coefficients related to silicon wafers which as a result reduce the mismatch that may occur between the film and the substrate. In the case of PZT the thermal expansion coefficient is close to that of silicon at the PZT MPB at temperatures below 500°C. While they are able to withstand processing temperatures as high as 900°C, at elevated temperatures reactions between Pb and the wafer have been found to occur producing lead silicate at the silicon-PZT interface resulting in delamination, and increases the conductivity of the SiO_2 layer (Dorey & Whatmore, 2004). Due to these limitations the processing of piezoelectric ceramic thick films is required to occur at lower processing temperatures to avoid the thermal and chemical instabilities of the silicon substrate.

For a capacitor to work it requires electrodes and in the case of piezoelectric thick film ceramic materials, the materials are placed in between two electrodes, with one applied prior to deposition of the thick film (back electrode) and the other applied above the thick film (top

electrode). This situation leads to a narrowing of the candidates that can be used as the back electrode as most conductive candidates may not withstand the high processing temperatures required to densify the ceramic thick films. Pt, Au, and Au/Pt/Pd, Ag/Pd alloys are some examples that have been shown to be effective back electrodes as they do not oxidise at the high processing temperatures of thick film ceramics. In this study a Pt based back electrode was utilised as the most suitable candidate to fulfil the requirements for a piezoelectric ceramic thick film. A Pt electrode forms a thin layer and is quite stable to 800°C which is ideal for the novel techniques developed to process piezoelectric thick films (Dorey & Whatmore, 2004). Consideration made for the top electrode involves compatibility with the thick film ceramic and its electrical conductivity as this material does not undergo the high ceramic processing temperatures as it is applied on completion of that step.

2.10. Powder preparation

The mixed oxide synthesis (MOS) is a solid state reaction which refers to a group of reactions that occur in the absence of a solvent. The conventional MOS is desirable for industrial applications due to the simplicity of the process. This is because –

- due to the absence of solvents in the MOS process the cost of acquiring solvents is removed,
- post reaction the product requires little or no purification step, to remove solvents,
- due to the high concentration of the reactants the reaction rates are very high making for high yields and making the process highly cost effective.

The MOS process with respect to KNN involves problems that are less common in PZT synthesis. The starting reactants for the process need to be stable materials. From a process of

elimination research found alkali metal carbonates, to be relatively stable precursors for this process and this results in the use of moisture sensitive K_2CO_3 (Ringgaard & Wurlitzer, 2005). As K_2CO_3 is hygroscopic and absorbs water when left in open air the need to ensure the correct weight ratio of precursors is added to avoid deviations from stoichiometry or the formation of phases with different stoichiometry (Malic, et al., 2008). Drying the K_2CO_3 prior to use in a dry atmosphere or using an excess is recommended in order to achieve proper stoichiometry and avoid unwanted properties (Birol, et al., 2005).

MOS with respect to KNN involves a high temperature calcination of the KNN oxide precursors with a long soak time to induce diffusion of the reactants. The main difficulty faced with the use of high temperature calcined KNN powders involved the precursor volatility that leads to compositional in-homogeneity (Rodel, et al., 2009). The high temperatures also lead to coarse particles, aggregation and low reactive activities of the powders (Yang, et al., 2005). This in turn leads to a ceramic product with varied grain sizes and poor piezoelectric activity (Li, et al., 2010). The precursor volatility and the related issues are due to the volatility of K_2O which may result in mass loss and stoichiometric imbalances that lead to low density materials and the resultant production of non-perovskite structures of potassium niobate (Zeng, et al., 2007) with poor piezoelectric characteristics. The volatility can be addressed by introducing excess alkali metal oxides and calcination and sintering in atmospheric powder in sealed crucibles, where mass loss is negligible (Rodel, et al., 2009).

To counter the deficiencies faced with KNN powder production, numerous low temperature synthesis routes were adapted and employed. Examples of low temperature powder production methods to produce KNN include the molten salt synthesis (MSS) (Zeng, et al., 2007) used in this study; the sol-gel method (Lai & Li, 2007) which involves mixing metal organic compounds (mainly alkoxides) in an organic solvent, the subsequent addition of

water generates two reactions, hydrolysis and polymerization, producing the gel which is dried and calcined and results in the crystalline ceramics. The disadvantages of sol-gel method is the expense of the precursors as well as expense involved in handling them due to the moisture sensitivity, therefore requiring equipment to allow handling in dry atmospheres (López-Juárez, et al., 2011). Another is the Pechini/citrate method which involves the formation of a polymeric resin involving an organic acid and an alcohol (generally ethylene-glycol). The precursor solution is then heated to evaporate the solvent and to promote the formation of the resin which is then crushed and calcined at different temperatures resulting in the crystalline powder. The Pechini/citrate route also utilises highly moisture sensitive precursor reagents (López-Juárez, et al., 2011) (Yang, et al., 2008). The hydrothermal process (Zhang, et al., 2008) method involves placing the reagents into a pressurized reactor or autoclave, where the reaction is carried out at a low temperature (< 300°C) and where the pressure generated depends on the temperature at which the reactor is heated. The processing time for the hydrothermal synthesis is between 6-24 hours after which this is dried and the crystalline powder is collected. A disadvantage related to the hydrothermal synthesis method is the presence of other phases beside the desired $K_{0.5}Na_{0.5}NbO_3$ perovskite phase. The advantage of the above mentioned low temperature powder production methods is the KNN powder produced is of a fine grain consistency (López-Juárez, et al., 2011).

The Molten Salt Synthesis method (MSS) was selected as the primary method to produce KNN powders in this project. The process involved mixing stoichiometric ratios of alkali carbonates and niobium (v) oxide with a NaCl/KCl salt mix that acts as a reaction aid (Li, et al., 2010). These were heat treated at a temperature above the eutectic melting point of the salts. Within the molten solvent the precursors are rearranged and then diffuse into the molten salt. Also, the molten flux increases the diffusion rates of the reactants (up to 10 orders of

magnitude), leading to a reduction of the reaction time and the heat treatment temperature (Madaro, et al., 2010). The perovskite phase begins to form through a nucleation and propagation process on continued heating (Yoon, et al., 1998) , with in theory $K_{0.5}Na_{0.5}NbO_3$ as the product.

The advantage of MSS when compared to other low temperature KNN powder synthesis processes is that the other methods lack the low cost, simplicity, robustness and ease required for effective scale up. The MSS is a short soak time, low temperature based method (due to the low melting points of the salts) when compared to MOS and as a consequence reducing the issue of K_2O volatility. In addition it makes use of relatively inexpensive precursors, which are non toxic, does not require specialist equipment and is scalable making it suitable for use in commercial environments. Enhanced powder characteristics, such as a relatively uniform distribution of particle size, smaller particle sizes and less particle agglomeration are characteristics that are thought to contribute to the resultant dielectric properties (Yoon, et al., 1998). Consequently due to the advantages of this process over MOS the project was tied to using this simple low temperature process.

The MSS powders have several unique characteristics when compared to those obtained by other powder synthesis methods. These characteristics are mainly governed by the chemical and crystallographic constraints given by the molten solvent and the features are more noticeable in the case of extremely anisotropic materials (Yoon, et al., 1998). The choice of the molten solvent is therefore extremely important due to the potential to influence the end product in a number of ways as shown in *Table 2*, which include the reaction rate, particle size and shape.

Table 2 effects of various parameters on particle size, shape and the effect on reaction rates

Processing Parameters		Reaction Rate	Particle Size	Particle Shape
Temperature		●	●	●
Time		x	●	●
Amount of salt		x	●	x
Type of salt -				
	Anion size	x	●	●
	Solubility effect	●	●	●
	Difference in melting point	●	x	x
Ratio between salts[a]		●	x	x

a – When using two different salts; ● – Predominantly dependent; x – Less dependent.
*Table by Ki Hyun Yoon, Yong Soo Choo, Dong Hoon Kang, Journal of Material Science **33** (1998) 2977-2984* (Yoon, et al., 1998)

From *Table 2* it is shown that besides the processing parameters the salt selection can affect the reaction rates and morphology characteristics. The molten solvents have an effect on the reactants' surface and interface energies, resulting in an inclination to reduce these energies and hence aid in forming the perovskite structure at lower temperatures. The resultant powders are more reactive, whereas in the case of the mixed oxide synthesis higher temperatures are required to create the perovskite structure resulting in powders with low reactivity (Yoon, et al., 1998).

The requirements of the salt are that it should have a low melting point a situation remedied by the use of two or more salts resulting in lower eutectic melting points. The salt is required to be display chemical inertness within the reaction mixture and thus avoid any side reactions with the reactants. The salt must be easy to wash away after powder synthesis and so should possess aqueous solubility (Yoon, et al., 1998). Therefore for this project the MSS fulfilled all the criteria required and the salt mix selected would in theory produce the ideal powders.

2.11. Doping powders

Chemical doping of powders intentionally introduces impurities at very low levels into pure piezoelectric ceramic powders for the purpose of controlling the electrical properties. In crystalline substances, the atoms of the dopant normally take the place of elements that were

in the crystal lattice of the material. The beauty of the perovskite structure is that it allows for multiple substitutions on the A-site and B-site, resulting in a number of valuable though more complex compounds (Jordan & Ounaies, 2001). Soft ceramics are characterised by large piezoelectric constants, large dielectric constants, high dielectric losses, high permittivity, low mechanical quality factors and poor linearity. Small quantities of donor dopants are added to a ceramic formulation to produce metal/cation vacancies in the crystal structure, consequently enhancing the aforementioned effects in soft ceramics. Donor dopants tend to have higher valency with respect to the ions they replace (Bortolani, 2010). Acceptor dopants form oxygen/anion vacancies in the ceramic crystal structure, creating hard ceramics that have properties such as small piezoelectric charge constants, large mechanical quality factors, higher Curie temperatures and large electromechanical coupling factors (APC International, 2002) and tend to have lower valency with respect to the ions they replace (Bortolani, 2010).

Hard ceramics generate smaller signal band widths and smaller displacements relative to soft ceramics though soft ceramics exhibit greater hysteresis and are more susceptible to depolarization or other deterioration. Soft ceramics also have a lower Curie temperature (generally below 300°C) which dictates that soft ceramics are used at lower temperatures compared to hard ceramics that are more stable at higher temperatures. As a result soft ceramics are used principally in sensing applications, rather than in power applications that require combinations of high frequency inputs and high electric fields where hard ceramics are utilised (APC International, 2002).

The resultant effects of doping KNN can usually be separated into two groups. The properties that result from doping KNN with particular dopants that results in improvements to the piezoelectric properties by preparing compositions close to an MPB or by shifting the orthorhombic to tetragonal (*O*–*T*) phase transition at 200°C to near or below room

temperature, is the first group. The second group involves doping KNN to improve its sintering behaviour while keeping its inbuilt structure and phase diagram aiming to improve particular properties like piezoelectric or coupling constants (Rodel, et al., 2009).

Discounting the effect of the altering of the sintering behaviour (the second group of effects) as with the nature of thick films they will not encounter sintering temperatures; focus was placed on the first group of effects that involve modifications to the phase diagram. The inducing of structural instabilities in a material can lead to the enhancement of its electromechanical properties which may be induced by compositional instability (MPB), thermal instability (PPT), stress fields or external electric fields. The MPB is the favoured route over the rest, because the composition does not change during use. As indicated earlier KNN displays numerous PPT's and MPB's resulting in a mixed phase transition character. Unfortunately in the case of most doped KNN powders, the MPB shows some temperature dependence due to the presence of PPT's, i.e., it is not close to vertical in the temperature-composition phase diagram as is the case with PZT and accordingly temperature changes do not always keep the material close to the MPB, i.e. close to the instability condition. With a temperature dependant MPB, properties will be improved close to the temperature of the phase transition and the MPB, but as temperature changes the material moves away from both MPB and PPT instabilities and properties start to decrease (Rodel, et al., 2009).

Despite temperature-sensitive properties, the chemical doping of KNN has seen a lot of interest in exploiting the enhancement of the properties at the T_{O-T} phase transition. Doping to modify the T_{O-T} phase transition by moving it to ambient temperature has been achieved though with a penalty that is a lowering of the Curie temperature. Consequently so far there are no methods for raising the T_{O-T} transition to much higher temperatures as it is said by Rodel *et al.* that all dopants have the opposite effect. It is also suggested that the key

mechanism of enhancement of the piezoelectric properties appears to be the close proximity of the T_{O-T} PPT to room temperature rather than MPB effects (Rodel, et al., 2009).

There are two different types of ion substitution that may occur these are isovalent substitution and aliovalent substitution. Isovalent substitution occurs when the dopant ion and the original ion have a similar oxidation state. Aliovalent substitution occurs when the dopant ion substituting the original ion has a different oxidation state. Aliovalent substitutions alter the overall charge within the ionic compound and therefore a charge compensation mechanism is required to maintain charge neutrality within the crystal. The introduction of the transition metal dopants with multiple oxidation states, alters the concentration of oxygen vacancies [responsible for increased dielectric loss in piezoelectric ceramics (Wang, et al., 2010)] and influences the structure and lattice energy of the piezoelectric material, since ionic sizes and charges of dopants differ from those of the main piezoelectric ceramic constituents (Zhang & Whatmore, 2001). Oxygen vacancies affect the microstructure of piezoelectric ceramics causing the direction of spontaneous polarization to be affected within the crystal lattice by either reducing or increasing the polarizability of the domains (Eichel, et al., 2009). The ability to fill A-sites allows transition metal dopants to fill any holes left by cation loss during calcination and with the ability of some to further oxidise (due to their aliovalent nature) they are able to absorb oxygen vacancies thus reducing incidences of dielectric loss in the resultant material and generally improving the piezoelectric properties (Wang, et al., 2010). The band gap/energy gap, between the conduction and the valence bands of a material, controls its level of resistivity. This gap is affected by the presence of impurities (e.g. dopants) or defects, which can release electrons into the conduction band, or add an energy level into the band gap. Dopant ions with charges greater than those of the ions they replace may act as acceptors i.e. the electron necessary to neutralize the excess positive charge may

be promoted into the conduction band; or the effect reversed by dopant ions with lower charges than the ion they substitute (Dauchy, 2007), (Kalantari, et al., 2011).

The various dopants selected for this study, were selected to dope either the A- or B-sites or in some cases, both sites. Lithium has been shown to enhance the piezoelectric and electro-mechanical properties of KNN at the MPB between the orthorhombic and tetragonal phases (Guo, et al., 2004) which it lowers from 200°C to room temperature (Rodel, et al., 2009) and the higher temperature cubic to tetragonal phase transition. Fu *et al.* found a level of 6% lithium to be the peak amount able to occupy the A-site cation vacancies resulting from alkali volatilisation (Fu, et al., 2011) and also a suitable level to enhance the properties of the MPB. At levels higher than 7% Li, only one MPB was observed in Yiping Guo *et al.* which was a cubic to tetragonal phase transition (Guo, et al., 2004). Thus the general issue of over-doping is a key factor to take into account, in order to avoid the creation of secondary phases that degrades several important piezoelectric properties (Meng, et al., 2006). The Li dopant acts to increase the Curie temperature of the resultant powder to 452°-510°C (100°C higher than conventional PZT) in Yiping Guo *et al.* from about 400°C and shifted the MPB transition of the T_{O-T} to a lower temperature (Fu, et al., 2011); a fact that contradicts the statement of Rodel *et al*; i.e. improved piezoelectric properties observed in Li-, Ta-, Sb-doped KNN is attributed to the effects of the PPT (Rodel, et al., 2009).

Manganese is unique as it is thought to occupy both oxygen and alkali cation vacancies during powder formation within the ABX_3 perovskite structure, thus reducing the concentration of these vacancies and improving electrical characteristics. Due to the volatility of the alkali metals, during the heat treatment stage to form KNN powders a small amount of the of alkali elements are lost resulting in oxygen vacancies. As the powder crystallizes some oxygen vacancies are oxidized into free carrier holes which co-exist in the powder with the

oxygen vacancies. The formation of the holes reduces the amount of oxygen vacancies, but leads to higher current leakage of the material. Manganese absorbs the holes by increasing its oxidation state from Mn^{2+} to Mn^{4+} (Wang, et al., 2010). The manganese also reduces the domain size and hence increases the density of the KNN domain which in turn improves the piezoelectric characteristics. Lin *et al.* suggested that amounts higher than 0.5% on Mn were reported to lead to lower piezoelectric characteristics and higher dielectric loss (Lin, et al., 2010). Various other dopants were introduced in this work and in general would be expected to act in a similar mechanism to either Li or Mn, dependant on the valency of the dopant.

The introduction of charged dopants can change the concentration of oxygen vacancies and influence the structure and lattice energy of the piezoelectric film, since ionic sizes and charges of dopants differ from those of the main powder constituents (Zhang & Whatmore, 2001) (Eichel, et al., 2009). The transition metal dopants selected had multiple oxidation states and were expected to fill both A-site and B-site positions and were thus added by the substitution of both A-site and B-site reagents. Tantalum was selected as it hinders abnormal grain growth, decreases both the T_c and the orthorhombic-tetragonal phase transition temperatures in KNN (Rodel, et al., 2009), it also has a similar valance to niobium, similar ionic radius and similar electro-negativity to niobium (Ta – 1.5; Nb – 1.6) (Gong, 2012). Titanium is commonly used as a dopant in combination with strontium and the effect of titanium on its own was investigated. Tungsten was added because, of its ability to adopt various valences, its position on the periodic table with respect to manganese i.e. close but in different period and its ionic radius that was near similar to manganese. It was also noted that Tungsten oxide hinders grain growth and densification (Rodel, et al., 2009).

$SrTiO_3$ was used in combination as it is said to produce relaxor behaviour in KNN powders, promotes densification and optimizes electrical properties (Chang, et al., 2007). ZrO_2 and

TiO_2 were used in combination as co-dopants as these reagents are the main components in the PZT powder system and it was envisaged that they may produce a positive effect in the resultant KNN thick films. Due to its use as a co-dopant with TiO_2, zirconium was selected as a dopant on its own to observe the effect it has on KNN, in the knowledge that it has a negative effect on KNN where it is said to impede grain growth (Rodel, et al., 2009).

Lithium and calcium were expected to occupy the A-sites and were thus added at the expense of the A-site reagents. Calcium is known to improve KNN sintering, decrease phase transition temperatures (Rodel, et al., 2009), promote densification and has near similar ionic radii to sodium and potassium with a higher electro-positivity (Barbara Malic, 2005) and therefore influence the structure and lattice energy of the piezoelectric film (Zhang & Whatmore, 2001).

2.12. Thick film deposition

As stated earlier it is impractical and a drawback to use ceramic bulk processes to produce thin and thick films. Numerous processes have been used to deposit piezoelectric thin films on to various substrates and include processes such as pulsed laser deposition, screen printing, electrophoretic deposition, pulsed vapour deposition and various chemical solution deposition (CSD) processes among them sol-gel technology, metallo-organic decomposition and the chelate process etc. The development of CSD processes for perovskite thin films, dates to the mid 1980's (Schwartz, 1997). Of the various physical and chemical methods investigated to deposit ferroelectric films, the sol-gel process has been widely used. This process uses metallo-organic compounds with the advantage of achieving high homogeneity,

low calcination process temperatures and the good control of chemical composition, including control of dopants (Lin, et al., 2007) (Nakashima, et al., 2007).

In order to be commercially viable the electromechanical properties of systems such as sensors, actuators and transducers need particular thicknesses of active material. The required thicknesses are difficult to fabricate using thin film production techniques due to the high levels of stress generated during processing, as a result leading to crack initiation and later crack propagation leading to poor piezoelectric properties and another issue worth noting is the slow deposition rates associated with these techniques (Huang, et al., 2006). Thick film fabrication routes allow the direct integration of films onto the substrate and hence removing the complexity of handling thin fragile ceramic components when using bulk processing routes (Dorey & Whatmore, 2004).

Various thin film deposition methods have been modified in order to produce piezoelectric ceramic thick films. Methods utilised in thick film deposition include screen printing, direct writing, electrophoretic deposition, a paint technique of deposition, the composite sol-gel technique etc. The composite sol-gel technique was utilised in this study due to its advantages of low preparation cost, good stoichiometric control and the means to lay down thick layers of between 0.1μm to 100μm, a thickness range that is difficult to achieve by other deposition techniques (Pérez de la Cruz, 2012).

It is well known that the composite sol gel process, is an exceptional technique used to develop high quality thick ceramic films of more than 1μm in thickness (Barrow, et al., 1995), while keeping all the benefits of the thin film sol gel process, i.e. ease of fabrication, ability to coat complex geometries, the relative cost effectiveness (Pérez de la Cruz, 2012) and also ability to produce thick layers without cracks by adding ceramic powder to reduce

the stress within the composite thick film (Lau, et al., 2011). The advantages of the method are associated with the possibility to obtain high quality thick films with thicknesses up to 100μm on a variety of substrate materials and shapes. The main disadvantage associated with the composite sol-gel process is the difficulty to obtain dense thick films that reproduce the ceramics' bulk electromechanical properties. This issue affects ferroelectric materials like PZT, where the dielectric, ferroelectric and piezoelectric properties are highly influenced by the density of the film (Pérez de la Cruz, 2012). The energy output by a piezoelectric film per unit area is proportional to the film thickness, hence making thickness control a mechanism by which to control electromechanical output (Huang, et al., 2006). The processes by which the thickness can be controlled are therefore very important and the layered nature of the composite sol-gel process allows this level of thickness control.

The composite sol-gel process is a combination of the low temperature sol-gel processing route and the ceramic powder processing route and yields a hybrid technique that allows thick film production at low temperatures (Dorey & Whatmore, 2004). The method normally involves the use of the solvent, 2-methoxyethanol, in the chemical synthesis of perovskite materials though other alcohol based solvents may be used. In any sol-gel process, the stable sol contains metal oligomer chains formed by the reactions of the metal-organic precursors, that are subsequently pyrolysed and heated in thin layers to form metal-oxygen-metal chain links which ensures uniformity in the final sol-gel (Chowdhury, et al., 2011). Solution processes based on the use of 2-methoxyethanol are said to be the most widely used of the CSD routes, due to the capacity for it to act as a solvent to a wide variety of starting reagents (Schwartz, 1997). The process involves producing a composite slurry by mixing the ceramic powder and an oxide ceramic producing sol (produced from a reflux reaction) to form the composite sol-gel. The composite sol-gel is then deposited using a spin coating process onto

a wafer spun at high speed resulting in a film. The film is pyrolysed to convert the sol to an oxide ceramic and remove the organic components of the slurry and successive layers may be deposited to increase the film thickness. On completion of the deposition the thick film is heat treated at temperatures above 600◦C to develop the perovskite phase. The largest disadvantage faced with composite sol-gel processed films are that the resultant properties of the film are typically lower than those of the corresponding bulk ceramics due to the high levels of porosity (Dorey & Whatmore, 2004). Another disadvantage is the use of 2-methoxyethanol which is a known teratogen presenting significant safety concerns especially with consideration during large scale manufacturing processes. A replacement of this solvent with 1,3-propanediol (considerably less toxic) in this process has been reported. An advantage to this process is that it has been demonstrated that through manipulation of the reflux reaction to produce the sol, the nature of the resulting solution precursors and gels may be controlled, allowing for eventual control of material properties (Schwartz, 1997).

One of the issues faced with the sol-gel deposition technique is constrained sintering, whereby difficulties are faced with the deposition thick films on rigid substrates which may lead to film shrinkage. This occurs due to differences in chemical properties between substrates and thick films i.e. heat affects the bulk properties and as a result the interface properties of the thick film and substrate which react differently. Constrained shrinkage occurs when the applied composite sol-gel film undergoes a reduction in volume while the dimensions of the substrate remain unchanged. The loss of the liquid phase and further volume reduction occurs continually from the application of the film to the eventual densification heat treatment processing step. On a rigid substrate the thick film is unable to shrink in the *x* or *y* axes, leading to the generation of in-plane tensile stresses within the film. Solutions include higher temperatures and longer dwell times with careful consideration

given to material mass loss that leads to a reduction in the electromechanical properties of the thick film. Other solutions include relief of the in-plane tensile stresses with stress relaxation which is achieved with the use of heat treatment chemical dopant aids which in turn enhance densification of the film structure. The heat treatment chemical dopant aid acts as a swift diffusion path for atomic species hastening the dissolution of material from areas of low stress and the subsequent deposition of material at areas of high stress (Dorey & Whatmore, 2004).

The use of a liquid phase, as the composite sol-gel process suggests, can act to reduce the stresses involved, as the liquid phase acting as a lubricant allows individual powder particles to move relative to one another. In practice both the densifying and stress relaxation heat treatment chemical dopant aid and the liquid phase heat treatment chemical dopant aid are active during the heat treatment process, acting at different times. At lower temperatures in the early stages the liquid phase heat treatment chemical dopant aid is most active and as that resource is depleted the solid phase heat treatment chemical dopant aid comes to the fore and stress relaxation is accomplished through a diffusion controlled shear relaxation resulting in a crack free thick film (Dorey & Whatmore, 2004).

Due to KNN's highly volatile alkali metal oxides, in many preparation processes of films containing sodium and potassium elements processed by e.g. pulsed laser deposition or RF-sputtering etc., these processes tend to result in significant sodium and potassium losses. The vacancies of volatile sodium and potassium ions are thought to be amongst the reasons for the low ferroelectricity observed in KNN films due to increased ionic conductivity (Lai & Li, 2007). The use of the composite sol-gel process offers the advantage of reductions in processing temperatures which reduces the tendency for loss of alkali metal oxides (Chowdhury, et al., 2010).

Over the years the uses of novel deposition techniques and solutions to obstacles faced have ensured the production of thick films with functional properties similar to those of bulk prepared ceramics (Dorey & Whatmore, 2004). Consequently with proper handling the composite sol-gel processes offer exceptional control and reproducibility of process chemistry with non-hydrolyzed solutions exhibiting minimal aging effects (Schwartz, 1997).

2.13. Summary

The key requirements of this study were to produce bio-compatible thick films that may find wider applications as MEMS. While it is possible to process bulk piezoelectrics into very thin elements and to dice very small elements in the fabrication of high frequency single element transducers and arrays, this was proven to be a very difficult task that had many disadvantages that the use of thick films ameliorated. Due to legislation it was required that a Pb-free material was utilised and thus KNN as the most researched and successful Pb-free material of the last two decades was selected to perform this task. Its popularity lies in the fact that it posses very good piezoelectric characteristics and is relatively cheap when compared to other bio-compatible Pb-free materials.

The processing techniques also required cost effective measures and hence low temperature production, robustness and simplicity were the by word of the research. This resulted in the selection of the low cost, robust and simple MSS powder synthesis method to produce the KNN powders. A hybrid sol-gel process the composite sol-gel process was selected to produce the KNN thick films again as it is a process that is cost effective, robust and quite simple. Consequently the MSS powder synthesis method and the composite sol-gel process methods that lend themselves suitably to eventual manufacturing scale-up. The main

parameters selected to characterise the properties of the KNN thick film were the piezoelectric coefficient, relative permittivity, dielectric loss and dielectric impedance spectroscopy.

Chapter 3

3. Experimental

3.1. Introduction

In order to produce $K_{0.5}Na_{0.5}NbO_3$ (KNN) thick films, KNN powder and a liquid KNN producing sol are required. The powder and the sol are mixed together to form a sol gel composite, then typically deposited onto a platinised silicon wafer. The spin coated wafer is heat treated and electrodes coated on the film surface. This is then ready for physical, chemical and electrical characterisation. PZT thick films were produced in a similar method to act as qualitative and quantitative guides to the KNN thick films produced.

Bulk KNN samples were prepared to also act as comparative standards for the KNN thick films through electrical testing. The KNN powders were doped with various transition and alkaline earth metals as well as lithium to enhance physical and electrical characteristics of the KNN thick films. A KNN thick film using polyvinyl acetate added as a binder to KNN powders was tested.

3.2. Powder production

Three methods of powder syntheses to produce KNN were used and are described below. All the starting reagents were used as received without further purification steps in all syntheses performed. Elemental and optical analysis of the powders prepared using these methods was carried out. The powders were combined with KNN sol to produce composite sol gel slurries for use to build up thick films.

3.2.1. Mixed Oxide Synthesis

The Mixed Oxide Synthesis (MOS) method, involves mixing stoichiometric ratios of K_2CO_3 (≥99.0% purity - Sigma Aldrich), Na_2CO_3 (≥99.0% purity - Sigma Aldrich) and Nb_2O_5 (99.9% purity - Sigma Aldrich) according to the $K_{0.5}N_{0.5}NbO_3$ formula. An excess (that fully submerged the reagents) of zirconia grinding media was placed in a 250ml borosilicate glass bottle and isopropanol added as the carrier in a quantity high enough to submerge both the reactants and zirconia balls. This was then milled for 12 hours to evenly distribute the reagents throughout the powder mix. The slurry was filtered using a stainless steel sieve (600µm mesh) to remove the zirconia balls and washed through the sieve with isopropanol. The slurry was placed in a glass bowl and dried at 120°C in an oven. Any aggregates were crushed in a pestle and mortar and the powder placed in an alumina crucible. This was placed in a furnace (Carbolite ELF 11/68) and heat treated at between 750°-950°C for 4 hours.

The ramp rate was dependant on the amount of powder present with a slower ramp rate applied when a large amount of powder was synthesised and a faster ramp rate with smaller amounts of powder. On completion KNN powder was collected. *Table 3* shows the classification of heating ramp rates (which was dependant on the amount of powder to be synthesised), used in this project to synthesize powders.

Table 3 classification of heating ramp rates

Description	Amount of Powder (g)	Ramp Rate
Fast	1-5	Greater than 20°C/min
Medium	6-19	10°-20°C/min
Slow	20+	1°-9°C/min

This powder synthesis method was used to make doped KNN powders which were added at the initial weighing stage with the other reactants. The dopants used are shown in *Table 4* below.

Table 4 showing dopants used

Dopants		
Mn [MnO_2 (99% -Sigma-Aldrich)]	**Zr** [ZrO_2 (99.9% -Sigma-Aldrich)]	**Li** [Li_2CO_3 (99% -Sigma-Aldrich)]
Ta [Ta_2O_5 (99% -Sigma-Aldrich)]	**Ti** [TiO_2 (99.9% -Sigma-Aldrich)]	**Ca** [$CaCO_3$ (Sigma-Aldrich)]
W [WO_3 (99% -Sigma-Aldrich)]		**Sr** [$SrCO_3$ (99.9% -Sigma-Aldrich)]

3.2.2. Molten Salt Synthesis

The Molten Salt Synthesis (MSS) method, involves mixing stoichiometric ratios of K_2CO_3, Na_2CO_3, Nb_2O_5 with a similar amount of salt [NaCl (≥99.5% - Sigma Aldrich) /KCL (≥99.0% - Sigma Aldrich) mix] according to the $K_{0.5}N_{0.5}NbO_3$ formula. An excess (that fully submerged the reagents) of zirconia grinding media was placed in a 250ml borosilicate glass bottle with isopropanol added as in ***section 3.2.1***. This was milled for 12 hours to evenly distribute the reagents throughout the powder mix. The slurry was separated from the zirconia grinding media and placed in a glass bowl as in ***section 3.2.1***, and dried at 120°C in an oven. A pestle and mortar was used to break any aggregates and the powder placed in an alumina crucible and heat treated at between 650°-800°C for 2 hours (Carbolite ELF 11/68). The ramp rate was dependant on the amount of powder present as in ***section 3.2.1***.

On cooling the powder was washed with lukewarm de-ionized water to remove the chlorine ions using a 0.20µm Whatman Nylon ZapCap™ filter which is re-usable. To detect the Cl ions: a 0.1M solution of $AgNO_3$ in de-ionised water was prepared. After each washing run approximately 1ml of filtrate was collected in a beaker and a couple of drops of $AgNO_3$ were added. A clear solution indicates the removal of the Cl ions while a colour change to white indicates the presence of Cl ions and the need to continue the washing. On completion the powder was washed out of the ZapCap filter and placed in a glass bowl and dried at 120°C for 12hrs. This powder synthesis method was used to make doped KNN powders.

3.2.3. Molten Hydroxide Synthesis

The molten hydroxide synthesis (MHS) method, involves mixing stoichiometric ratios of K_2CO_3 and Nb_2O_5 with an excess of KOH (≥90% flakes – Sigma Aldrich) according to the $K_{0.5}N_{0.5}NbO_3$ formula. These were ground in a pestle and mortar to breakdown agglomerates, reduce the particle size of the large grained reactants and mix them. This was then placed in an alumina crucible and heat treated at 315°C-500° for 2 hours; on cooling, the reactants were broken down in a pestle and mortar.

In the second stage a molar excess of Na ions (from Na_2CO_3 or NaCl) (a molar excess with respect to the KNN stoichiometric ratio – see *Table 5*) was added to the reaction mixture and ground with a pestle and mortar to a fine powder consistency and to mix the reactants.

Table 5 showing molar mass of reactants

Reagent	Molar Mass (moles)
Nb_2O_5	0.0129
K_2CO_3	0.0064
KOH	0.0520
Na ions	0.0376

The powder was placed in an alumina crucible and heat treated at 650°-800° for 2 hours. The ramp rate was dependant on the amount of powder present as in ***section 3.2.1***. On cooling the powder was washed with warm de-ionized water, using a 0.45µm Whatman PTFE ZapCap™ filter (due to the corrosive nature of the hydroxide) which is re-usable. This is done in order to remove the hydroxides and any other unreacted water soluble niobate materials present. Due to the hydrophobic nature of the PTFE ZapCap™ filter before the washing procedure is started, a few drops of isopropanol were used to temporarily nullify the hydrophobic nature of the PTFE filter material and therefore allow water through. 5-8 washings (dependant on the amount of powder) are carried out to ensure complete removal of soluble material. XRD

tests were carried out to determine this number of washings. This was then washed out of the filter, placed in a glass bowl and dried at 120°C in an oven for up to 12 hours. This powder synthesis method was used to make doped KNN powders.

3.3. Sol production

The glassware for the reflux reaction was placed in a dry oven, overnight before use. The reactants were stored and measured in a dry glove-box (N_2 atmosphere). Sodium ethoxide (95% - Sigma Aldrich) and potassium ethoxide (95% - Sigma Aldrich) were mixed following the formula $K_{0.5}Na_{0.5}NbO_3$, in the desired stoichiometric amounts at a concentration of 0.3M, in 2-methoxyethanol (99.8% - Sigma Aldrich) (2-ME) and glacial acetic acid (Alfa Aesar - 99.7+%) (2% of all 2-ME used in the full reaction) and refluxed while stirring for 3 hours at 120°C. Niobium ethoxide (99.99% - Multivalent Ltd.) was added to this with 2-methoxyethanol to the desired molar concentration (0.3M) and again refluxed for 3 hours at 120°C. On cooling to room temperature, 4.17 wt. % (relative to the solvent) of ethylene glycol (99.8% - Sigma Aldrich) was added and stirred for 30mins. On completion a 0.45µm Whatman PTFE ZapCap™ filter (which is re-usable) was used to filter undissolved material into the borosilicate glass sample bottle and stored in a cool dry place. Doping of the sol did not occur, as this would have introduced further complexity to the thick film production.

3.4. Slurry production

The slurry was a mixture of powder and sol that was deposited on a substrate to produce thick films.

3.4.1. KNN slurry production

The composite slurry was produced by mixing the KNN producing sol with the KNN powder in a 1:1 mass ratio. 2 wt. % (relative to the KNN powder mass) of a dispersant, KR55 (Kenrich Petrochemicals, Inc.) was added to ensure thorough dispersion. Zirconia grinding media were placed in a borosilicate glass bottle at a level high enough to cover the slurry and milled for 24 hours in order to achieve a fine powder particle size.

3.4.2. PZT slurry production

Lead titanate zirconate (PZT) slurry was prepared by mixing PZT powder (Meggit-Ferroperm-PZ26 2627-N2) and PZT sol (sourced from fellow researchers). The PZT sol was produced from the combination of two separately prepared reflux reactions involving; the lead acetate solution and the 2-methoxyethanol solution. The lead acetate solution was prepared by mixing 52.5g of lead (II) acetate trihydrate (Sigma-Aldrich ≥99%) with 30ml of glacial acetic acid and refluxed for 3 hours, followed by complete dehydration of the solution using vacuum distillation at 102-104˚C until 20ml of distillate was gathered. The 2-methoxyethanol solution was prepared by mixing 17.685g, 27.328g and 50ml of titanium (IV) isopropoxide (Sigma-Aldrich ≥99.7%), zirconium (IV) propoxide (Sigma-Aldrich ≥99.7%) and the solvent 2–methoxyethanol anhydrous, respectively were refluxed for 3 hours. The two solutions were mixed together by further refluxing. The solution at this stage had a cloudy appearance. Vacuum distillation was then conducted at 84-90˚C to remove excess water until a clear yellow solution was obtained. The amount of distillate removed was replaced by additional 2–methoxyethanol to obtain a sol concentration of 1.1M, this was followed by the addition of 5g of ethylene glycol to stabilise the sol. The powder and the sol were missed in a 3:2 mass ratio respectively. 2 wt. % (relative to the PZT powder mass) of a

dispersant, KR55 was added to ensure thorough dispersion. Zirconia grinding media were placed in a borosilicate glass bottle at a level high enough to cover the slurry and milled for 24 hours after which the material was ready for deposition.

3.4.3. Polymer modified KNN slurry production

KNN powder was mixed with polyvinyl acetate (PVAc) (Polysciences Inc. M.W. 500,000) in a mass ratio of 48% KNN powder to 52% PVAc. 2 drops of a dispersant, Ingepal® 630 (Sigma Aldrich) were added to ensure thorough dispersion. The 250ml borosilicate glass bottle was filled with acetone (ratio of PVAc to acetone 1:20 respectively). The slurry was left standing for 24 hours to allow the PVAc to dissolve in the acetone. This was ball milled with zirconia milling media for 24 hours. This was then ready for deposition.

3.5. Deposition

A back electrode was deposited on silicon wafers with a titanium-platinum electrode sputtered [Nordiko Magnetron Sputter machine (Ti = 10nm; Pt = 100nm – {preferred orientation (111)})]. At this stage in some cases the wafer was diced into between 4 to 10 sections to be used individually while in other cases whole wafers were used. The wafer was cleaned with isopropanol and acetone by spinning at 3000rpm for 30s (SCS Cookson G3-8 Spincoat) and dried with compressed air. These wafers were then cleaned using oxygen plasma (Polaron PT7160 RF plasma barrel etcher,13.56 MHz, 2 min @ 12 W power) to remove residual surface contaminants.

The KNN thick film was built up by covering the wafer with the composite slurry and spinning at between 2000-3000 rpm for 30s using the spin coater. This layer was then

subjected to calcination (200°C for 60 seconds and 450°C for 30 seconds) in order to remove the organic component, solvent and to pyrolyse the sol. Sol was then deposited on the deposited composite slurry, passing it through a 0.2µm Whatman filter and subjected to a similar spinning and heat treatment. This was repeated until 4 layers of composite slurry, each infiltrated by two sol layers had been deposited i.e. 4(C + 2S); C = composite slurry; S = Sol.

The same processing was applied to the PZT films. In the case of the KNN-PVAc, films sol was not used and the layers were built up to between 10 and 20 layers of slurry with heating for 1min at 65°C after each deposition of slurry. *Figure 9* shows a schematic illustration of the deposition process.

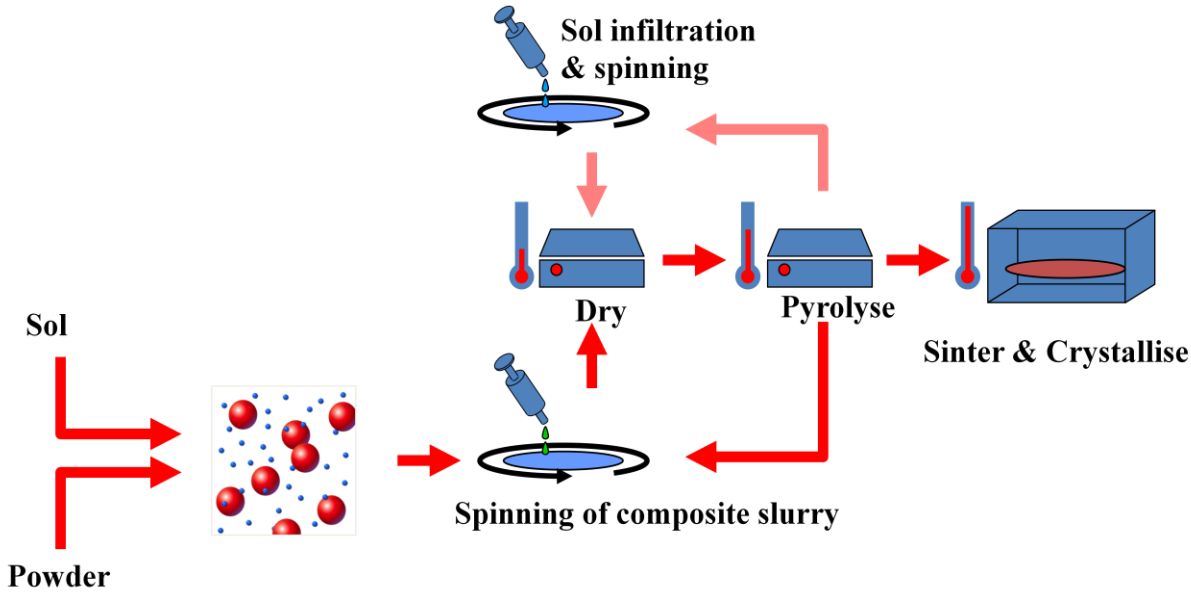

Figure 9 schematic illustration of thick film deposition (Dorey, 2010)

A small section of the thick film was mechanically abraded in order to later establish contact with the platinum back electrode. The spin coated wafer was then subjected to a thermal annealing process (700°C/30min) to develop the perovskite structure, in a furnace (Carbolite

ELF 11/68). A fast ramp rate was used to reach maximum temperature in the shortest space of time.

3.6. Preparation of bulk disc compacts

Deionised water and water soluble polyvinyl alcohol binder [Alfa-Aesar 87-89% hydrolyzed, low molecular wt.] (at 2% the weight of KNN powder used) were mixed with 5g of KNN powder in a borosilicate glass bottle and ball milled for 24hrs with zirconia balls. The zirconia balls were removed by sieving the material through a stainless steel sieve and using deionised water to wash through then dried at 120°C. They were then pressed into discs, 30mm in diameter and 3mm in height, under 3 tons of pressure (322kPa). These powder compacts were sintered in air for 4hrs at 1050°C with a 5°C/min ramp rate.

The sample surfaces were wet polished until visually smooth and smooth to the touch. They were then dried at 120°C for 6 hours. Cr/Au electrodes were deposited on either side of the bulk compact (using Edwards E480) by evaporation prior to electronic characterisation.

3.7. Physical characterisation

Prior to physical characterisation testing, all powders were ground with a pestle and mortar to break up any agglomerates.

3.7.1. X-Ray Diffraction

The crystalline structure and chemical composition of the powders and thick films on wafers were investigated using X-Ray diffraction (Siemens D-5005). Two methods of testing powders were carried out. The first involved the use of a metal boat attached to a glass slide,

where approximately 0.5g of the powder was held during measurement. In the second method powder was deposited directly onto double sided carbon tape attached to a glass slide. Thick films were measured without further treatment. Using Bragg's Law the lattice-spacings were calculated.

3.7.2. Surface profilometry

The Dektak™ Surface Stylus Profiling analyser was used to determine the thickness of the thick films by measuring the depth of a groove scratched into the thick film. The film thicknesses varied between 5 -12 μm.

3.7.3. Scanning electron microscopy

The micro-structures of the films and powders were examined by scanning electron microscopy (SEM) micrographs (ESEM FEI XL30 and SFEG FEI XL30) to characterise particle shape and size, establish film thickness and observe the film density and micro-structure.

Chemical analysis of the powders and films was carried out using the Energy Dispersive X-ray spectroscopy (EDX) attached to the ESEM.

3.8. Electrical characterisation

The thick films and bulk ceramic samples were prepared for electrical testing by deposition of top electrodes.

3.8.1. Electrode deposition

The thick films were placed on a mask with an array of 2mm and 1mm diameter holes to evaporate Cr/Au electrodes (Edwards coater E480) onto the surface of the thick films with a thickness of 10nm Cr and 50nm Au. In the case of the bulk ceramic compact the entire surface had 10nm Cr and 50nm Au electrodes deposited on both sides.

Silver conductive paint (RS Components 186-3593) was applied to the back of the wafer and on the small abraded section on the front to make contact with the platinum back electrode and the two sections of Ag paint connected on the edge of the abraded section.

3.8.2. Electrical poling

Contact electrical poling of the thick films was carried out on a departmental custom made electrical poling rig that had a hot plate attached. Poling of thick films occurred from room temperature to 200°C. The maximum poling voltage used was dependent on the thickness of the thick film with poling occurring from 0V/µm to a maximum of 10V/µm. Thick films were poled at either room temperature or elevated temperatures (room temperature to 200°C) for 5 minutes then cooled while poling to 60°C, after which dielectric coefficient, capacitance and dielectric loss measurements were carried out.

The bulk KNN disc compact samples were poled (Brandenburg Alpha Series II) at both room temperature and 130°C (silicone oil bath) with poling occurring from 0V/µm to a maximum of 10V/µm for 15mins and on cooling to 60°C tested for piezoelectric constant, capacitance and dielectric loss.

3.8.3. Capacitance & dielectric loss measurement

Capacitance (C) and dielectric loss ($tan\delta$) measurements were carried after each electrical poling step (as described in ***section 3.8.2***) using a Wayne Kerr Precision Component Analyzer 6425 at 1 kHz, on the 2mm diameter Cr/Au electrodes. The two pin electrodes were connected to the Pt back electrode via the abraded section with Ag paint and the Cr/Au electrodes on top of the thick films. The AC field was 100mV with no bias applied. The relative permittivity (ε_r) was calculated from the capacitance and knowledge of the sample geometry using ***Equation 3-1***.

$$\varepsilon_r = \frac{Cd}{\varepsilon_0 A} \qquad \textit{Equation 3-1}$$

Where C is capacitance, d is the thickness of the film, ε_0 is permittivity of free space ($8.85418781 \times 10^{-12}$ F/m) and A is the area of Cr-Au top electrode.

3.8.4. Piezoelectric coefficient (d_{33}) measurement

The d_{33} measurements were conducted using a Berling Court piezometer (Take Control PM25) after each electrical poling interval (as described in ***section 3.8.2.***). Two readings were taken for each electrode tested.

3.8.5. Impedance analysis

Impedance analysis was carried out over the full range of the Hewlett Packard LF Impedance Analyzer's (5Hz-13MHz) frequencies. The magnitude of the impedance and phase angles of the samples was collected and used to calculate the real and imaginary parts of impedance.

Chapter 4

4. KNN powder production

4.1. Molten salt synthesis

The Molten Salt Synthesis (MSS) method was adopted as the primary $K_{0.5}Na_{0.5}NbO_3$ powder synthesis method in this project initially. When the NaCl-KCl salt mix was used in the MSS method, a sodium rich alkali niobate and related derivatives were formed in place of the desired KNN, despite starting with equimolar amounts of Na_2CO_3 and K_2CO_3, as seen in the XRD results shown in *Figure 10* (NOTE: all XRD traces are normalised and offset to enhance clarity). The XRD results show peaks at higher 2θ angles with respect to the reference KNN XRD powder trace and match the XRD pattern of $NaNbO_3$ (NN). A similar behaviour was observed in studies of the hydrothermal synthesis (HS) of KNN, where to achieve a 1:1 ratio of K-Na ions in the final product the ratio of the precursors needed to be greater than 3:1 of K-Na (Zhang, et al., 2008). In contrast in the high temperature Mixed Oxide Synthesis (MOS) process, $K_{0.5}Na_{0.5}NbO_3$ is produced with the use of equimolar quantities of K and Na precursors. In the lower temperature synthesis methods i.e. MSS and HS, potassium deficient species are produced, indicating that there is an issue associated with K diffusion or reactivity that does not occur in MOS. Potassium ions are known to have a lower diffusion rate with respect to sodium ions (Zeng, et al., 2007) (Zhang, et al., 2008) and this may in part explain the imbalanced stoichiometry in the end product.

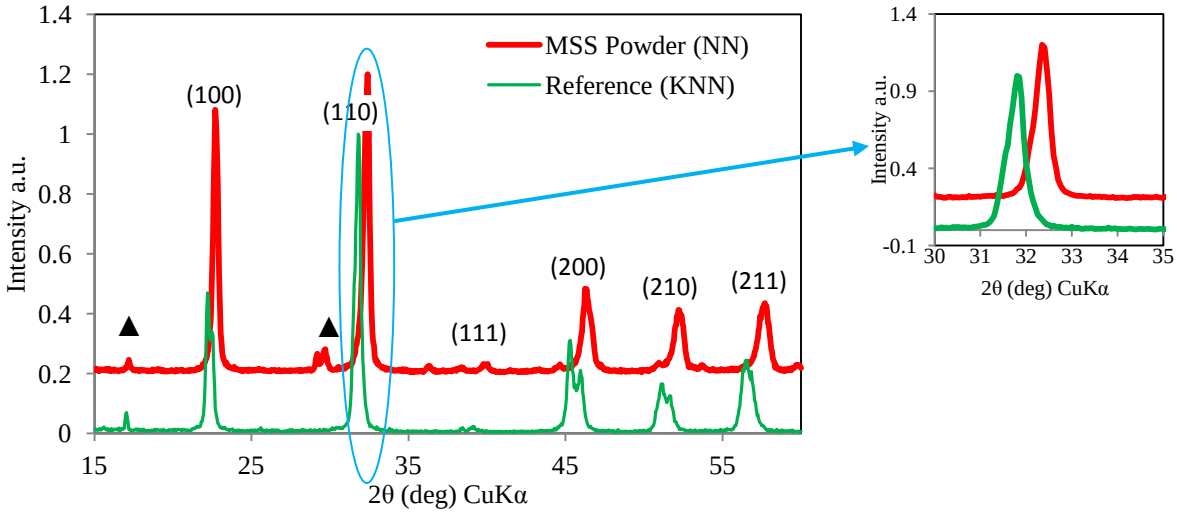

Figure 10 XRD patterns of powder made from MSS method (that formed $NaNbO_3$) compared with KNN reference powder sample. ▲- unreacted Nb_2O_5 (the XRD traces are normalised and offset to enhance clarity).

The XRD analysis indicates the formation of a Na-rich alkali niobate and the presence of residual Nb_2O_5 in the end product as seen in *Figure 10*. ESEM-EDX analysis supports this observation showing a K-Na ion ratio of 1:14 as seen in *Table 6*.

Table 6 ESEM-EDX analysis of powder made using MSS showing atomic percentages of constituent parts

ESEM EDX analysis - Molten Salt Synthesis (MSS) produced powder				
Element	Nb	Na	K	Total
Theoretic atomic (%)	50.0	25.0	25.0	100.0
Actual atomic (%)	58.9	38.3	2.8	100.0

The result shows that the potassium reactant is lost in some way from the reaction either by evaporation or as a water soluble product washed away during the washing step. Further work was carried out to establish the cause of the $NaNbO_3$ production and find a solution to this issue.

4.1.1. Effect of calcination temperature on product of MSS

Due to the result achieved with the standard MSS process further investigation was carried out to better understand the process in order to produce KNN. The effect of varying the dwell time and temperature of the MSS process were investigated, as it was hypothesised that

longer times or higher temperatures would allow more K to diffuse into the final product. Powders were prepared at 700°, 750° and 800°C with a two hour heat treatment dwell time. A further powder heat treated at 700°C was prepared with a calcination dwell time of 4 hours to examine if an extended treatment time would allow further K diffusion to take place. The powders were examined by XRD to determine their crystal structures (*Figure 11*).

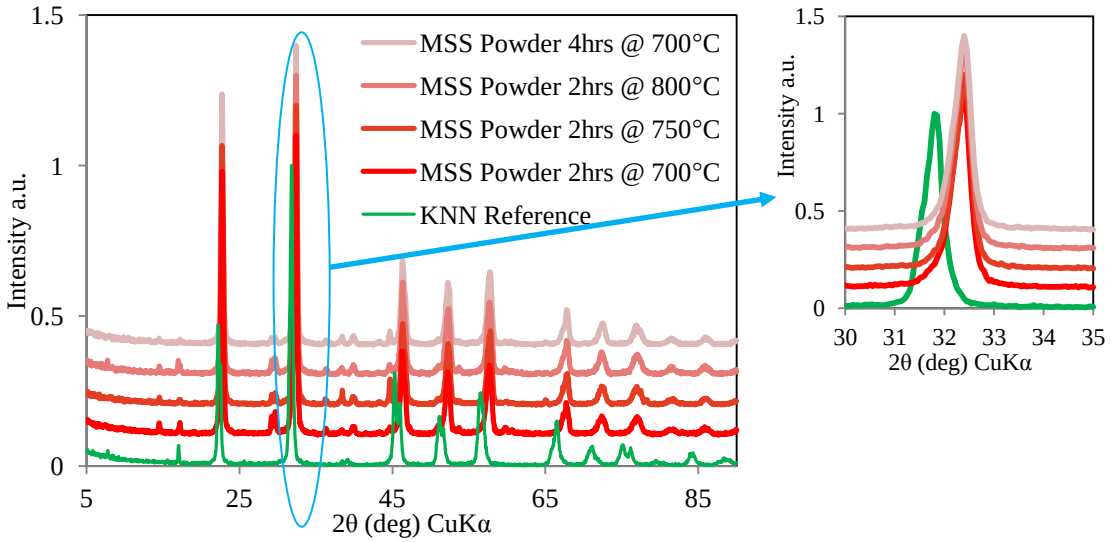

Figure 11 XRD patterns of powder made using the MSS method at different conditions compared with reference $K_{0.5}Na_{0.5}NbO_3$.

From the XRD patterns shown in *Figure 11* it was observed that increasing the reaction temperature (700°C – 800°C) and the reaction soak time (2hrs – 4hrs) failed to produce any significant changes in the reaction product.

4.1.2. Excess K_2CO_3

Following the results reported from the use of the hydrothermal synthesis method by Zhang *et al.* (Zhang, et al., 2008), the proportion of potassium ions was increased in a stepwise manner with respect to the level of sodium ions in the system. The aim was to increase the concentration of K ions in the reaction mix so increasing the possibility of KNN formation.

Table 7 shows the molar ratios of the starting reagents (K_2CO_3: Na_2CO_3: Nb_2O_5) used in the synthesis.

Table 7 molar ratios of starting reagents in MSS synthesis

K_2CO_3	Na_2CO_3	Nb_2O_5
1.25	1	2
1.50	1	2
1.75	1	2
2.00	1	2
3.00	1	2

The powders were heat treated for 2 hours at 700°C, then washed, dried and analysed using XRD (*Figure 12*).

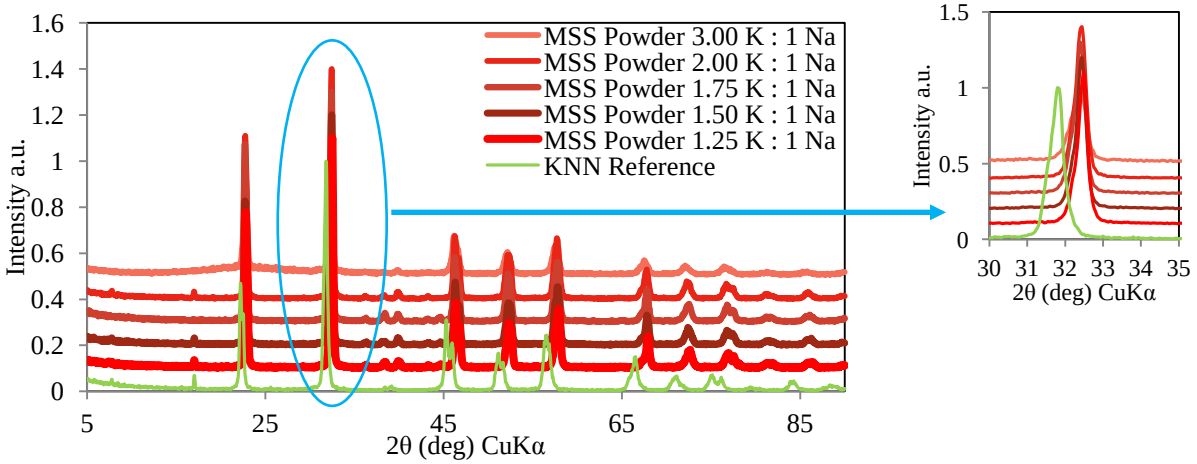

Figure 12 XRD patterns of powders with varying amounts of K_2CO_3 starting reagent made using MSS method compared to a KNN reference powder.

From the XRD patterns shown in *Figure 12* it was observed that, despite the increases in the concentration of K ions in the reaction mix, a sodium rich alkali niobate was still produced shown by the position of the peaks with respect to those of the reference KNN. Equally worth noting is that increasing the potassium ion excess up to 3:1 K-Na, as in the hydrothermal synthesis (HS), also failed to increase the level of K incorporation into the final product. The ratio of K: Na ions of 3.5:1 in hydrothermal synthesis, was seen to result in the formation of KNN with a long dwell time of between 6-24 hours (Zhang, et al., 2008). Modifying the MSS by increasing the concentration of K ions would lead to an inefficient

and expensive process and with no gradual shift observed it was considered unlikely that a 3.5:1 ratio would show any difference; thus matching the successful concentration used in the HS method was not investigated.

4.1.3. Stepwise removal of starting reagents

The results obtained indicate that the potassium ions from the K_2CO_3 did not react sufficiently with the niobium (v) oxide, with XRD and ESEM-EDX analysis showing a deficiency of K ions in the end product. It is known that Na ions diffuse into the niobium oxide matrix an order of magnitude faster than K ions to form $NaNbO_3$ (Zeng, et al., 2007) (Zhang, et al., 2008) and this in part explains the deficiency of K ions in the end product. Another observation made from the XRD analysis was the near purity of the $NaNbO_3$ product with a low presence of unreacted Nb_2O_5 despite the stoichiometric ratios of Na_2CO_3 and K_2CO_3 added initially. The number of moles of Na ions from the Na_2CO_3 was half that of the niobium oxide and as a result besides producing $NaNbO_3$ a large amount of unreacted Nb_2O_5 or other products were also expected. This suggested either a secondary source of Na ions from the salt, which diffused faster than the K ions into the niobium oxide matrix creating the $NaNbO_3$; or as suggested before a water soluble potassium niobate phase that was washed away during the washing step.

To investigate the hypothesis that NaCl may be the secondary source of the Na ions, MSS was conducted to observe the resultant product in the absence of both alkali metal carbonates in the reaction mix. Consequently niobium oxide was mixed with sodium and potassium chloride salts only and heat treated for 2 hours at 700°C (*Figure 13*).

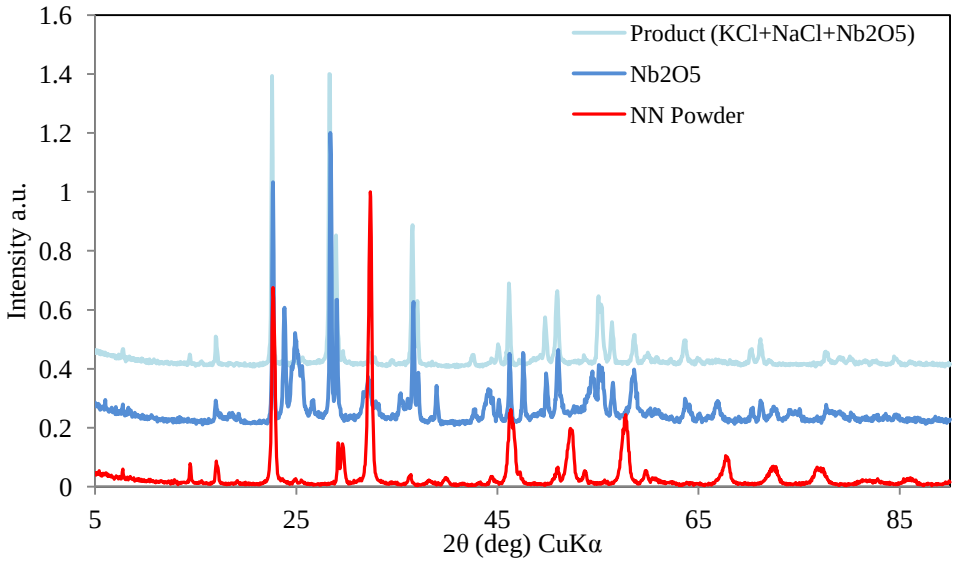

Figure 13 XRD patterns of Nb_2O_5 heat treated in the presence of NaCl & KCl compared with Nb_2O_5 & $NaNbO_3$ powder.

From the XRD patterns shown in *Figure 13*, there was no evidence of an alkali niobate formed by a reaction of Nb_2O_5, KCl and NaCl. The KCl and NaCl showed no significant reaction with the niobium (V) oxide, showing that Na and K ions from the salts are not available to diffuse into the Nb_2O_5 in the absence of the alkali carbonates. A further observation made was that following the heat treatment the resultant niobium (V) oxide powder pattern did not contain evidence of second phases as seen in the pattern of the unheated as received niobium (V) oxide powder.

To evaluate if K could be incorporated, K_2CO_3 was added to the simple reaction mixture. The XRD pattern of the product is shown in *Figure 14*.

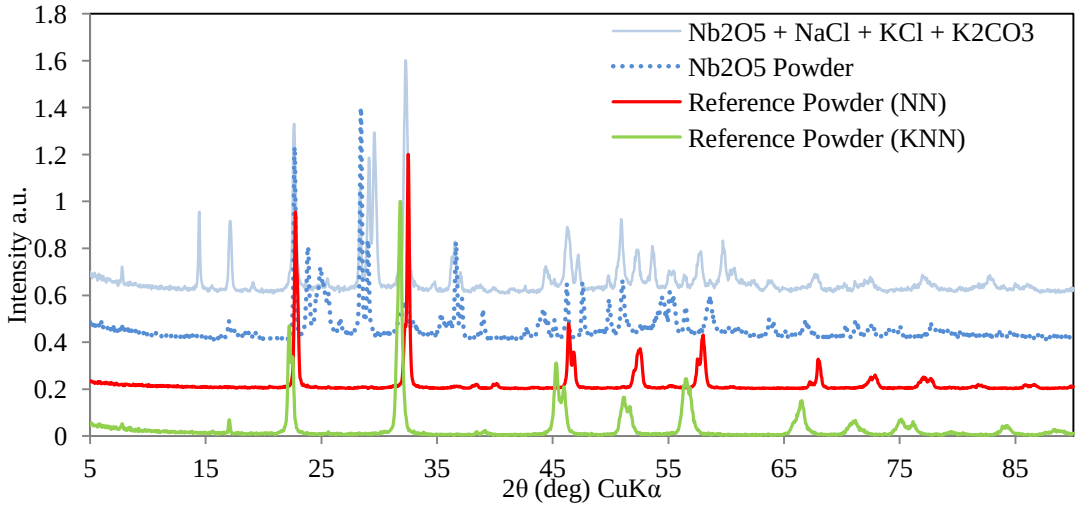

Figure 14 XRD pattern of products of Nb_2O_5 and K_2CO_3 heat treated in the presence of NaCl & KCl for 2hrs @ 700°C compared with reference KNN, NN and Nb_2O_5 powder.

The reactants were heat treated at 700°C for 2 hours (*Figure 14*) and washed. The product appeared to be a mix of materials with signs of the nascent development of the perovskite structure with the peaks most closely aligned to those of $NaNbO_3$. $Na_2Nb_4O_{11}$ is thought to be the first phase of the reaction to form the perovskite structure at the interface of sodium carbonate and Nb_2O_5 at 500°C. The perovskite phase is thought to form only after heating at 700°C at the boundary between $Na_2Nb_4O_{11}$ and Na_2CO_3 (Malic, et al., 2008). This indicates that the reaction proceeds through various phases prior to the production of the perovskite phase.

This showed that despite overloading the system with potassium ions the reaction did not yield KN or KNN powder. Furthermore, this result also indicates that there is an interaction between K_2CO_3 and NaCl that liberates some Na ions that are able to interact with the Nb_2O_5 to produce the Na rich niobate perovskite structure. A proposed reaction is shown below.

$$K_2CO_3 + 2NaCl \longrightarrow 2KCl + Na_2CO_3 \qquad \textit{Equation 4-1}$$

$$Na_2CO_3 \longrightarrow 2Na^+ + O^{2-} + CO_{2(g)} \qquad \textit{Equation 4-2}$$

$$2Nb_2O_5 + 2Na^+ + O^{2-} \longrightarrow Na_2Nb_4O_{11} \qquad \textit{Equation 4-3}$$

$$Na_2Nb_4O_{11} + 2Na^+ + O^{2-} \longrightarrow 4NaNbO_3$$ *Equation 4-4*

The hypothesis is that the Na ions react with the K_2CO_3 to form Na_2CO_3, which then reacts with the niobium (V) oxide. Comparison of the XRD trace of this product with the XRD Powder Diffraction File data file database shows some similarities to various potassium and sodium niobates (e.g. KNb_3O_8, $KNb_{13}O_{33}$, $KNbO_3$, $Na_2Nb_4O_{11}$, Na_3NbO_4, Na_5NbO_5, $NaNb_3O_8$ etc) were observed, but no definitive identification could be made due to the complex nature of the product i.e. a mixture of products/phases.

4.1.4. Two step molten salt synthesis

Based on the observations in ***section 4.1.3*** where the difficulty of reacting K_2CO_3 with Nb_2O_5 in the presence of NaCl was highlighted; a two stage powder synthesis process was proposed. In the first stage $KNbO_3$ (KN) would be produced and any unreacted Nb_2O_5 would be present; in a second stage Na ions would be introduced which would react with unreacted Nb_2O_5 and KN to form KNN.

The partial reaction reported in ***section 4.1.3*** where signs of the formation of a Na rich niobate, was driven further by the addition of Na_2CO_3 in a 2nd stage. The intention was to observe what the product of this reaction would be considering the absence of Na_2CO_3 from the 1st stage. Also knowing that from the earlier experiment where the 1st stage powder appeared to be a mixed phase powder that contained a sodium rich niobate this experiment would provide clarity. The resultant powders were washed, dried and examined by XRD, (*Figure 15*).

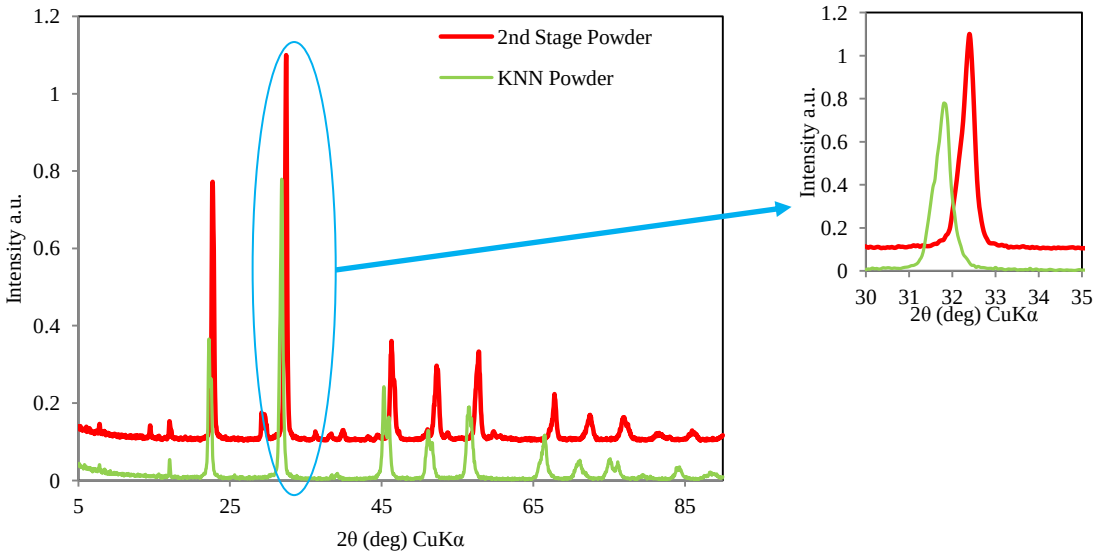

Figure 15 XRD pattern of 2nd stage powder made from a two stage MSS method compared with KNN reference powder where Na_2CO_3 was added in the 2nd stage.

From the XRD plot of the *1st stage* powder (*Figure 14*), the *1st stage* product can be seen to be a mixture containing a sodium rich alkali niobate and other potassium or sodium niobate derivatives. After the *2nd stage* (*Figure 15*) with the addition of Na_2CO_3, $NaNbO_3$ is formed indicating that the Na ions diffused into the *1st stage* product mixture. These results further highlight the observation made that depriving the system of Na ions under these conditions still will not yield KNN. It also appears that if the unidentified phases were potassium niobate phases then these were displaced by the Na ions.

Based on these observations it was decided to use a *1st stage* reaction that was devoid of Na ions. In this two step MSS reaction it was proposed that $KNbO_3$ would be the product of the first step. It was anticipated that K ions would diffuse into the niobium (V) oxide crystal matrix in a first stage of the reaction, due to the absence of Na ions and as a result the elimination of competition between the two ions. A *2nd stage* of the reaction would see the introduction of Na ions which would react with K + Nb mixed phases and form KNN. The XRD patterns of powder from both stages are shown in the *Figure 16*.

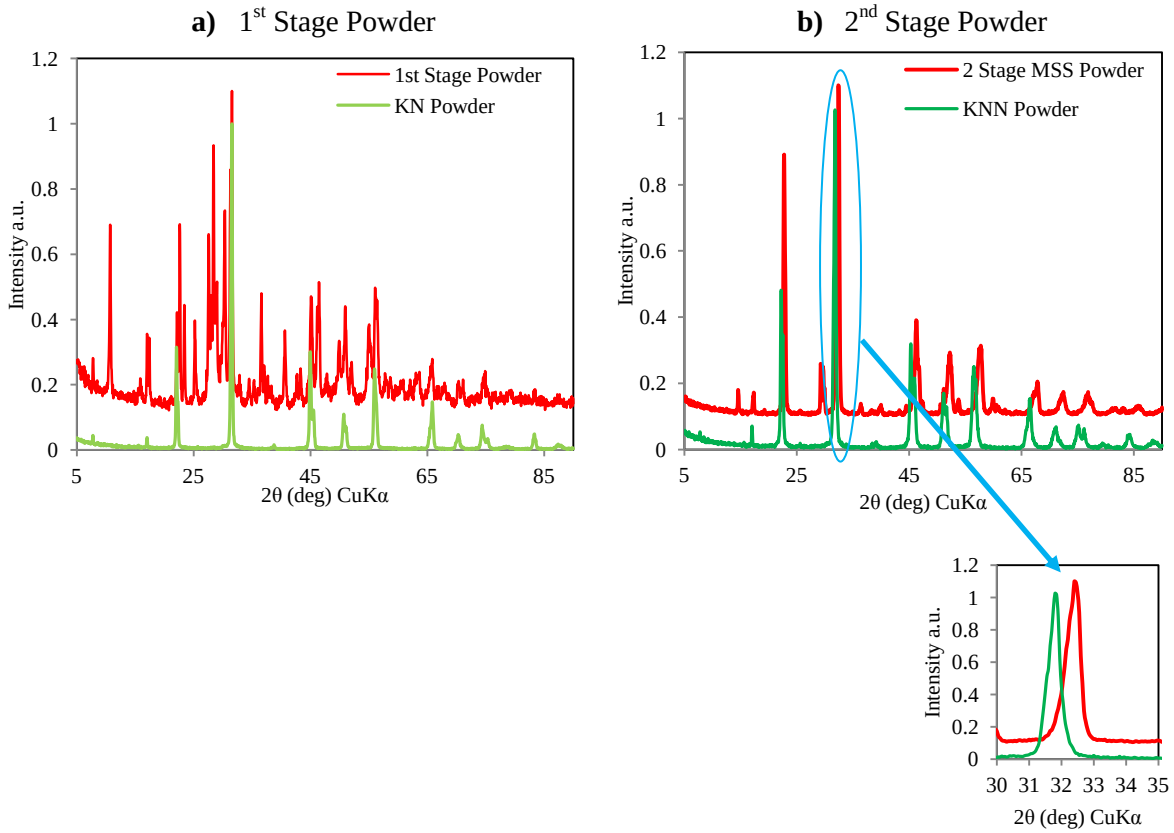

Figure 16 XRD patterns of powder made from a 2 stage MSS method compared with reference powders showing **a)** 1st stage MSS powder with K_2CO_3 + Nb_2O_5 + KCl, compared with reference $KNbO_3$; **b)** 2nd stage MSS powder with NaCl and Na_2CO_3 added, compared with reference $K_{0.5}Na_{0.5}NbO_3$.

The XRD plot (*Figure 16a*) shows the product from the *1st stage* compared with a $KNbO_3$ reference powder. A mixed phase powder appears to have been produced which when compared to that of $KNbO_3$ appears to have some peaks in similar positions, but with multiple unidentified peaks present. When the unwashed *1st stage* powder was mixed and reacted with Na_2CO_3 and NaCl in the *2nd stage*, $NaNbO_3$ was formed as shown in *Figure 16b*. This result appeared to suggest the displacement of K ions from the K rich niobium (V) oxide matrix by Na ions, described in the previous reaction. As shown in the XRD scans in *Figure 15* and *Figure 16b* neither method produced KNN despite the complete removal of sodium ions in the second case, and $NaNbO_3$ was produced in both powder syntheses methods. This

shows that unlike the HS, overloading the system with K reagent will still not yield a KNN powder instead the greater reaction rates of sodium ions prevail.

4.2. Molten hydroxide synthesis

4.2.1. Introduction

Based on the results of the MSS system, where it was found that there is a detrimental interaction between the potassium carbonate and the sodium chloride solvent which resulted in $NaNbO_3$ production rather than KNN, an alternative solvent mix that would eliminate the side reactions was considered.

4.2.2. Hydroxide solvent

To eliminate the effects of the K – Cl interaction an alternative solvent system was investigated; NaOH – KOH system has the advantage of low melting temperature, presence of K and Na ions and the elimination of the K – Cl interaction. KOH (mp 420°C) and NaOH (mp 318°C) have lower melting points with a eutectic melting point of 170°C; compared to KCl (mp 770°C) and NaCl (mp 801°C) with a eutectic melting point of 657°C.

Initially the standard reactants were mixed in stoichiometric ratios, with NaOH and KOH and heat treated for 2 hours at 315°C (though furnace fluctuated between 315°C-350°C), a temperature selected for being just below the NaOH melting point. Also, a higher heat treatment temperature of 500°C was used to attempt to create a single phase powder which would give a clear indication of the alkali niobate that the MHS would produce. The resultant powders were washed, dried and characterised by XRD (*Figure 17*).

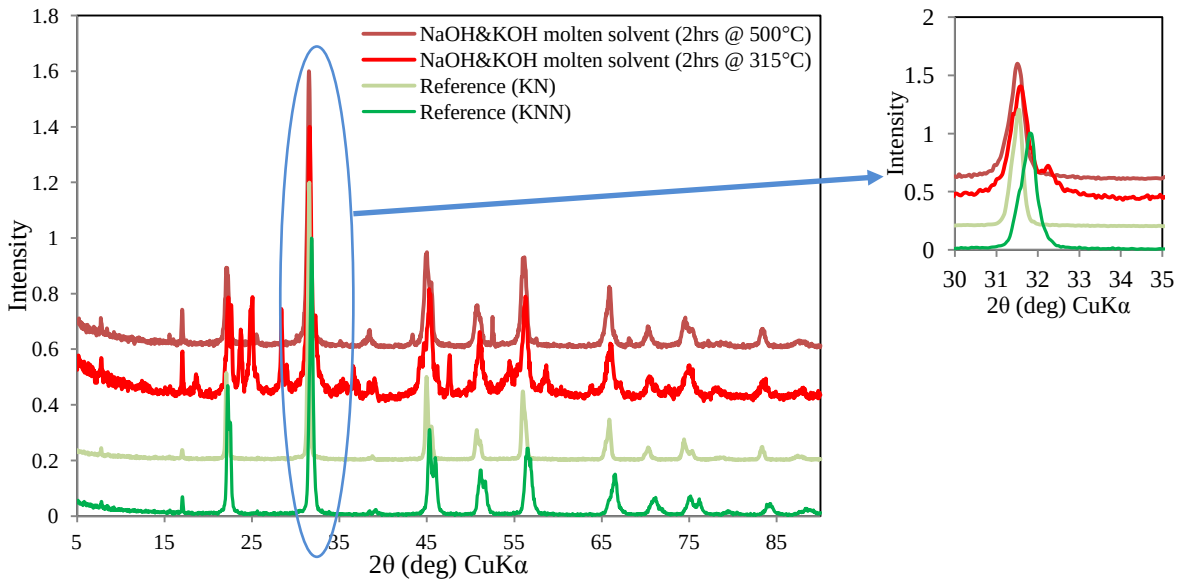

Figure 17 XRD patterns of powder made from a Molten Hydroxide Synthesis method with heat treatment temperatures at 315°-350°C and 500°C compared with KN and KNN reference powders.

The powder from the lower heat treatment temperature (*Figure 17*) showed a mixed phase powder containing numerous phases of possibly reacted and unreacted material with positive signs of the development of a perovskite structure. The position of the perovskite peaks, at slightly lower *2θ* angles with respect to the reference KNN sample, suggests a K rich alkali niobate. From the XRD data (*Figure 17*) it can be seen that at a 500°C heat treatment temperature the powder still contains impurities though a clear potassium rich alkali niobate was formed, a result directly opposite to the effect seen in MSS. The MHS technique resulted in the formation of a K ion-rich niobium oxide lattice. The results suggest that K ions are more reactive compared to Na ions with niobium (v) oxide at lower temperatures in the molten hydroxide solvent system.

Consequently with the result achieved, the removal of the Na ions from the starting materials in order to produce single phase $KNbO_3$, which could be further reacted in a second step with the addition of Na ions to produce KNN, was investigated. The resultant powder was washed, dried and characterised by XRD as shown in *Figure 18*.

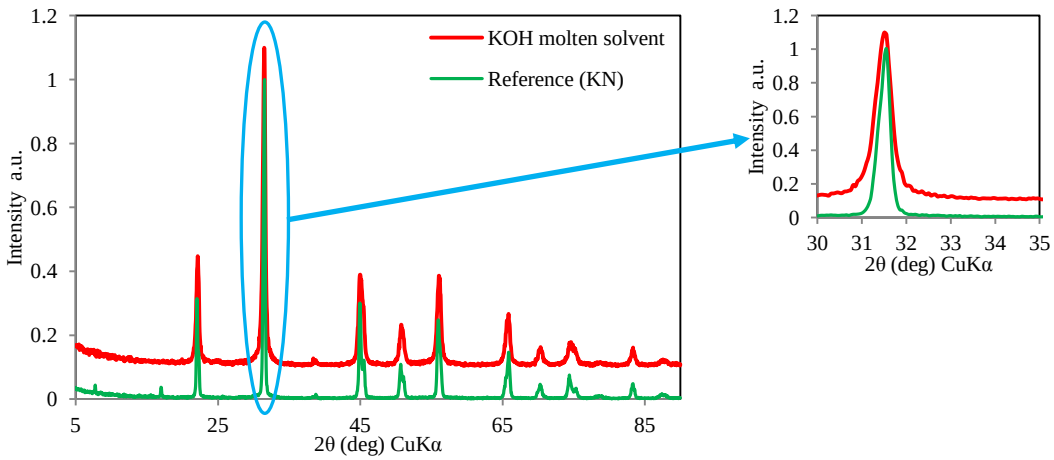

Figure 18 XRD pattern of powder made from a Molten Hydroxide Synthesis method heat treated for 2 hours at 500°C.

The XRD data shown in *Figure 18* showed a relatively pure reaction product of $KNbO_3$ which could not be achieved in an earlier test, as discussed in ***section 4.1.4.***, using the MSS route that had all the Na ions removed. Removal of NaOH did not affect the resultant product, so henceforth KOH was used in isolation to ensure the production of pure $KNbO_3$.

4.2.3. Two stage molten hydroxide synthesis of KNN

In order to produce KNN, the incorporation of Na ions in a second stage was examined. Two procedures were used to form the powders –

1. The 1st stage powder was not washed and so KOH was present going into the 2nd stage.
2. The 1st stage powder was washed and so KOH was absent going into the 2nd stage.

The powders were mixed with NaCl and Na_2CO_3 as shown in *Table 9*. The powders were then heat treated and washed to remove water soluble ions. The resultant XRD data is shown in *Figure 19*.

Table 8 formulation – two stage MHS investigating intermediate washing stage and source of Na ions

	Unwashed First Stage Powder			Washed First Stage Powder		
	Powder 1	Powder 2	Powder 3	Powder 4	Powder 5	Powder 6
Stage 1	K_2CO_3					
	Nb_2O_5					
	KOH					
	Powder Heat Treated - 2hrs @ 500°C					
	Not washed. KOH & water soluble ions present.			KOH & water soluble ions washed out		
Stage 2	Na_2CO_3		Na_2CO_3	Na_2CO_3		Na_2CO_3
	NaCl	NaCl		NaCl	NaCl	
	Powder Heat Treated – 2hrs @ 700°C					

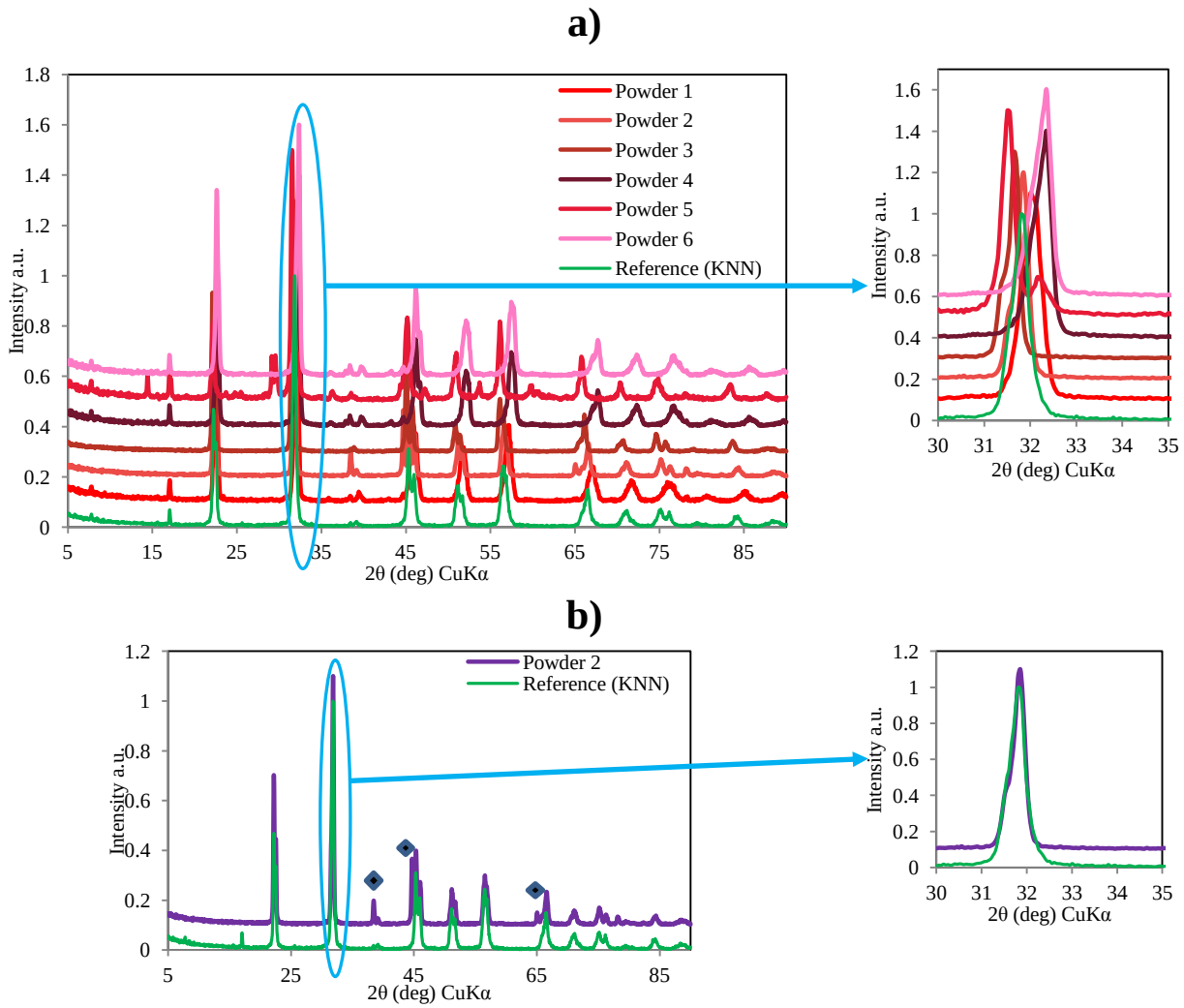

Figure 19 XRD patterns of powders made from a two stage method compared to a KNN reference powder. **a)** All the powders from ***Table 9*** made in 2 stages; **b)** XRD pattern of *powder 2* which had NaCl added in the 2nd stage. ◆ - Represents the XRD powder sample holder trough.

In *Powder 2*, which had KOH present in the second stage and NaCl as a source of Na ions, KNN was formed and the XRD data in *Figure 19b* shows that the main peaks match those of the reference KNN. The additional peaks associated with *powder 2* can be attributed to the metallic sample holder.

The XRD pattern for *powder 3* where the source of Na ions was Na_2CO_3 and KOH was present, gave an indication that increasing the amount of Na_2CO_3 may lead to the formation

of KNN. There was a slight increase in the *2θ* angles observed on the XRD data indicating incorporation of Na into the lattice.

In the case of *powder 5* (KOH absent; NaCl source of Na ions), no favourable reaction appeared to occur, with the KN peaks remaining at the same *2θ* angles. This suggests that in the absence of KOH the Na ions from the NaCl are unable to diffuse into the K-rich niobium oxide matrix to displace some of the K ion, as was seen in *powder 2*. *Powder 1* (KOH present; NaCl & Na_2CO_3 source of Na ions), *powder 4* (KOH absent; NaCl & Na_2CO_3 source of Na ions) and *powder 6* (KOH absent; Na_2CO_3 source of Na ions), all reacted with the KN to form Na-rich niobate powders. *Powder 1* formed the least Na-rich powder of the three NN producing powders and did so in the presence of KOH, thus suggesting the influence of the KOH in favouring a K ion-rich system. *Powder 1*'s XRD plot exhibits peaks at slightly higher *2θ* angles with respect to the KNN peaks and slightly smaller *2θ* angles with respect to NN peaks, suggesting a powder formed midway between the two that would be sodium rich.

Powder 4 (KOH absent; NaCl & Na_2CO_3 source of Na ions) and *powder 6* (KOH absent; Na_2CO_3 source of Na ions), formed Na-rich powders that had *2θ* angles closest to NN XRD peaks; although with *2θ* angles slightly smaller compared to the NN. This suggested that the Na ions were able to diffuse into the K ion-rich niobium oxide matrix and displace most of the K ions from the crystal lattice. The reaction in *powders 1* (KOH present; NaCl & Na_2CO_3 source of Na ions), *4* and *6* is also interesting for the fact that they all formed the same Na ion-rich powder. *Powders 4* and *6* reacted in the absence of KOH, suggesting a solid state MOS reaction route. The lack of a reaction in *powder 5* which did not have any KOH and also no Na_2CO_3 served to highlight this point.

KNN was successfully produced using the 2 step MHS method as shown by *powder 2* reacting K_2CO_3, Nb_2O_5 and KOH in the first stage and introducing NaCl in the 2nd stage.

4.2.4. Further investigation MHS with NaCl as source of Na ions

Following the successful synthesis of KNN it was observed that the stoichiometric amount of K ions available from the K_2CO_3 was not sufficient to react with the entire amount of niobium oxide in the 1st stage in order to form pure $KNbO_3$, as seen in *Figure 19b*, as the molar ratio between the two reactants was 2:1. Therefore the hypothesis for the reaction is that K ions supplied by the KOH react to form K ion-rich alkali niobates. The Na ions are able to substitute the K ions present within the niobate supplied by the KOH to form KNN in the second stage. Examination of reaction products at each stage of the successful KNN MHS synthesis reaction led to the following reaction process being proposed –

Stage 1 - K_2CO_3 + Nb_2O_5 in KOH solvent

The initial reaction is thought to lead to the formation of multiple potassium niobate compounds such as $KNbO_3$, KNb_3O_8 (Wang, et al., 2007), $K_4Nb_{16}O_{17}.3H_2O$ (Wang, et al., 2007) (Santos, et al., 2002) and water soluble potassium hexaniobates of the general formula $K_{8-x}H_x[Nb_6O_{19}].nH_2O$, x = 0-3 (Wang, et al., 2007) (Santos, et al., 2002) whose formation depends on the temperature and concentration of KOH used (Santos, et al., 2002), though in the MHS pure KOH was used. *Figure 20* shows the XRD pattern for both the unwashed and washed powders after the 1st stage synthesis. Comparison between the two shows the presence of phases in the unwashed sample that are absent in the sample that was washed. Evaluation of XRD data between the unwashed sample and the starting reagents indicated the extra phases could not be attributed to the starting reagents. The unwashed KN powder XRD trace showed similarities in part to the niobates mentioned above; indicating the possible

presence of soluble species, though due to the complexity of the unwashed samples XRD data and those of the materials quoted in literature, led to an inability to isolate a structure. The reaction of K_2CO_3 and Nb_2O_5 is known to progress through various stages (i.e. $K_6Nb_{10.88}O_{30}$ to $K_4Nb_6O_{17}$) before $KNbO_3$ (Malic, et al., 2008) is produced, which may account for the extra phases observed in the unwashed sample.

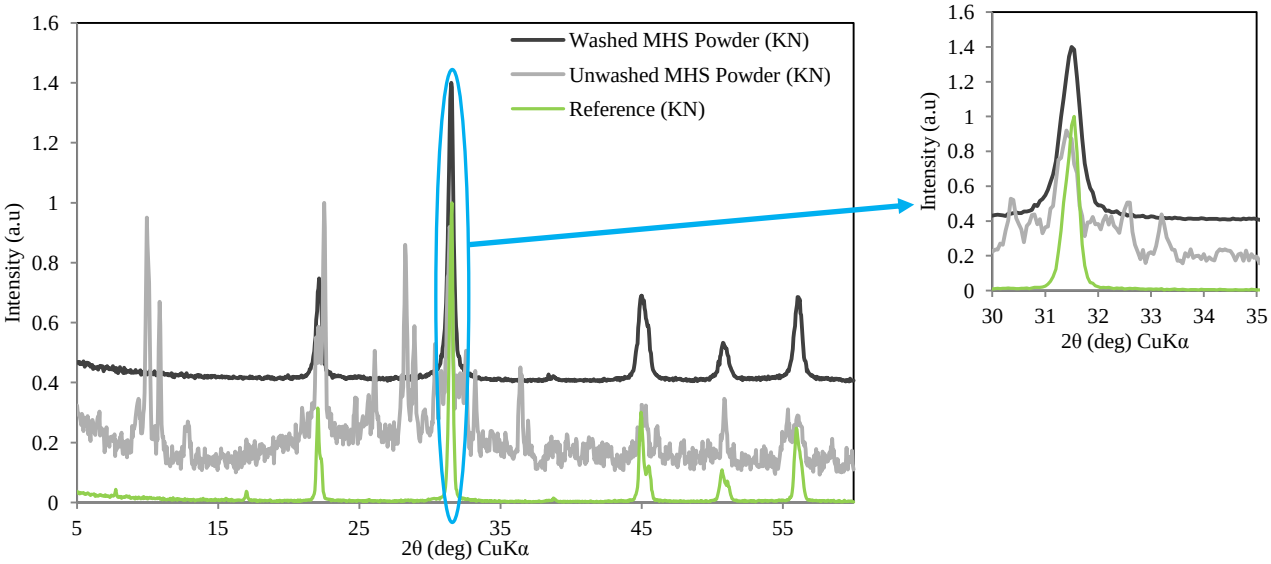

Figure 20 XRD pattern of the powder with the single KOH molten solvent that formed $KNbO_3$, compared with a reference $KNbO_3$ sample.

Stage 2 – $K_xNb_yO_z$ products + Na source

On the introduction of Na ions in the second stage, the Na ions are thought to diffuse into the various potassium niobate derivatives to form KNN. *Figure 21* shows the product of the second stage reaction.

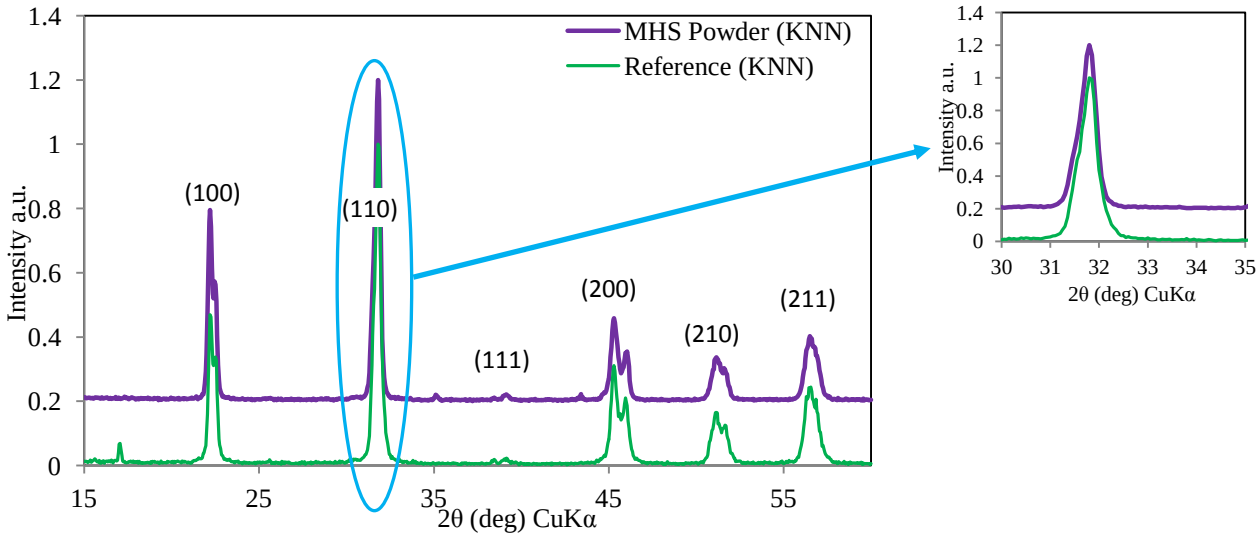

Figure 21 XRD patterns of MHS KNN powder compared with KNN reference powder.

The XRD pattern shown in *Figure 21* confirms the successful production of KNN. The ESEM-EDX analysis results (i.e. actual atomic ratio – Nb = 53.9%, Na = 22.6% & K = 23.5%) show the ratios of each element to fit the stoichiometric ratio of the formula $K_{0.5}Na_{0.5}NbO_3$. To differentiate it from the standard MSS this process was named the Molten Hydroxide Synthesis method (MHS). *Figure 22* is a schematic illustration of the process involved in the MHS.

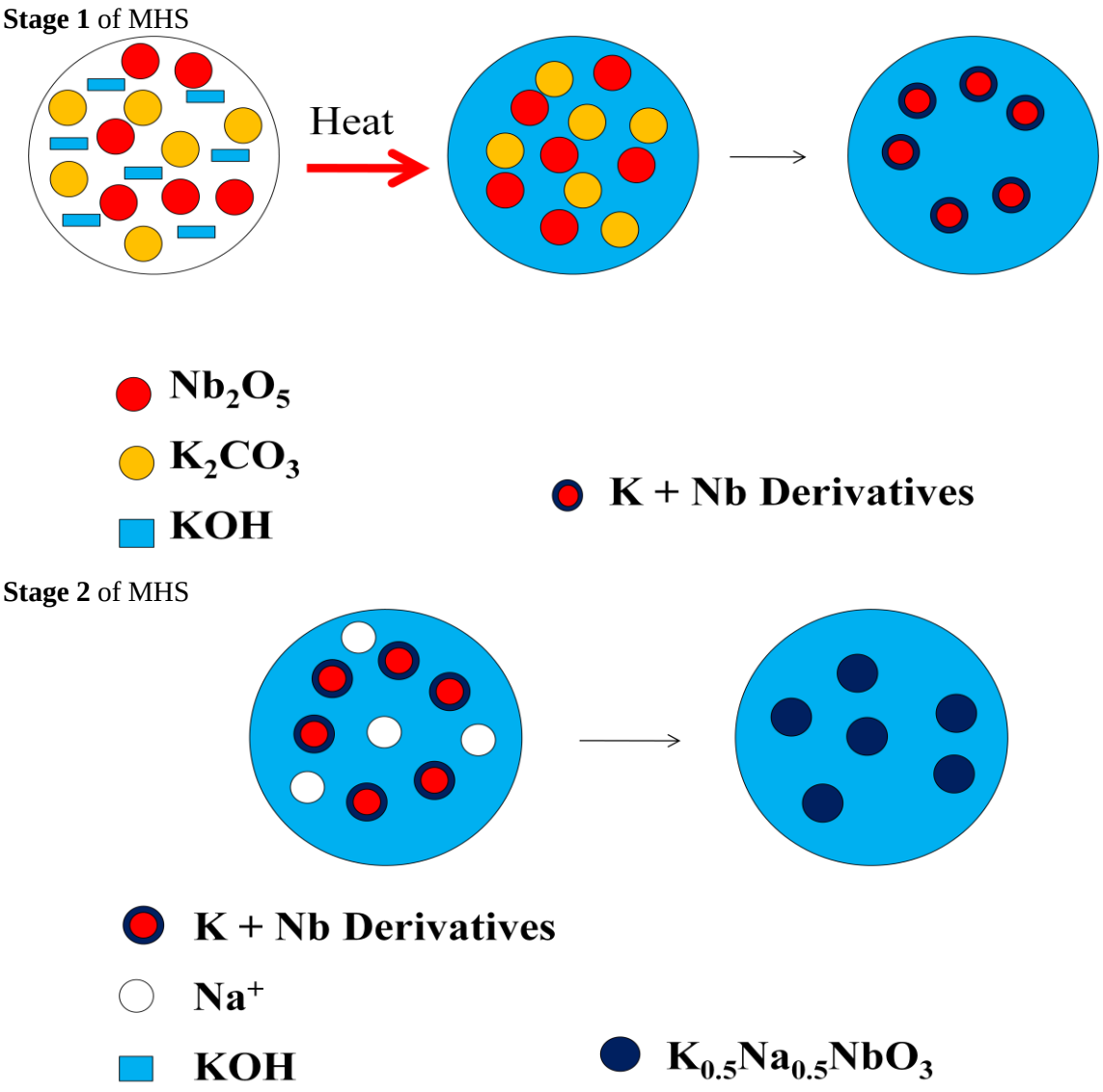

Figure 22 schematic illustrations of Molten Hydroxide Synthesis (MHS) (Dorey, 2010)

4.2.5. Effect of NaCl & Na_2CO_3 loading

While KNN was successfully produced using the MHS method it was found that a molar excess of Na ions with respect to niobium oxide was required for the reaction to proceed to the desired conclusion. The first stage product of the MHS method reacted effectively with 0.038moles of NaCl combining in the second stage to form KNN. From the amount of Nb_2O_5

(0.012mol) present it is understood that only 0.006moles each of K ions and Na ions were required to form KNN. Consequently powder was produced to observe whether the number of moles of Na ions added in the second stage could be reduced from 0.038moles to 0.03moles and 0.02moles of NaCl and still produce KNN.

Based on the result in ***section 4.2.3*** where *powder 3* [KOH present throughout with Na_2CO_3 (0.006moles) acting as source of Na ions] appeared to indicate it would form KNN if the amount of Na_2CO_3 was increased; powder was made through the MHS route in a two stage synthesis with the formation KNN anticipated in the 2nd stage by reacting potassium niobate derivatives with Na_2CO_3 in the presence of KOH. Increasing the number moles of Na_2CO_3 to 0.038moles, with the intention of matching the positive result from the use of 0.038mol of NaCl, powder was produced. *Figure 23* shows the XRD patterns of these powders.

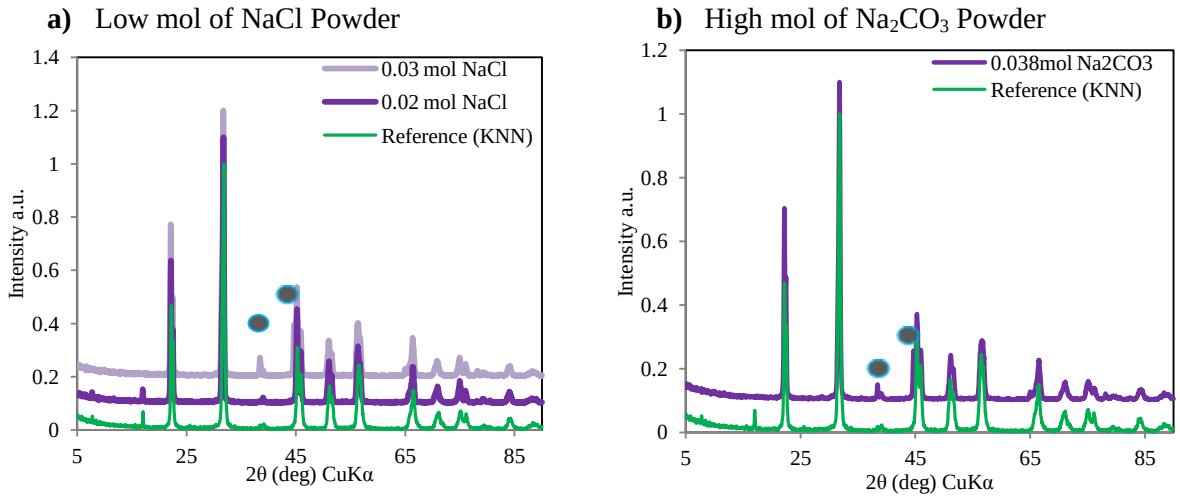

Figure 23 XRD patterns of powder made from a 2 stage method compared to KNN reference powder; **a)** are the XRD patterns of the two low mol NaCl powders; **b)** is the XRD pattern of the high mol Na_2CO_3 powder. ⬬ – XRD peaks of metallic sample holder**.**

KNN was formed from the reaction of the first stage MHS product with a lower number of moles of NaCl as shown from the XRD plot in *Figure 23a*. It is also instructive to see the small peaks at 7.5° and 17° *2θ* which are related to unreacted niobium (V) oxide, are present

on both the reference KNN powder XRD trace and the 0.02 mole KNN powder XRD trace, suggesting that 0.03 mole of NaCl is able to ensure the production of a pure product.

KNN was formed from the reaction of the potassium niobate derivatives with a higher number of moles of Na_2CO_3 as can be seen from the XRD plot in *Figure 23b*. A disadvantage of carbonates is that they are hygroscopic and as a result with the ability to use NaCl in place of sodium carbonate is a distinct advantage when it comes to the practicalities of achieving stoichiometric measures. The success in making KNN with Na_2CO_3 and NaCl also indicated the possibility that different sources of Na ions could be used to achieve the same end product, though dependant on simplicity of purification.

Tests of the 2nd stage of the MHS showed that stoichiometric amounts of Na ions were not sufficient for the reaction to progress. While a lower limit to the excess of Na ions required was not established, a level of 1.5 – 2.9 molar excess of Na ions with respect to Nb_2O_5 was found to be essential to produce $K_{0.5}Na_{0.5}NbO_3$.

4.3. Single salt molten salt synthesis

KCl was used as a single molten solvent in a one step MSS method with the desire to create a simple powder synthesis method producing KNN. Equimolar amounts of the standard precursors i.e. Nb_2O_5, K_2CO_3 and Na_2CO_3 were reacted in an excess of KCl salt with a heat treatment temperature of 800°C for 2 hours. The XRD plot in *Figure 24* shows the product of this reaction compared with that of a reference KNN.

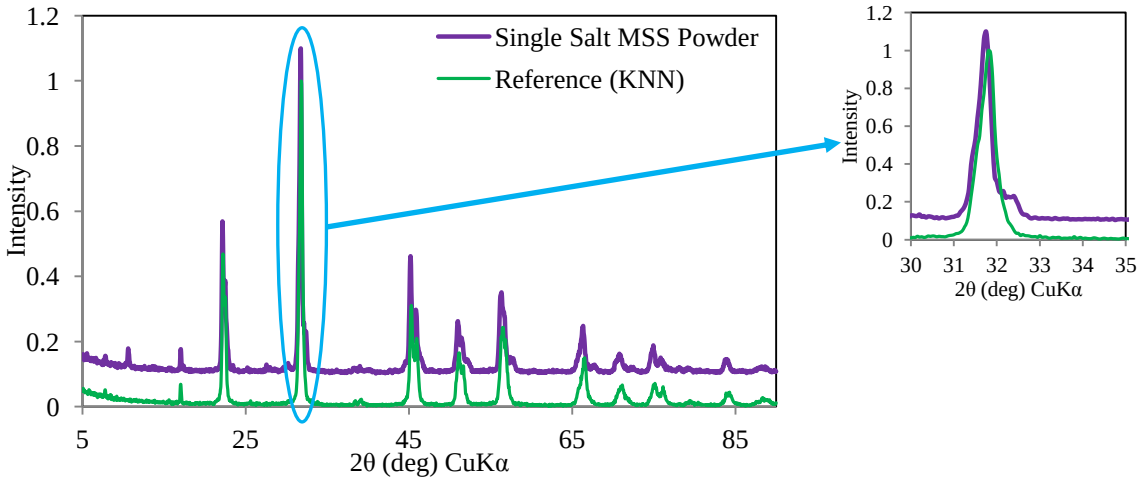

Figure 24 XRD patterns of single salt MSS KNN powder compared with KNN reference powder.

$K_{0.5}Na_{0.5}NbO_3$ was successfully produced using the KCl single salt MSS (ssMSS) route allowing for multiple methods of KNN powder synthesis. This result showed that in a higher heat treatment temperature and a K-rich environment with NaCl absent the negative effects observed in the MSS earlier may be countered, allowing for the production of a KNN powder with the desired stoichiometric balance.

4.4. Comparison of powder synthesis methods

The KNN powders produced from the MOS, MHS and the ssMSS were compared by XRD and optically to observe any differences. A comparison of the ESEM micrographs of the three powders synthesised using MOS, MHS and ssMSS is shown in *Figure 25*.

a)

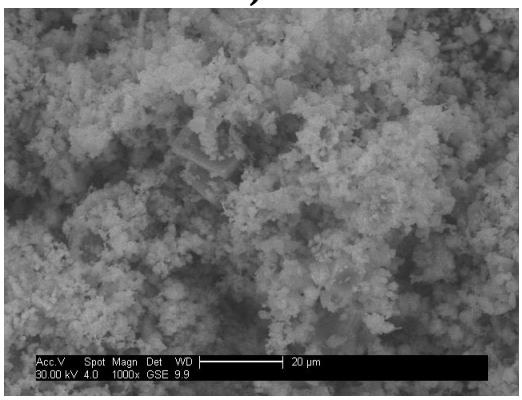

KNN Powder from single salt MSS – 2hrs @ 700°C

b)

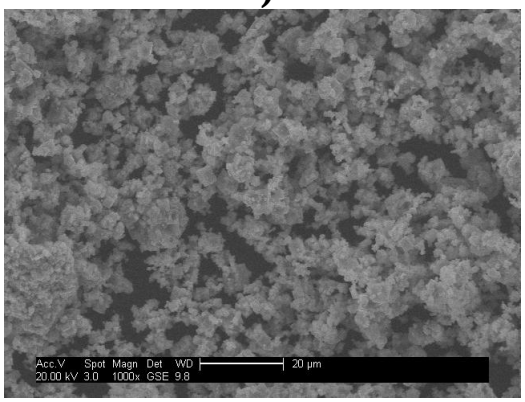

KNN from MHS – 2hrs @ 800°C

c)

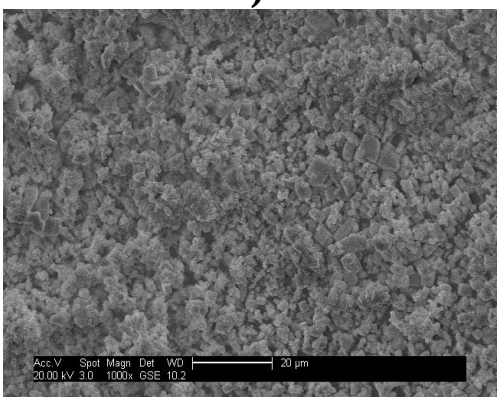

KNN from Mixed Oxide Synthesis – 4hrs @ 950°C

Figure 25 ESEM micrographs of KNN powders produced using **a)** single salt MSS, **b)** MHS & **c)** MOS

A small particle size improves micro-structure and hence dielectric properties of resultant films (Yoon, et al., 1998) and thus would be beneficial to the resultant thick films produced. The MOS powder (*Figure 25c*) had larger particle sizes, which concur with the information in *Table 2* which suggests higher temperatures and longer dwell times result in larger particles. This is because smaller particles coalesce at faster rates and with a longer dwell time present in the MOS, the particles have more time to grow. The other methods using lower temperatures and shorter dwell times show smaller particles compared to the MOS method. The advantage of MHS method over the single salt MSS in *Figure 25* was that even a 100°C difference in heat treatment temperature resulted in a difference in particle size as some large particles are visible in the ESEM images of the single salt MSS processed powder

that are not present in the MHS method. The results show that the MHS powder synthesis method is the method best tailored to achieve small particles for use in thick film micro-systems devices.

A comparison of the XRD patterns of the 3 processes can be seen in *Figure 26*.

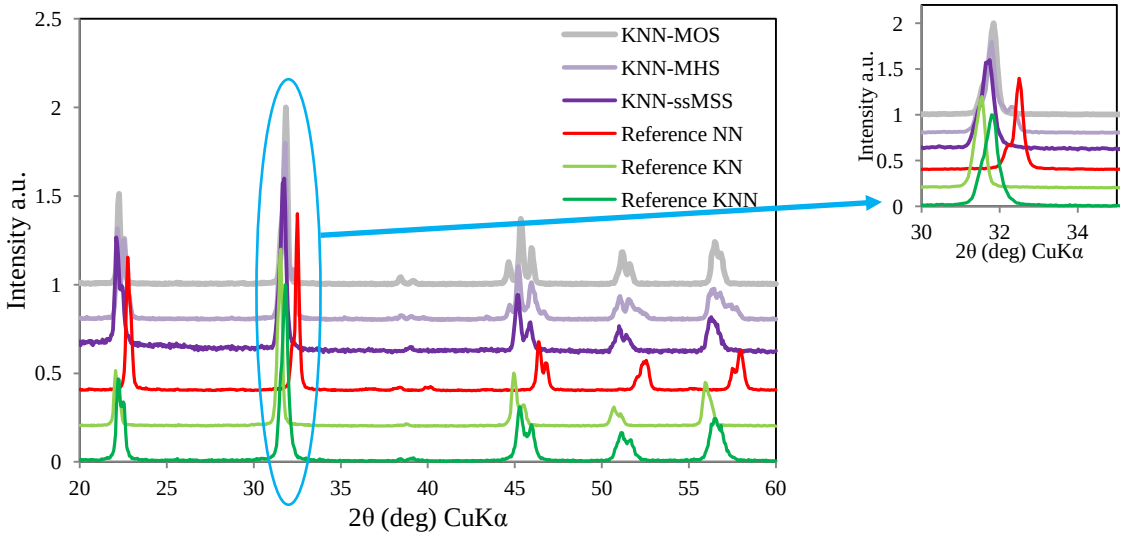

Figure 26 XRD trace comparison of KNN made from MOS, MHS and ssMSS with reference $K_{0.5}Na_{0.5}NbO_3$, $KNbO_3$ and $NaNbO_3$.

The XRD patterns (*Figure 26*) of the KNN powders made using the three powder synthesis methods show similarities to the pattern of the KNN reference powder. The MHS method appears to be the closest match in terms of *2θ* data. The lattice-spacings were calculated and compared with those of reference KNN, MSS prepared $NaNbO_3$ and MHS prepared $KNbO_3$, as shown in *Figure 27*.

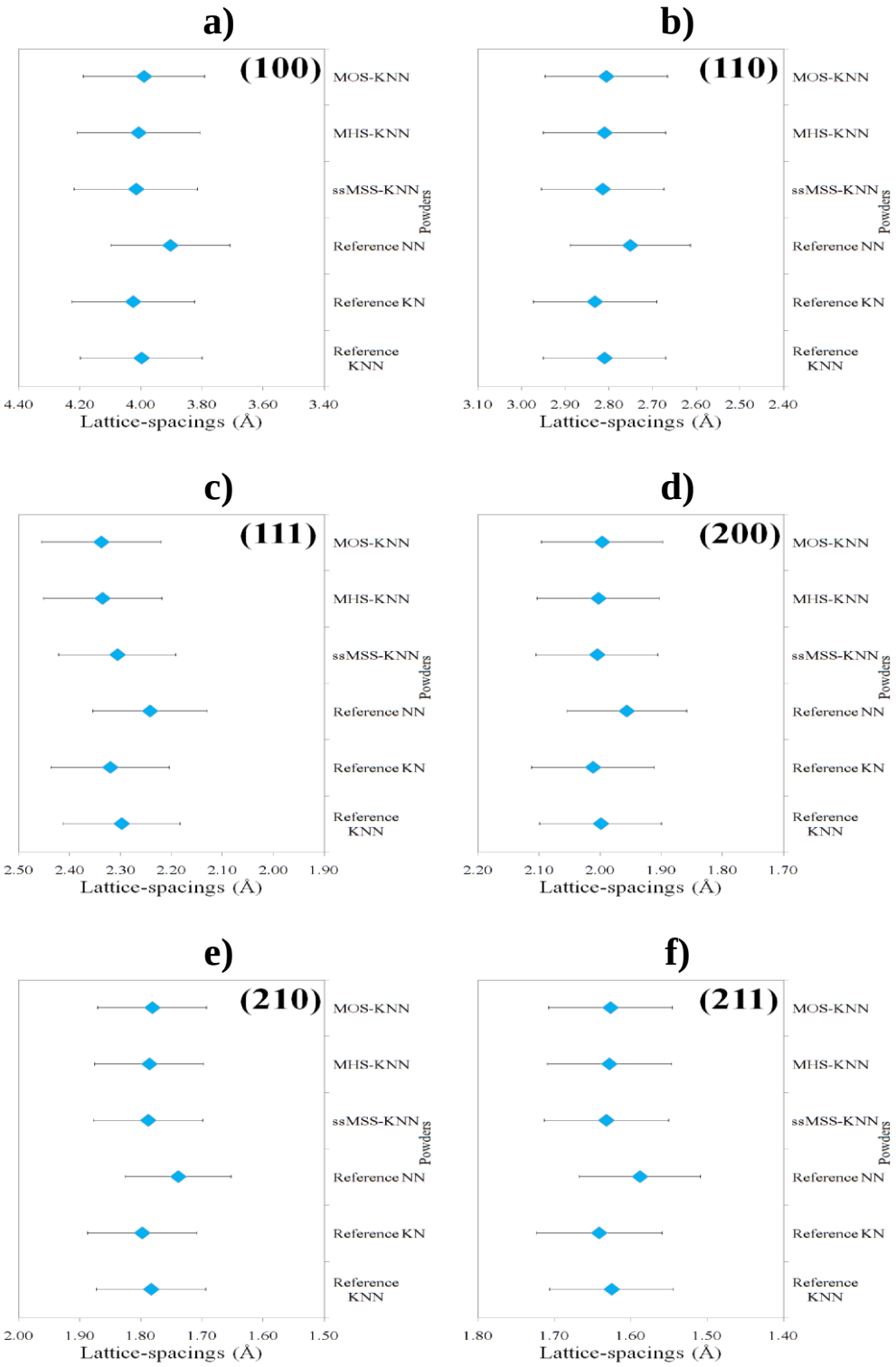

Figure 27 a comparison of 6 selected perovskite planes' lattice-spacings of KNN powders prepared by MOS, MHS and ssMSS with reference KNN, KN and NN. ±5 atomic % error determined by Siemens-D5005 X-ray machine.

The lattice-spacing data (*Figure 27*) shows that the various methods used to make KNN powder resulted in powders with lattice-spacings with slight variation from the reference KNN with the MHS powder showing the closest lattice-spacing to the reference among most of the Miller indices planes selected allowing for the 5% error.

ESEM-EDX analysis on the levels of each constituent in the powders highlighted the differences observed in the lattice-spacing data (*Table 8*).

Table 8 elemental analysis of different KNN powder processing routes

ESEM-EDX analysis (Atomic %; ±0.1% error)			
	Na	K	Nb
Theoretical	**25.00**	**25.00**	**50.00**
MHS	22.63	23.45	53.92
ssMSS	20.46	26.22	53.32
MOS	21.17	24.55	54.28

The results show an imbalanced stoichiometry in the powders with a larger level of sodium loss when compared to the level of potassium loss. The MHS method appears to have the closest match to the theoretical stoichiometry. The volatility of the alkalis especially the sodium appears to be responsible for the imbalance.

4.4.1. Yield comparison

When powders were synthesised to achieve a mass of between 5-20g it was observed that the MHS produced average yields of 50% which was much lower than the yields achieved with single salt MSS and MOS. *Table 9* shows a comparison of yield between MHS, single salt MSS (discussed in ***section 4.3***) and the mixed oxide process.

Table 9 analysis of powder yields made using different synthesis methods.

Powder Synthesis Process	Process	Yield
MHS	1st Stage – 2hrs @ 500°C 2nd Stage – 2hrs @ 700°C	50%
Single salt MSS	2hrs @ 800°C	80%
Mixed Oxide Synthesis	4hrs @ 950°C	88%

The high yield from the MOS is expected to be due to the higher and longer temperature and dwell time used, providing for a more complete reaction. As stated before the reaction of K_2CO_3 and Nb_2O_5 is known to progress through various intermediate stages before $KNbO_3$ (Malic, et al., 2008) is produced. Similarly Na_2CO_3 when reacting with Nb_2O_5 to produce an alkali niobate passes through various intermediate products prior to the formation of desired product. As a result combined with the lack of a ball milling stage in the MHS (avoided due to the solubility of the KOH in the alcohol solvents used) poor reagent mixing may result in reactions that do not proceed to the desired conclusion. Some of the intermediate products are known to be water soluble and as a consequence are washed away leading to a lower yield of 50% with the MHS. Both the MOS and ssMSS were also prepared occasionally with the ball milling stage replaced with a pestle and mortar mixing stage, but still resulted in yields stated in *Table 9*. This suggested that the hydroxides used in the MHS had an effect on the resultant yield. Further work on the MHS method where powder was made on a larger scale i.e. 25-100g, resulted in a good yield of 80% similar to the yield in the single salt MSS system suggesting that with lower amounts of reactants the MHS method is not as productive as the other two methods used.

4.5. Doped KNN powders

4.5.1. Introduction

Three methods were used to produce doped KNN powders, these were the MOS, MSS and MHS described above. Dopants were added at 0.5% - 6% molar mass of the powder relative to the $K_{0.5}Na_{0.5}NbO_3$ formula, either substituting at the A-site or both the A- and B-sites depending on the dopant. The dopants were added at the initial stage when weighing out the KNN reactants in all the different powder synthesis methods used. In the case of the MHS synthesis method the dopants were added during the first stage. Other processing remained the same as before.

4.5.2. Doping with Li and Mn

Initial doping of KNN powder was carried out with Li as this was the most common dopant used for KNN powder in literature and Li_2CO_3 was a cost effective and readily available reagent. Lithium is known to enhance the piezoelectric and electro-mechanical properties of KNN at the MPB between the orthorhombic and tetragonal phases (Guo, et al., 2004). With a temperature dependent MPB, doping KNN ensures that as temperature is increased, the material remains close to the MPB. Lithium also decreases the orthorhombic – tetragonal (T_{O-T}) transition temperature found in KNN at 200°C to room temperature (Rodel, et al., 2009) and increases the KNN T_c in the higher temperature cubic to tetragonal phase transition (Guo, et al., 2004). Using both the MHS and the ssMSS powder processing methods, $Li_{0.06}Na_{0.47}K_{0.47}NbO_3$ was produced as shown by the XRD trace in *Figure 28* which shows the successful production of the perovskite structure.

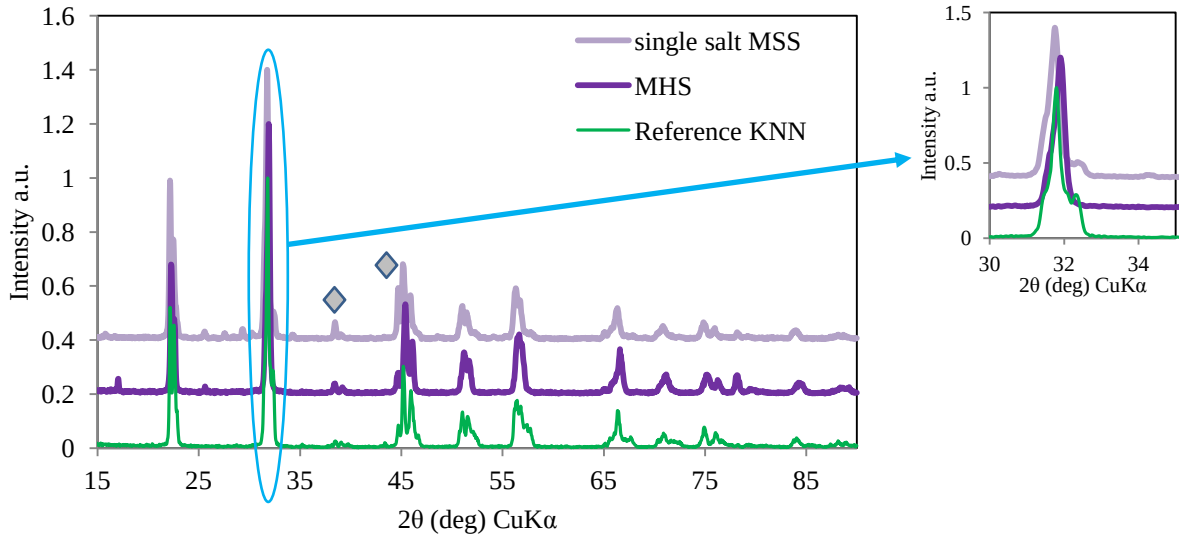

Figure 28 XRD powder trace of 6% Lithium doped KNN powder synthesized using MHS and single salt MSS. ◇ – Symbol indicates peaks attributed to the sample holder.

Aliovalent manganese was also selected as a dopant as it is known to increase the piezoelectric properties (Lin, et al., 2010), dielectric constant, reduce dielectric loss (Wang, et al., 2010) in KNN. Using the MHS method Mn doped KNN was successfully produced as shown in the XRD plot in *Figure 29*, creating a powder with a characteristic off-white colour.

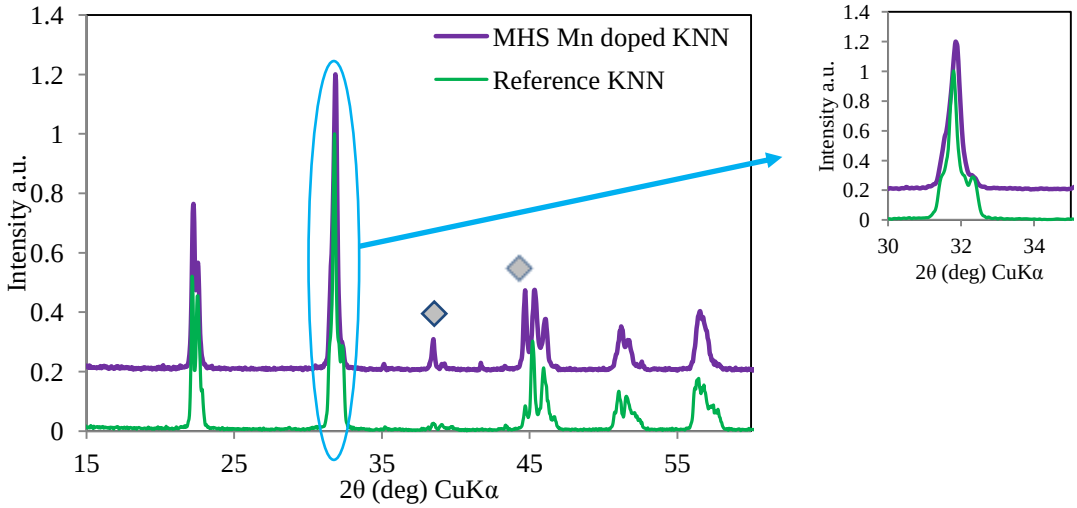

Figure 29 XRD powder trace of MHS produced 0.5% Mn doped KNN powder compared with reference KNN powder. ◇ – Symbol indicates peaks attributed to the sample holder.

With the positive ability for manganese to exist within the KNN powder in multiple oxidation states the resultant benefit to the KNN thick films envisaged was an improvement in the doped KNN thick film piezoelectric properties (Wang, et al., 2010).

4.5.3. Transition metal dopants

Following the successful incorporation of Li and Mn into KNN powders, more dopants were selected to observe the effect that they would have on the KNN thick films. KNN thick films being relatively novel, most recorded use of dopants with KNN powders in literature, refers to their use to produce sintered bulk ceramics rather than low temperature produced thick films and as a consequence the stated effects in literature may not be observed, due to the widely dissimilar processing routes. Donor dopants were utilised to dope the KNN powders in order to produce doped KNN thick film ceramics characterised by large piezoelectric constants, high permittivity; though with the intention of avoiding the accompanied high dielectric losses, low mechanical quality factors and poor linearity, that come with the use of donor dopants (Bortolani, 2010). As many aliovalent elements have been used as dopants to modify the dielectric properties of piezoelectric ceramics (Meng, et al., 2006), several transition metals were also selected for this task in order to utilise the advantages of the multiple oxidation states. *Table 10* shows the ionic radii and oxidation states of K, Na and Nb as well as the transition metal dopants used. The ionic radius determines whether a particular dopant would successfully fit into the material's crystal lattice structure while the oxidation state it adopts within the structure has fundamental effects on the electrical properties of the material (Eichel, et al., 2009). Strontium while not a transition metal was used in conjunction with a transition metal dopant hence its inclusion here.

Table 10 ionic radii (nm) (Atomistic Simulation Group, 2012) (Shannon, 1976)

Ionic Charge	1+	2+	3+	4+	5+	6+	7+
Na	**0.102**						
K	**0.138**						
Nb			**0.072**	**0.079**	**0.064**		
Mn		0.083	0.065	0.053	0.033	0.0255	0.025
W				0.066	0.062	0.06	
Ti		0.086	0.067	0.0605			
Ta			0.072	0.068	0.064		
Zr				0.072			
Sr		0.118					

The ionic radii data (*Table 10*) shows that the transition metal dopants would fit comfortably in the Nb sites at most oxidation states, while the strontium would fit in the A-site, when used as a co-dopant. The doped powders were prepared using the three main powder synthesis methods in this research, then examined by XRD and their lattice-spacings calculated and compared with each other as well as to reference KNN, KN, NN powders and un-doped KNN powders from specific powder synthesis methods, as shown in *Figure 30*. The lattice-spacings were represented graphically using the (110) perovskite plane with the highest intensity.

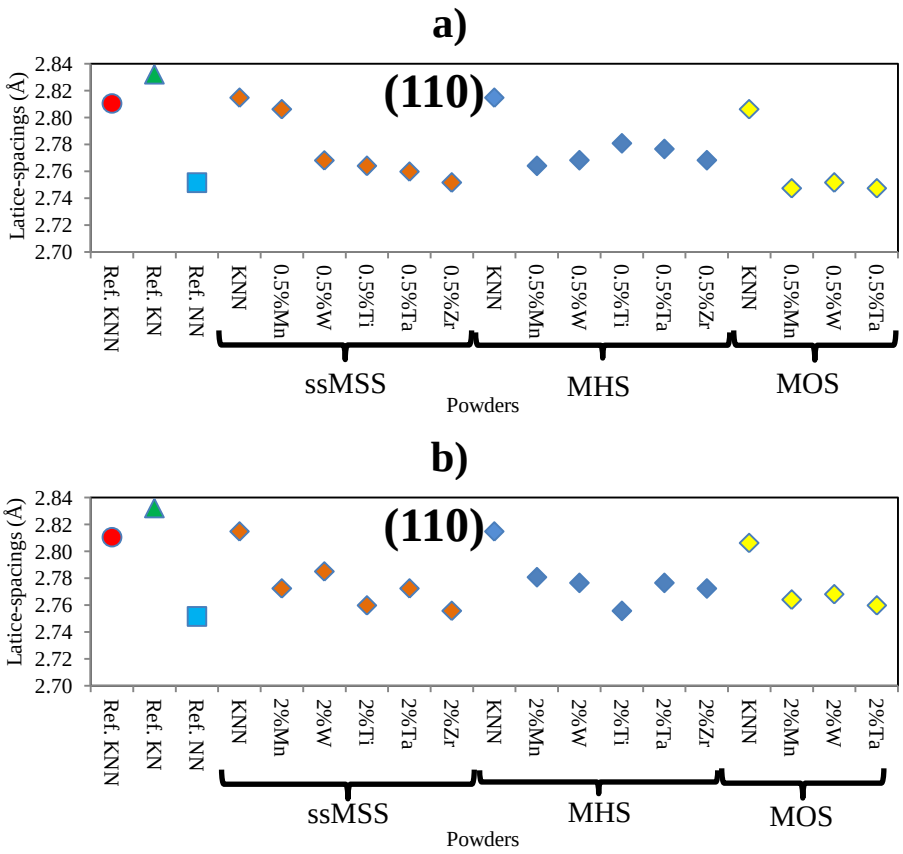

Figure 30 the (110) perovskite plane showing lattice-spacings of KNN powders doped with **a)** 0.5at. % and **b)** 2at. % transition metals, prepared by ssMSS, MHS and MOS compared to reference powders.

● – Reference KNN, ▲ – reference KN, ■ – reference NN. ±5 atomic % error determined by Siemens-D5005 X-ray machine.

The un-doped KNN powders produced by MOS, MHS and ssMSS have lattice-spacings that most closely match the KNN reference. As the actual oxidation state of the dopants within the KNN powder was unknown, it was not possible to determine a trend in the size of the lattice-spacings that corresponded to the size of the ionic radii data. Further complexity was added by the ability of the transition metal dopants with several oxidation states, to adopt at least two of these states in order to occupy both A- and B-sites (Wang, et al., 2010).

A general observation from the lattice-spacing results of the doped KNN powders was that the addition of dopants resulted in smaller distances between the planes in the crystal lattice, indicating lower lattice volumes. Two hypotheses were made, the first that the dopants with

smaller or near similar ionic radii cause the plane spacing to reduce, resulting in a KNN powder that has stoichiometric balance or the dopants may cause an imbalance in the stoichiometry of the KNN (i.e. K substituted in preference to Na), in favour of Na ions and as a consequence, leading to the smaller lattice-spacing, taking into account the 5 atomic percentage error. The KNN powder doped with 0.5 at. % Mn produced by ssMSS method (*Figure 30*) shows close similarity to the KNN reference with lattice-spacing slightly smaller than the KNN reference, when compared to the other doped powders.

Figure 31 shows a comparison of the lattice spacings of KNN powders doped with a combination of either zirconium and titanium or strontium and titanium at selected levels, which were produced by the ssMSS powder synthesis method and compared with reference powders - KNN, KN, NN and an in-house un-doped KNN. The co-dopant use has been used successfully to produce highly active ceramic powders.

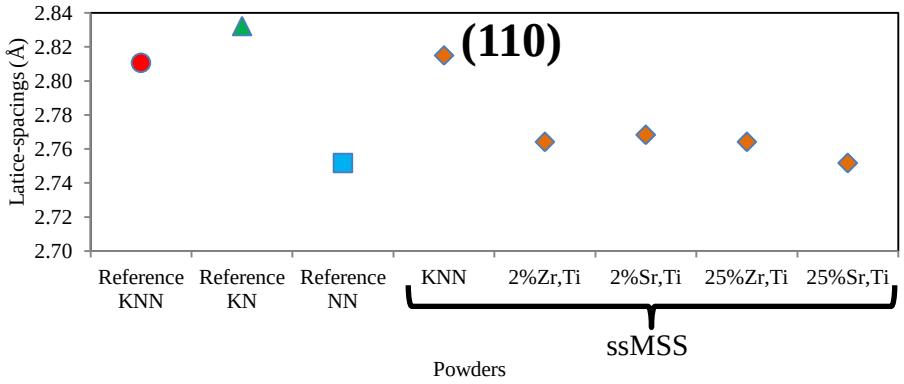

Figure 31 the (110) perovskite plane showing lattice-spacings of co-doped KNN powders compared to a reference KNN.

● – Reference KNN, ▲ – reference KN, ■ – reference NN. ±5 at. % error determined by Siemens-D5005 X-ray machine.

The combined dopants (*Figure 31*) showed a similar effect to the mono-doped powders where the lattice-spacing results showed a reduction in distance between the planes in the crystal lattice when compared to the reference KNN. It was envisaged that the introduction of the transition metal dopants would alter the concentration of oxygen vacancies [responsible

for increased dielectric loss in piezoelectric ceramics (Wang, et al., 2010)] and additionally, they would influence the microstructure and lattice energy of the eventual KNN thick film, since ionic sizes and charges of dopants differ from those of the KNN constituents (Zhang & Whatmore, 2001). The ability to fill A-sites allows transition metal dopants to fill any holes left by alkali loss during heat treatment (***Equation 4-5***) and with the ability of some to further oxidise (due to their aliovalent nature) they are able to absorb the cation vacancies resulting in a reduction of the oxygen vacancies (***Equation 4-6***), thus reducing incidences of dielectric loss in the resultant material and generally improving the piezoelectric properties (Wang, et al., 2010).

$$V_O^{\bullet\bullet} + \frac{1}{2O_2} \longrightarrow O_O^* + 2h^{\bullet} \qquad \textit{Equation 4-5} \text{ (Wang, et al., 2010)}$$

Where $V_O^{\bullet\bullet}$ represents oxygen vacancies, O_O^* represents O^{2-} at the oxide ion site and $h^{\bullet}$ indicates the free carrier holes produced from alkali loss.

$$Mn^{2+} + h^{\bullet} \longrightarrow Mn^{3+}$$

$$Mn^{3+} + h^{\bullet} \longrightarrow Mn^{4+}$$

Equation 4-6 (Wang, et al., 2010)

The oxygen vacancies and the free carrier holes are able to coexist within the KNN films and the formation of the holes can decrease the amount of oxygen vacancies, but results in the increase in dielectric loss. Thus the use of aliovalent dopants, Mn in this example, can reduce the amount of both oxygen vacancies and holes (Wang, et al., 2010).

4.5.4. A-site metal dopants

Calcium was used as an A-site dopant with Lithium doped powders used for comparison. Calcium with an ionic radius of 0.1nm and Lithium with an ionic radius of 0.076nm were

much smaller than the A-site cations they were substituting and thus following the results observed with the transition metal dopants, smaller lattice-spacings were expected. *Figure 32* shows a comparison of the lattice spacings of KNN powders doped with the A-site dopants at 6 at.%, produced using the three main powder synthesis methods used in this research and compared with reference powders namely KNN, KN and NN and an in-house un-doped KNN powders from different powder synthesis methods.

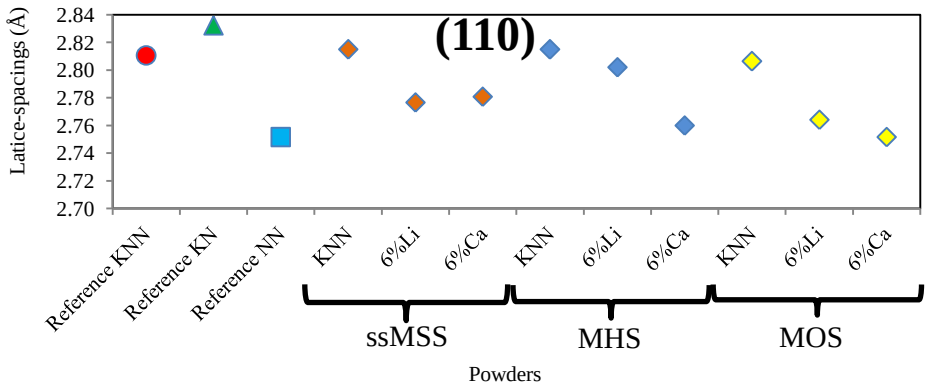

Figure 32 the (110) perovskite plane showing lattice-spacings of KNN powders doped with 6 at.% Li or Ca, prepared by ssMSS, MHS and MOS compared to a reference KNN.

● – Reference KNN, ▲ – reference KN, ■ – reference NN. ±5 at. % error determined by Siemens-D5005 X-ray machine.

The MHS produced 6at. % Li doped KNN powder (*Figure 32*) shows close similarity to the KNN reference with lattice-spacings slightly smaller than the KNN reference compared to the other doped powders and their un-doped versions. The smallest lattice-spacing results were produced by Ca (*Figure 32*) made from the MOS and ssMSS methods. The differences between powders synthesised through different powder synthesis methods, but using similar dopants further highlights the point that as the powder heat treatment conditions change the resultant powders may have different levels of dopant absorption. The use of Ca as an A-site dopant with a smaller ionic radius, higher electro-positivity relative to the K and Na atoms it substitutes, may explain the reductions in lattice-spacings observed.

4.5. Summary

The MSS method known to produce highly reactive, small particle powders due to the low heat treatment temperatures used when compared to the MOS method was initially selected as the desired powder synthesis route. The MSS was found to favour the incorporation of Na ions at the expense of the K ions resulting in a Na ion-rich alkali niobate due to the detrimental reaction of the molten salt reaction aid (NaCl), that was meant to be benign, with the K_2CO_3 reactant leading to the formation of KCl and K substitution from the carbonate by Na. This therefore generated more Na ions that reacted with the niobium oxide to produce the K ion-deficient niobate. This led to research to find an alternative method to produce KNN.

A method for making KNN powder was achieved with the removal of the NaCl molten reaction aid in favour of hydroxide based reaction aids. In a two step powder synthesis process, K_2CO_3 + KOH + Nb_2O_5 were reacted at 500°C to produce potassium niobate derivatives and in the second stage Na ions were introduced for a two hour heat treatment at 700°C producing KNN. A disadvantage of this MHS system is that it is a two step heat treatment method and when synthesizing small amounts results in low yields. An advantage is that the operating heat treatment temperatures have remained similar to the earlier envisaged MSS method for producing KNN.

A MSS method utilising KCl as the single solvent in the absence of NaCl, was also successfully utilised to produce KNN, further highlighting the unfavourable nature of NaCl in close proximity to K_2CO_3 within the MSS powder synthesis of KNN. The advantage that the synthesis occurred in a single stage, though the heat treatment was 100°C above the desired operating heat treatment temperature. The various powder synthesis methods also displayed alkali losses leading to powder that had a stoichiometric imbalance. Using the MOS, MHS

and ssMSS, KNN powders were successfully doped with various metal dopants which on the whole appeared to reduce the lattice-spacings present in the KNN due to smaller ionic radii.

Chapter 5

5. Thick films

5.1. Introduction

The main quantitative and qualitative electrical tests involved in evaluating the thick films were the piezoelectric coefficient measurement (d_{33}), dielectric permittivity (ε_r & $\varepsilon^T{}_{33}$) and dielectric loss ($tan\delta$). These were compared to results obtained from KNN and PZT from literature and in-house prepared bulk KNN compacts and PZT thick films. Impedance measurements were carried out to further characterise the material. The aim of the research on thick films was to create films that exhibit high d_{33} and ε_r with low $tan\delta$.

5.2. Bulk KNN

Bulk KNN samples were prepared in order to observe and analyse the KNN powder properties independent of the additional processing and additives present in the composite sol-gel thick film process. The samples were poled and electrically characterised at room temperature with dielectric and piezoelectric measurements carried out. The highest reported value of $tan\delta$ for bulk KNN discs is 8.4% (Hollenstein, et al., 2005) while the in house bulk sample had a room temperature peak $tan\delta$ of 10%. The KNN bulk sample tested showed a peak room temperature $\varepsilon^T{}_{33}$ of 620. In literature the highest relative permittivity seen by the author was 1164 for a bulk un-doped KNN sample (Jarupoom, et al., 2008). The lowest d_{33} value seen for bulk KNN discs in the literature is 30pC/N (Guo, et al., 2004) with the highest at 218pC/N (Li & Sun, 2009). The in-house bulk KNN disc had a room temperature d_{33} of 95pC/N.

5.3. Standard KNN thick films

The initial deposition and infiltration method selected for this project was 4(C+2S) generally established by Barrow *et al.* (Barrow, et al., 1995) and specifically adapted from Dorey *et al.* (Dorey, et al., 2002). The standard heat treatment temperature and dwell time of 7 00°C and 20 minutes for the KNN thick film, which was derived from work on PZT thick films heat treated in a near similar manner (Dorey, et al., 2008) (Dorey, et al., 2002).

5.3.1. Na ion-rich alkali niobate thick films

The powder used for this film was the initial MSS produced Na ion-rich alkali niobate, which is anti-ferroelectric at room temperature. This sample displayed a peak piezoelectric coefficient value of 11.5pC/N. Anti-ferroelectric materials are known to weaken their anti-ferroelectric characteristics (Pulvari, 1960) during high temperature poling and so it is possible to electrically pole the material to produce a d_{33} response. Relative permittivity of 252 and *tanδ* of 9.8% where measured for this sample after electrical poling at up to 6.89V/µm. A ferroelectric hysteresis loop measurement revealed the film to be a lossy capacitor i.e. possessing the response properties of both an ideal capacitor and an ideal resistor as opposed to the standard non-linear ferroelectric hysteresis loop response of good ferroelectric capacitors (Stewart, et al., 1999).

5.3.2. Initial KNN thick films

With varying results displayed by initial KNN thick films, that were related to early familiarisation with the film processing method, the preeminent KNN thick film at this preliminary stage displayed a peak d_{33} of 34pC/N; relative permittivity of 442 and a minimum *tanδ* of 19%, though with an average *tanδ* for the whole thick film beyond 100%.

This was an improvement on the earlier produced Na ion-rich alkali niobate thick film with respect to the two parameters of d_{33} and ε_r, but incredibly poor when the average *tanδ* across the thick film was calculated, as the average *tanδ* for the whole Na ion-rich alkali niobate thick film was 29%. High *tanδ* is a sign of a material that will display poor dielectric characteristics with the possibility of these affecting the piezoelectric response, highlighting the significance of the high *tanδ* result from the KNN thick film. Impedance measurements carried out on the best KNN thick film showed the film to have extremely low phase angle of -16.8° and a magnitude of impedance of 8341 ohms recorded at 1 kHz. The sample showed a response closer to that of a resistor than a capacitor.

The high *tanδ* proved to be a recurrent issue faced with the KNN thick films. The bulk KNN disc provided a quantitative and qualitative indication of the KNN material performance expected. The d_{33} and ε_r results for the KNN thick films were lower than those displayed by the bulk KNN disc. The different processing to produce the KNN thick film resulted in highly divergent *tanδ* results when compared to the bulk material result, indicating the source of the issue was related to the part of the thick film processing or new constituents added rather than a KNN powder issue.

5.4. Processing and constituents of KNN thick films

In order to understand the source of the high *tanδ* results, the new constituents and processing involved in producing KNN thick films were investigated. The differences between the thick film and bulk samples are:

- calcination temperature whereby the bulk sample was sintered at 1100°C for 4 hours while the thick film was heat treated for 30 minutes at 700°C,
- the deposition of the thick film on a platinised silicon substrate,
- the use of a KNN producing sol in the thick film,
- the use of binder material to aid green strength of the bulk material prior to sintering.

With these facts established, investigations were carried out on these differences to better understand the cause of the high *tanδ*.

5.4.1. Effect of heat treatment temperature on KNN thick films

KNN thick films were deposited on Si wafers to observe the effect that increasing the calcination temperature would have on the phase and elemental structure of the films as shown in *Table 11*.

Table 11 elemental analysis of MHS KNN thick films

ESEM-EDX analysis (Atomic %; ±0.1% error)			
	Na	K	Nb
No heating	20.5	26.2	53.3
450°C	17.3	24.7	58.1
500°C	16.7	25.6	57.7
550°C	5.4	15.4	79.3
600°C	5.7	15.2	79.1
650°C	5.2	15.6	79.2
700°C	5.4	15.8	78.8

The initial stoichiometry of the film is imbalanced with the unheated film showing a deficiency in Na as shown in *Table 11*. The initial imbalance in the ratio of potassium and sodium was observed in the KNN powders in ***section 4.4*** and also in a KNN sample where the EDX analysis showed a near similar deficiency of Na (Centre Interdisciplinaire de Microscopie Electronique, 2009). Poor stoichiometry leads to deterioration in the electrical properties of piezoelectric ceramics which are induced during ceramic processing (Li, et al., 2010). The stoichiometric ratios with the best piezoelectric characteristics for KNN are 50:50 of K-Na and any deviation reduces the piezoelectric response (Egerton, 1959). Consequently, the elastic properties may be affected and can vary by as much as 5%, the piezoelectric properties 10% and the dielectric properties 20% within the same batch (Jordan & Ounaies, 2001).

After processing at 550°C and above, the levels of both K and Na ions reduce drastically, with Na particularly affected. It is thought that the alkali metals either evaporate or diffuse into the wafer. From the formula $K_{0.5}Na_{0.5}NbO_3$ it was shown from the elemental analysis that elevated temperatures led to an extreme imbalance in the stoichiometric ratios within the thick film. An alkali ion imbalance affects the electrical functionality of the thick film and may be a reason for the high *tanδ* (Li, et al., 2010) (Zeng, et al., 2007). At 550°C the Nb appears to shield further alkali losses.

PZT samples are normally sintered in the presence of a lead source, such as $PbZrO_3$, and placed in covered crucibles. This reduces Pb loss and as a consequence allows sintering at temperatures between 1200°-1300°C (Jordan & Ounaies, 2001); therefore transferring this idea to KNN thick films, a KNN thick film was covered with KNN powder, creating a KNN rich atmosphere during heat treatment processing. Unfortunately with this method, powder

adhered to the film making a poor surface for deposition of electrodes and thus was not pursued further.

Increasing the alkali to niobate ratio from 1:1 to 1.5:1 during powder synthesis was another suggested route to curtail the alkali losses, though long-term stability and resistance to humidity may be affected (Rodel, et al., 2009). In practical terms this method is un-workable with the MHS and ssMSS powder synthesis methods, due to the washing step which would wash away the soluble excess alkali.

XRD analysis of the films indicated the formation of the perovskite phase at all temperature ranges examined and the production of additional phases (*Figure 33*).

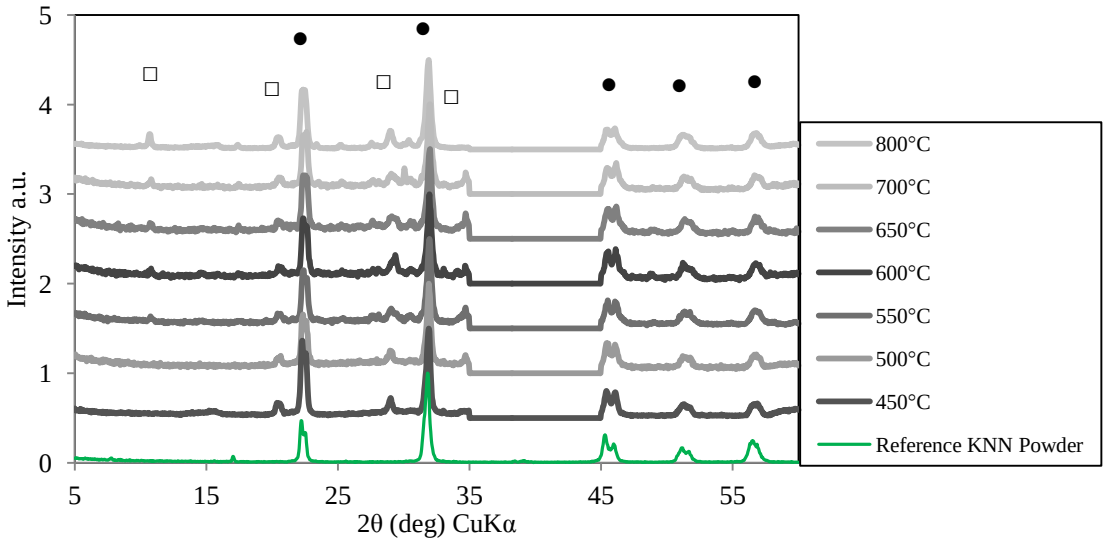

Figure 33 XRD trace of MHS KNN 4(C+2S) thick films heat treated at a range of temperatures. Section between 35°-45° is Pt peak that has been removed.
● – perovskite phases; □ – unknown phases.

Extra phases within piezoelectric ceramics have a detrimental effect which critically decreases the functional response the ceramics. Comparison of the extra phases with XRD records of numerous alkali niobates such as $K_6Nb_{10.88}O_{30}$, $K_4Nb_6O_{17}$, $K_2Nb_4O_{11}$, $KNbO_3$, $Na_2Nb_4O_{11}$, $NaNbO_3$, etc. did not match. Further investigation to identify the extra phases was carried out with ESEM-EDX analysis of KNN thick films (*Table 12*).

Table 12 cross sectional elemental analysis of a MHS KNN thick films

ESEM-EDX analysis atomic %						
	Na	Si	K	Nb	Ag	Pt
KNN Thick Film - 4(C+2S) - Heat Treated – 20min @ 450°C	2.6	75.5	3.2	11.2	6.3	1.2
KNN Thick Film - 4(C+2S) - Heat Treated – 20min @ 700°C	5.4	57.5	5.7	19.7	8.9	2.8

The ESEM-EDX analysis showed the presence of high levels of silicon within the KNN thick film, which suggested diffusion into the film from the Si substrate. This led to further analysis of the film-substrate interface. It is worth taking note that the ESEM-EDX analysis of these samples with large Si or alumina substrates below thin KNN or PZT films, may result in the possible sampling analysis detrimentally including the substrates.

KNN deposited on substrates was found to possess an imbalanced stoichiometry prior to the application of any heat processing. As the thick films were heat treated, they experienced large alkali losses with the hypothesis being these were lost to evaporation and/or inter-diffusion with the Si wafer substrate. This possible inter-diffusion may have resulted in the production of silicon induced extra phases within the thick films that are known to impede electromechanical functionality.

5.4.2. Investigating the film-substrate interface

Silicon diffuses into the piezoelectric ceramic thick films at similar elevated temperatures utilized in this process; Kosec *et al.* found the inter-diffusion of Pb and Si occurred at temperatures as low as 500°C (Kosec, et al., 2001). The purity of the piezoelectric thick film enables it to be piezo-electrically active and contamination hinders that ability. An ESEM-EDX cross sectional line scan confirmed the presence of silicon in the KNN thick film as shown in *Figure 34* and therefore was thought to have an effect on the measured parameters of the films.

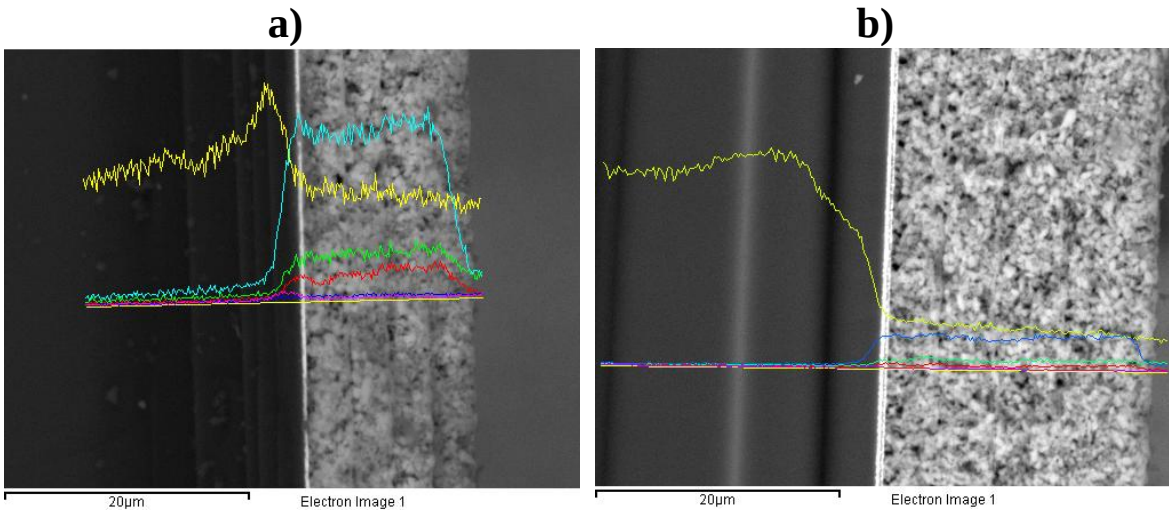

Figure 34 elemental ESEM-EDX cross sectional line scans of MHS KNN thick films on wafer **a)** KNN Thick Film - heat treated at 450°C **b)** KNN thick film - heat treated at 700°C

Pink = Pt, Blue = Nb, Green = K, Yellow = Si, Red = Na.

Further analysis was carried out on the thick film to determine where the elements are to be found within the film-substrate interface as shown by *Figure 35* which shows the areas of analysis used to produce the data in *Table 13*; which were the 100nm platinum back electrode (*Spectrum 1*), KNN thick film (*Spectrum 2*) and the silicon substrate (*Spectrum 3*).

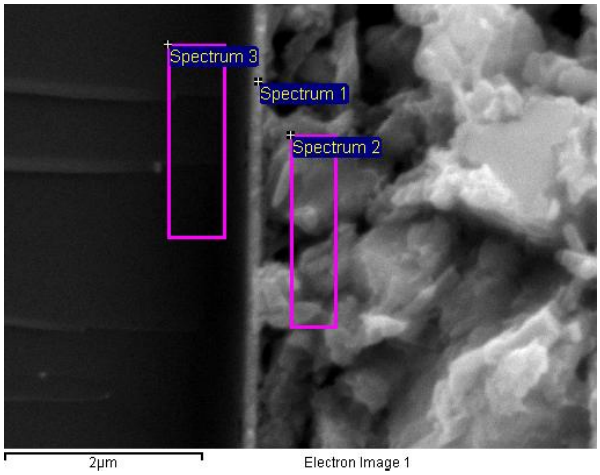

Figure 35 elemental ESEM-EDX cross sectional analysis at interface between Si wafer and MHS KNN thick film

Table 13 cross sectional elemental ESEM-EDX analysis of MHS KNN film

ESEM-EDX analysis atomic %								
Spectrum		Si	Pt	Na	K	Nb	O	Total
Spectrum 3	Si substrate	48.91	37.76	n/a	3.04	n/a	10.28	100
Spectrum 1	Si/Pt/KNN interface	9.22	22.05	2.27	8.83	40.37	17.27	100
Spectrum 2	KNN thick film	7.93	n/a	3.09	10.59	48.48	29.91	100

Silicon appears to diffuse through the Pt back electrode into the thick film (*Spectrum 1*) and the Pt diffuses into the Si wafer (*Spectrum 3*). There is a negligible diffusion of sodium into the wafer while potassium diffuses into the wafer (*Spectrum 2*). Niobium on the other hand does not diffuse into the wafer (*Spectrum 3*). The results suggest that sodium is lost through evaporation; potassium by both evaporation and diffusion into the wafer and niobium is neither evaporated nor diffused into the wafer at a considerable level hence leading to the observed stoichiometric imbalances. The extra phases observed in the XRD patterns may be related to silicon diffusion into the thick film as they did not match with numerous alternative alkali niobate XRD patterns examined.

The inter-diffusion observed between the Si wafer and the KNN thick film raised the question about whether this phenomenon would be observed in the PZT system. A cross sectional line scan ESEM-EDX analysis of a PZT thick film is shown in *Figure 36*.

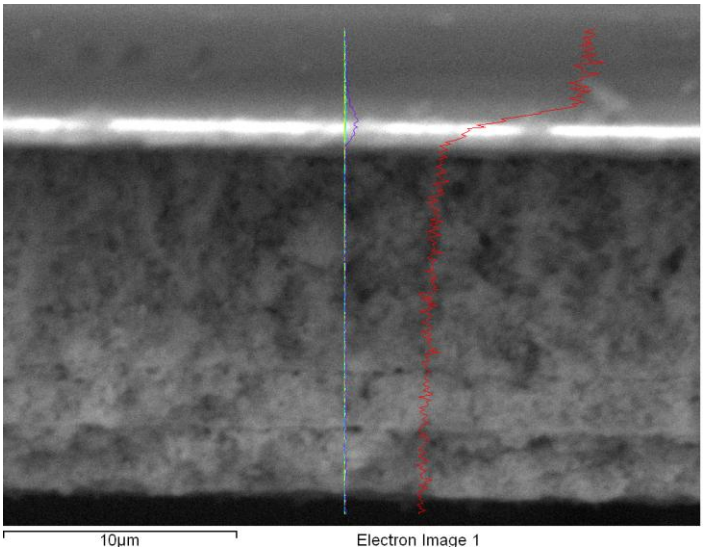

Figure 36 elemental ESEM-EDX cross sectional line scan of a PZT thick film on a Si wafer - heat treated at 700°C

Purple = Zr, Blue = Ti, Green = Pb, Red = Si.

The ESEM-EDX line scan shows the diffusion of Si into the PZT thick films. The piezoelectric and dielectric properties of the PZT thick film were far superior to those of the KNN despite the supposed Si diffusion. In the work of Kosec *et al.*, inter-diffusion of Si and PbO and alumina and PbO was noted to result in detrimental effects on the functionality of the films (Kosec, et al., 2001).

Following these results and the knowledge that alumina is more chemically inert when compared to silicon; an elemental ESEM-EDX line scan analysis was made of KNN deposited on an alumina sheet (*Figure 37*).

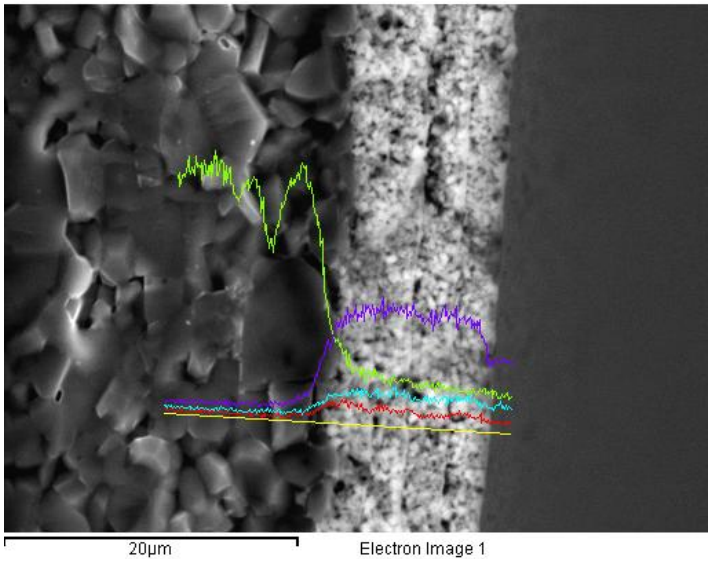

Figure 37 elemental ESEM-EDX cross sectional line scan of a MHS KNN thick film on an alumina sheet - heat treated at 700°C

Purple = Nb, Blue = K, Green = Al, Red = Na.

The results suggest diffusion occurs in both directions, similar to the situation seen with the Si wafers. Research by Su *et al.* into the stability of alumina suggested that at high temperatures it was found to interact with barium strontium titanate thick films at high sintering temperatures (>1250°C) and also as mentioned earlier where Kosec *et al.* found diffusion of alumina to occur (Su & Button, 2001) (Kosec, et al., 2001), thus indicating alumina may also suffer inter-diffusion issues. A KNN thick film was deposited on a platinised alumina substrate. Poor results were recorded for each of the parameters tested including $tan\delta$ beyond 100% and peak d_{33} of 4.25pC/N.

A point of note concerning the ESEM-EDX is the sampling size where it is thought that with a large Si or alumina substrate below a thin KNN or PZT film there is a possibility of the sampling analysis including the Si wafer substrate. This may explain the observed result where in various films the level of silicon appears to be more than the actual thick film and hence the hypothesis on silicon diffusion requires more experimental work to clarify what is occurring.

The overall results indicate that inter-diffusion occurs between the KNN thick film and the substrate (Si wafer and alumina) and similarly with PZT and this is known to result in lower functionality of the films electromechanical response. The functionality of the PZT films was not affected as much as was the case with the KNN thick films.

5.4.3. Use of ZrO_2 barrier layer

Inter-diffusion between the film and the wafer were shown to occur despite the use of lower calcination temperatures in the composite sol-gel route that are expected to curb these occurrences. ZrO_2 is a well known material used as a diffusion barrier layer when producing PZT films (Dorey, et al., 2008). The requirements of a good barrier layer are that no atoms go through it, it should not be a weak link through poor adhesion to the substrate or film and it should be as thin as possible so as not to affect the performance of the device as a whole (Dorey & Whatmore, 2004). The buffer layer was utilised to stop the inter-diffusion of the elements from the thick film and the silicon from the wafer and thus improve the piezoelectric and electric properties. This involved the use of a 40nm ZrO_2 layer spin coated on the Si wafer to form the ZrO_2 buffer layer after which the Ti/Pt electrode layers were applied (Dorey, et al., 2008), and was applied and annealed in a similar manner to the composite sol-gel deposition process. Such a thin layer is thought not to affect the functional performance of the resultant piezoelectric thick film. Four samples deposited on ZrO_2 buffered Si wafers were examined and the results of electrical characterisation displayed in *Figure 38*.

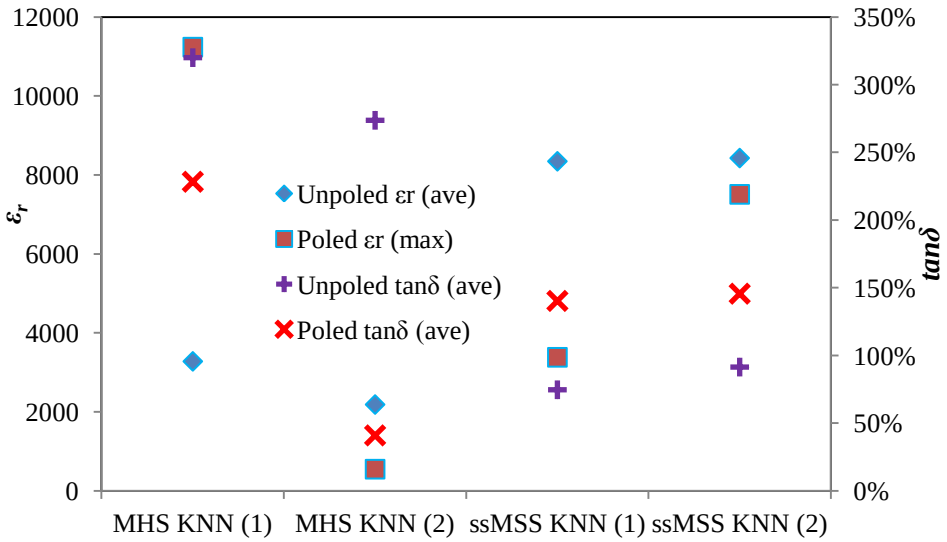

Figure 38 KNN 4(C+2S) thick films on ZrO_2 buffered Si wafers; ε_r and *tanδ* data before and after electrical poling (5-8V/μm) at 200°C

Inter-diffusion between the KNN thick film and the silicon was thought to result in the production of extra-phases, resulting in a reduction in the measured parameters. Use of the ZrO_2 barrier layer was expected to reduce incidences of this occurring and result in improved performance of the KNN thick films. Overall the results (*Figure 38*) were poor with no apparent improvement in the measured piezoelectric and dielectric characteristics when compared to previous samples. The *tanδ* and ε_r results did not show the envisaged decreases and stabilisation. Elemental ESEM EDX analysis of the film-Si wafer substrate interface of the sample that displayed the lowest dielectric loss i.e. *MHS KNN (2)* was conducted (*Figure 39*).

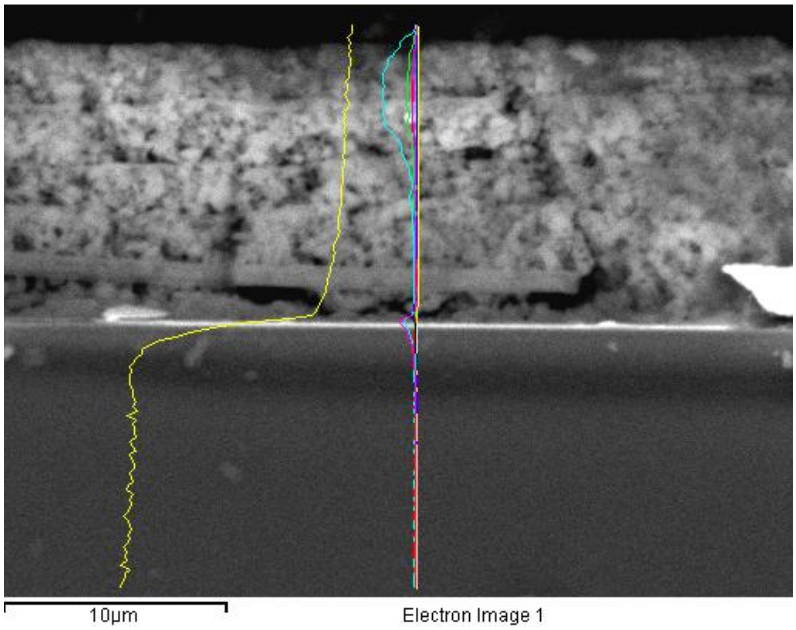

Figure 39 elemental ESEM-EDX cross sectional line scan of *MHS KNN (2)* thick film on a Si wafer – with 40nm ZrO_2 barrier layer

Red = Na, Yellow = Si, Green = K, Light Blue = Nb, Dark Blue = Pt, Pink = Zr.

Figure 39 suggests the ZrO_2 barrier layer may have failed to stop the inter-diffusion at the interface as it shows a large presence of Si within the film. It is again worth noting that this may be a limitation of the equipment and the small scale of the thick film being examined as the data suggest a larger amount of silicon present in the film when compared to KNN. If indeed ESEM-EDX results are a failing of the equipment and no silicon diffused through, then the dielectric and piezoelectric results may suggest the KNN thick film does indeed suffer from self induced issues of alkali loss, stoichiometric imbalance and porosity leading to compromised dielectric and piezoelectric properties. The ESEM-EDX results coupled with the dielectric results resulted in a halt to further investigation of the ZrO_2 buffer.

5.4.4. KNN thick film porosity

Following the hypothesis that the high *tanδ* was attributed to the high porosity of the KNN films and alkali loss; the film was examined further using S-FEG SEM and compared to a

PZT thick film known to have good density and excellent piezoelectric and dielectric characteristics (*Figure 40*).

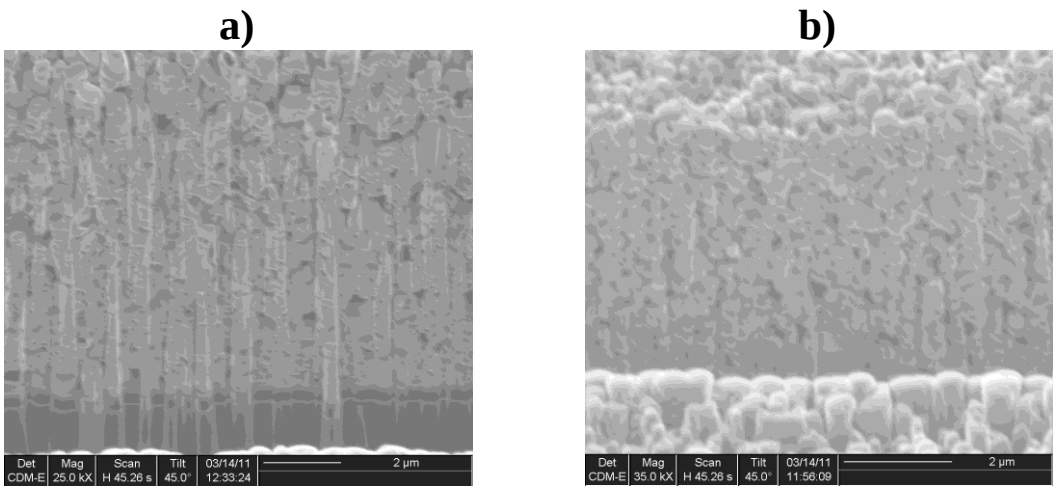

Figure 40 S-FEG SEM micrograph of **a)** MHS KNN 4(C+4S) thick film and **b)** PZT 4(C+4S) thick film

Figure 40 shows the density in the KNN thick film to be comparable to that of the PZT thick film. The heat treatment step is an extremely crucial step for piezoelectric thick films as it ensures that full crystallization and densification of the sol-gel phase are complete and thus forming the perovskite phase. Previous XRD results and the S-FEG SEM micrographs in combination indicate a perovskite structure with high density was formed and thus on the micro-scale significant porosity was not observed. Despite the noted similarity in density to the PZT film, the KNN displayed far inferior piezoelectric and dielectric properties to the PZT. One hypothesis suggests that the inter-diffusion between the substrate and the film, created a dense film that contained silicon impurities that filled space vacated due to alkali loss.

5.4.5. Increased heat treatment temperature

With the underlying hypothesis that alkali loss, leading to an imbalanced stoichiometry and porosity may be responsible for the high *tanδ*, a MHS KNN thick film was produced in the

standard fashion and heat treated for 30 minutes at 800°C. With the increased calcination temperature, a denser film was envisaged with improved piezoelectric and dielectric properties, due to increased densification of the KNN sol-gel. Higher alkali loss and increased film-substrate inter-diffusion were the expected downsides to this procedure.

The resultant thick film was visually different to other KNN thick films produced at the standard temperature, being whiter than the standard films. The colour change could indicate that higher levels of crystallisation of the sol occurred resulting in a more crystalline KNN thick film compared to KNN thick films produced at 700°C.

An issue found with this thick film was poor inter-granular adhesive force leading to a powdery consistency that easily disintegrated, when touched (e.g. poling electrodes etc.). The poor inter-granule adhesion resulted in Cr-Au electrodes with poor adhesion to the film and hence easily disintegrated during testing, making parameter measurements difficult. This suggested that the optimum temperature to create a dense and fused KNN thick film on a silicon wafer had been surpassed.

When possible, dielectric testing revealed an improved un-poled *tanδ* of 21% and *tanδ* after electrical poling of 20% which were the best results achieved with a KNN thick film on a silicon wafer. The relative permittivity properties of this film were unstable with ε_r prior to electrical poling of 349 which dropped after electrical poling (at 10V/μm) at 200°C to 131. Impedance measurements revealed a previously unmatched phase angle of -80.4% at 1kHz. The d_{33} was poor at 3.25pC/N, suggesting the granular structure did not support the polarisation of the domains.

Higher alkali loss and increased film-substrate inter-diffusion were expected to affect both the piezoelectric and dielectric properties of the film by producing a highly conductive film

or an inactive film with low loss, but no dielectric or piezoelectric functionality. The result led to a number of hypotheses; the first that the high calcination temperature reduced the dielectric loss characteristics of the thick film, though at a cost, i.e. the loss of inter-granular adhesion, and low d_{33}. The effect on the relative permittivity appeared to be minimal suggesting a dielectric functionality.

The colour (pure white) compared to that of standard KNN thick films prepared at 700ºC (off-white) and the contrasting granular adhesion issues, highlighted the presence of a binding material in the standard films which is thought to be derived from the KNN sol.

It has been suggested that the use of a sol-gel composite with its complex microstructure, results in material defects in the ceramic (e.g. porosity, dislocations, ion vacancies, impurities) which are said to be the most important source of dielectric loss. Each defect causes a correction in the surrounding ions relative to their state when the defect is absent and as a consequence induces screening charges which act against the polarization induced by the applied electric field (Dauchy, 2007); resulting in the hypothesis that suggests, the level of the binding material derived from the KNN sol-gel, was much lower in the sample heat treated at 800ºC. This was due to the evaporation/deactivation of binding properties at the higher calcination temperature. The binding material may have a detrimental effect on the dielectric properties of the KNN thick films and thus the lower levels of the binding material resulted in a KNN thick film that exhibited lower dielectric loss when compared to standard films calcined at 700°C.

5.5. Sol infiltration treatments

5.5.1. Number of sol infiltrations

Further sol infiltrations were added mainly to reduce the film porosity (Dorey, et al., 2002), with another advantage being to compensate for alkali loss and hence reduce the *tanδ*, as low density is known to increase *tanδ* in KNN ceramics (Rodel, et al., 2009). Sol infiltrations were increased from 2 to 4 per composite slurry layer. Each sol layer deposited flows into the thick film increasing the density of the film as shown in *Figure 41*.

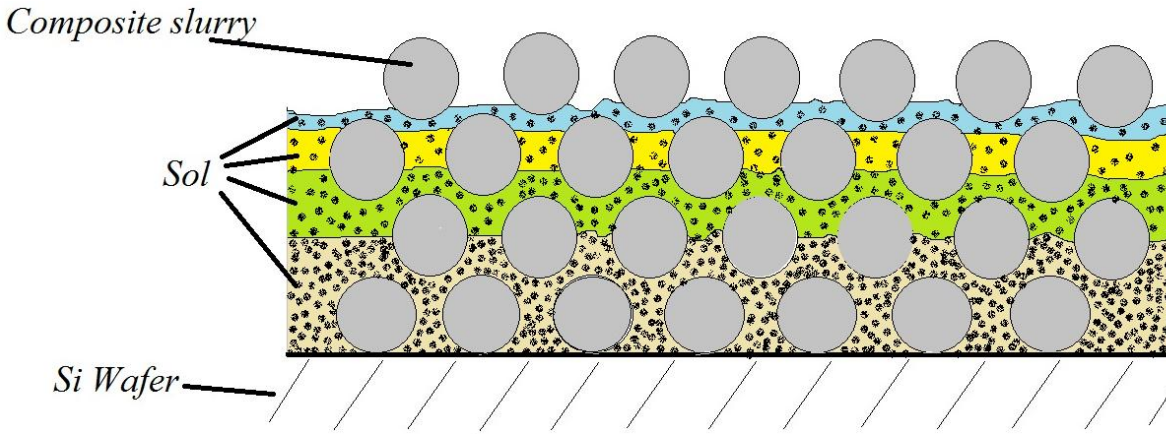

Figure 41 increased sol infiltration into composite slurry layers creating denser film

The dielectric loss of KNN 4(C+**2S**) thick film is shown in *Figure 42a* and is high and exhibits a large variation across the range, with values ranging from a low of 60% to a peak of 93% after electrical poling. Increasing sol infiltrations resulted in a considerable increase in *tanδ* as shown on *Figure 42b* with a low of 323% and a high of 770%.

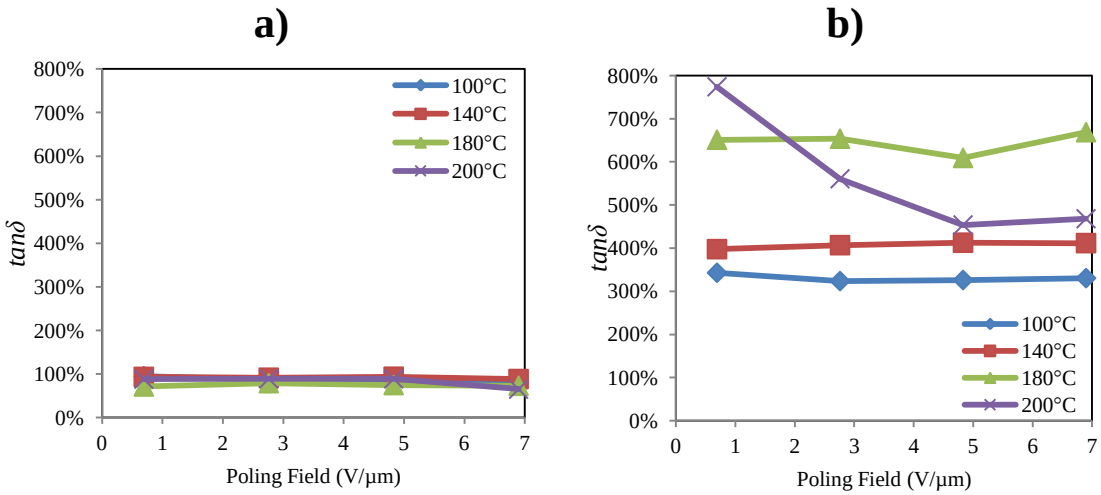

Figure 42 *tanδ* as a function of poling voltage of two MHS KNN thick films poled at increasing poling voltages and a series of increasing poling temperatures and tested at room temperature. **a)** 4(C+**2S**) – 5.6µm thick, **b)** 4(C+**4S**) – 5.8µm thick.

The high *tanδ* result for the sample with 4 sol infiltrations (*Figure 42b*) showed that increasing the number of sol infiltration had the effect of increasing the level of dielectric loss, suggesting the sol had a negative impact on this property. This effect coupled with the result in ***section 5.4.5***, where higher temperatures resulted in a reduction of the sols effect on the properties of the thick film; both indicated that the sol was in part responsible for the high dielectric loss.

Figure 43a, shows the relative permittivity of the KNN 4(C+**2S**) thick film which had a high level of *tanδ* that peaked at 80%. The KNN 4(C+**4S**) thick film sample with an even higher level of *tanδ* appeared to have very high relative permittivity as shown in *Figure 43b*.

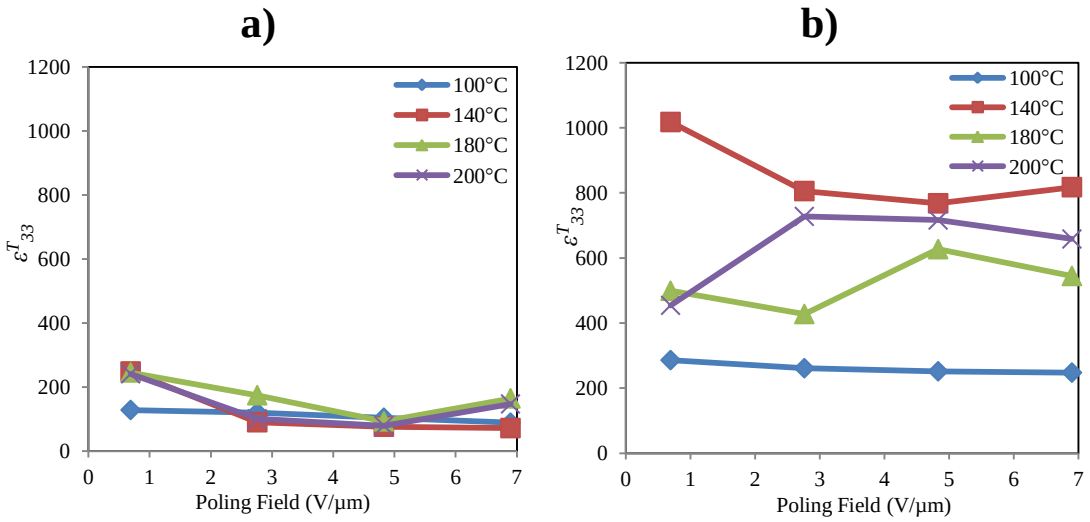

Figure *43* ε^T_{33} as a function of poling voltage of MHS KNN thick films poled at increasing poling voltages and a series of increasing poling temperatures and tested at room temperature. **a)** 4(C+**2S**) – 5.6µm thick, **b)** 4(C+**4S**) – 5.8µm thick.

Increased sol infiltrations have the effect of increasing the relative permittivity even further (*Figure 43b*). A good dielectric material is considered to have low *tanδ* and a large ε_r (Johnson, 2001). The overall result from these samples shows the dielectric properties are severely affected by the conductivity of the film resulting in large relative permittivity readings. One way of describing dielectric losses is to consider the permittivity as a complex number (***Equation 2-10***).

The real part (ε_r') represents AC capacitance and the imaginary part (ε_r'') represents the dielectric loss factor (Johnson, 2001). The degree to which a dipole is out of phase with an applied AC electric field and the dielectric losses that result, determine how large ε_r'' is. The larger the ε_r'', the more energy is dissipated through dipole motion and thus in this KNN thick film system large dielectric losses contribute to high ε^T_{33} properties characterised by high contribution from the ε_r'', rather than from the desired AC capacitive component.

Figure 44a shows very low d_{33} values for the 4(C+**2S**) KNN thick film of between 1.4pC/N and 10pC/N; while (*Figure 44b*) the KNN 4(C+**4S**) thick film sample is shown to exhibit higher d_{33} values of between 0.75pC/N to 18.25pC/N.

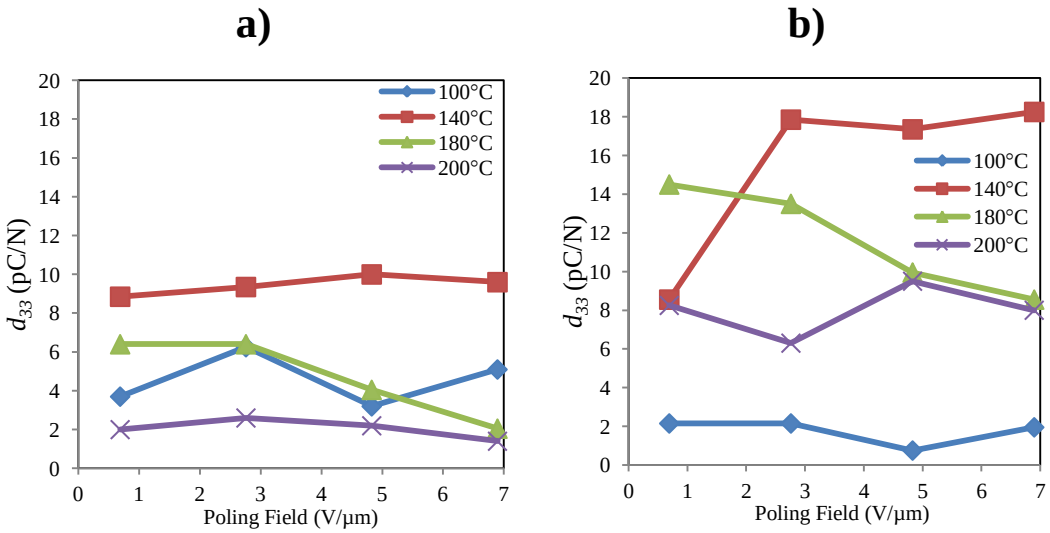

Figure 44 d_{33} as a function of poling voltage of two composite thick films poled at increasing poling voltages and a series of increasing poling temperatures and tested at room temperature. **a)** 4(C+**2S**) – 5.6µm thick, **b)** 4(C+**4S**) – 5.8µm thick.

This result showed that despite the high *tanδ* and inconsistent ε_r, the 4(C+**4S**) thick film sample was able to be poled to give a higher d_{33} result (*Figure 44*). The d_{33} response indicated that the high *tanδ* did not curtail the ability to polarise the material.

It was noted that increasing the level of KNN sol infiltration resulted in a film with poor dielectric characteristics, exhibiting much higher *tanδ* and even more variable ε_r properties. However, increased infiltration of the KNN sol appeared to have a positive effect on the piezoelectric properties corroborated by the result in ***section 5.4.5*** where with an evidently reduced level of KNN sol, d_{33} was much lower.

5.5.2. KNN-PZT composite

Mixing KNN powder with PZT sol as well as KNN sol with PZT powders was undertaken to isolate the potential effects of the KNN sol and powders. It was envisaged that with the KNN sol suspected of being the source of the poor dielectric properties, isolating it with a material known for its superior properties would highlight this hypothesis. *Table 14* shows the dielectric and piezoelectric results of the samples tested.

Table 14 piezoelectric and dielectric characteristics of various inter-mixed KNN and PZT based thick films

Powder	KNN	PZT
Sol	PZT	KNN
Spin coating	4(C+2S)	4(C+2S)
Film Thickness	6µm	5.8 µm
Phase Angle @ 1kHz	-54.8°	-20.6°
Un-poled ε_r	2,150	2,157
Un-poled $tan\delta$	138%	364%
Poled d_{33} (pC/N)	2	12
ε^T_{33}	2,300	81
Poled $tan\delta$	586%	116%

An increase in the phase angle was noted with the use of PZT sol with KNN powder, with very high dielectric loss and relative permittivity results and a poor piezoelectric response (*Table 14*). The sample with the KNN sol and PZT powder had a low phase angle, high dielectric loss, very low relative permittivity and an average piezoelectric response.

The results suggest the lower volume sol dictates the dielectric response in both cases, resulting in the sample with KNN powder and PZT sol displaying a PZT sol induced phase angle while the sample with KNN sol displayed a low KNN-like phase angle. After electrical poling at elevated temperatures the larger volume powders dictate the piezoelectric response

where PZT powders mixed with KNN sol display high d_{33} while the opposite is true with the KNN powder based thick film.

5.6. Sol base-layer

With the hypothesis that porosity issues, in particular the DC conductive component of the dielectric loss, were at the heart of the poor dielectric properties displayed by the KNN thick films that resulted in a film with low resistance, a single layer of sol was deposited prior to the standard 4(C+2S) spin coating procedure to create a dense KNN sol base-layer (*Figure 45*). The high density KNN sol base-layer was expected to act as a barrier to the current and thus reduce the dielectric loss and produce more consistent relative permittivity.

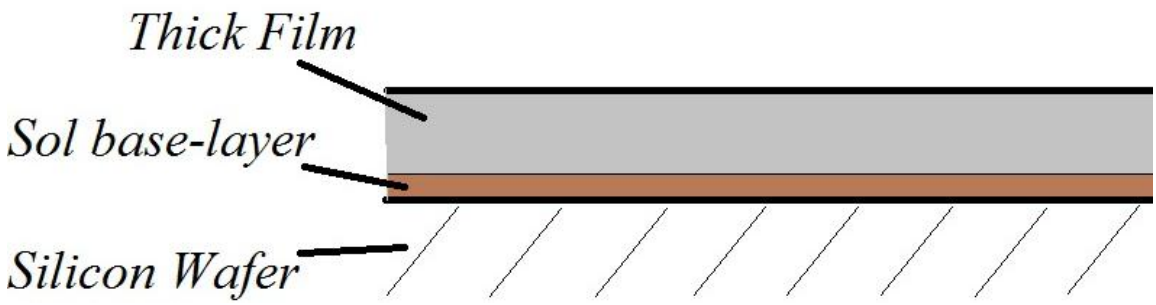

Figure 45 the addition of the sol base-layer to the 4(C+2S) thick film deposition process

A single sol base-layer, i.e. **1S**[4(C+2S)] was applied and dielectric and piezoelectric measurements recorded (*Figure 46a*). Following the analysis of the results of the **1S**[4(C+2S)] sample the sol base-layers were increased to five in order to enhance the barrier properties derived from the sol base-layer (*Figure 46b*).

a)

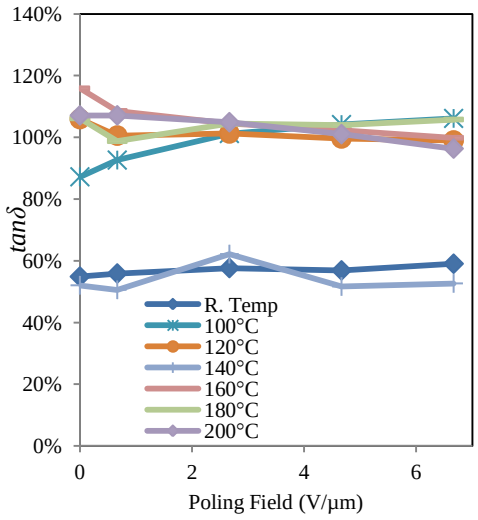

b)

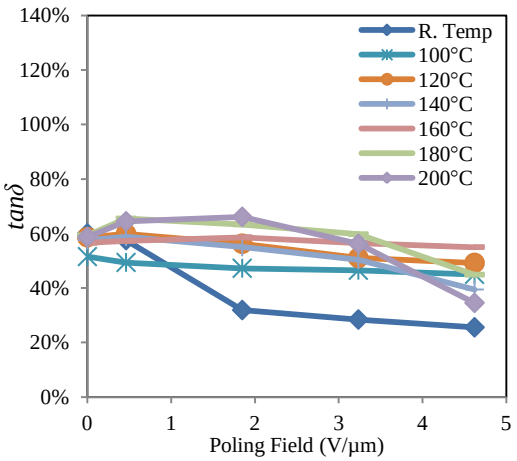

Figure 46 *tanδ* as a function of poling voltage of two composite thick films poled at increasing poling voltages and a series of increasing temperatures and measured at room temperature. **a)** MHS KNN thick film **1S**[4(C+2S)] (film thickness - 6µm) and **b)** MHS KNN thick film **5S**[4(C+2S)] (film thickness – 8.65µm)

Deposition of a single sol base-layer, showed a reduction of the *tanδ* prior to electrical poling at elevated temperatures from beyond 100% seen in most KNN thick films, to 60% on average across several samples. After electrical poling the dielectric losses were higher as shown in *Figure 46a* where the sample had a peak *tanδ* beyond 100%. The **5S**[4(C+2S)] sample, exhibited further improvements, with a pre-poled average *tanδ* of 36% and after electrical poling an average *tanδ* of 52% as seen in *Figure 46b*.

A doubling of the number of sol base-layers, i.e. **10S**[4(C+2S)] resulted in a further reduction in the *tanδ* observed with a tighter spread of results showing an increase in robustness of the sol base-layer, despite the increase in poling voltage when compared to previous samples, as shown in *Figure 47*.

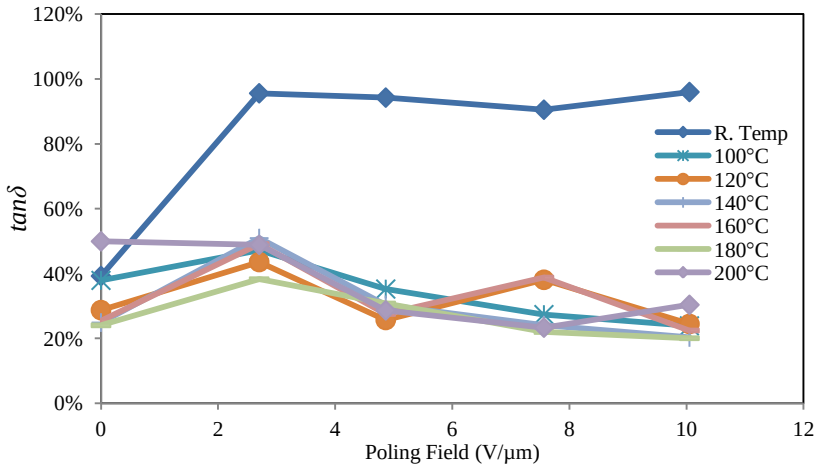

Figure 47 *tanδ* as a function of poling voltage of **10S**[4(C+2S)] MHS KNN thick film (film thickness – 23µm) poled at increasing poling voltages and a series of increasing temperatures and measured at room temperature

The KNN results were poor in comparison to that of PZT thick films, but an improvement on earlier KNN thick films was observed. The un-poled PZT 4(C+2S) thick film had an average *tanδ* of 6% and on poling the average dielectric loss across all electrodes tested was 1.7%. It was noted that in the case of PZT the *tanδ* prior to electrical poling was higher than the *tanδ* after poling which was a behaviour opposite to that observed with KNN thick films which had lower *tanδ* before poling which increased after electrical poling.

The relative permittivity of the KNN thick films electrically poled at room temperature (*Figure 48a*), were higher than the results from the bulk KNN sample, suggesting other factors affecting the result e.g. moisture; as after electrical poling at elevated temperatures the ε^{T}_{33} was more consistent and lower. Increasing the sol base layers to 5 and 10 layers appeared to improve the *tanδ*, but the effect on ε^{T}_{33} was inconsistent as shown in *Figure 48b* and *Figure 48c*.

Comparing the relative permittivity of the KNN films to the PZT thick film results shown in *Figure 48d*; the results of the PZT film are packed in a narrow band showing greater consistency in the film's ε^{T}_{33} with increasing poling voltages and temperatures applied. The KNN results show widely divergent results implying poor consistency of the films' dielectric properties. It has been suggested by West *et al.* that at low frequencies, grain boundary impedances may at times lead to anomalously high capacitance values (West, et al., 1997), which may be the case with the KNN thick films measured at 1 kHz.

The KNN 1S[4(C+2S)] (film thickness – 6µm), 5S[4(C+2S)] (film thickness – 8.65µm), and PZT samples (film thickness – 6µm), were poled at a maximum of 40V, while the 10S[4(C+2S)] KNN sample (film thickness – 23µm), which was much thicker required higher electrical poling in order to achieve a result and combined with different film thicknesses resulted in the contrast in the poling field *x*-axis.

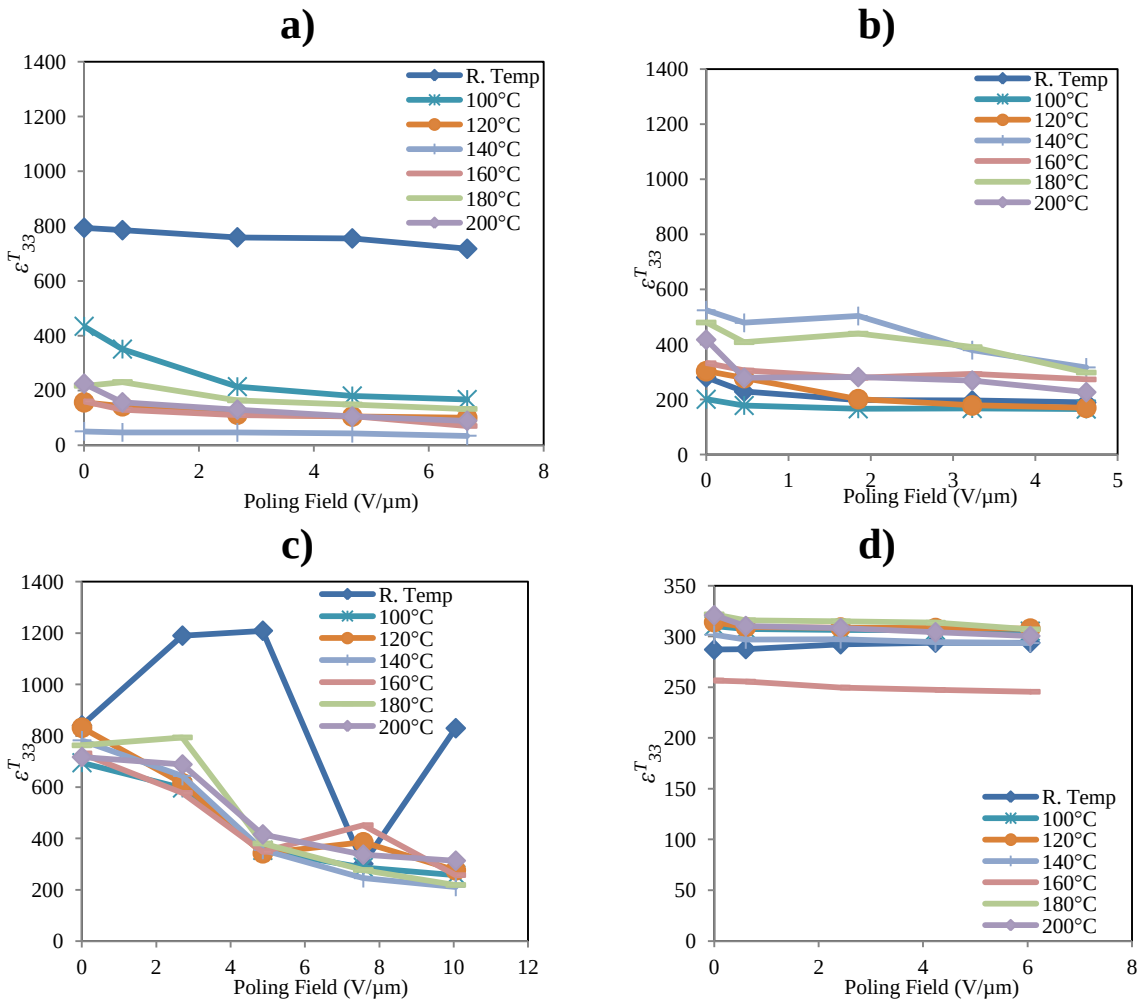

Figure 48 ε^T_{33} as a function of poling voltage of an un-doped KNN thick film poled at increasing poling voltages and a series of increasing temperatures and measured at room temperature. **a)** MHS KNN thick film **1S**[4(C+2S)] (film thickness – 6µm); **b)** MHS KNN thick film **5S**[4(C+2S)] (film thickness – 8.65µm); **c)** MHS KNN thick film **10S**[4(C+2S)] (film thickness – 23µm); **d)** PZT thick film 4(C+2S) (film thickness – 6µm)

$BaTiO_3$ ceramics are said to have constricted grain boundaries that possess capacitance, that is a combination of the capacitance of air gaps surrounding the grain to grain contacts and the capacitance of the neck region connecting the grains with the air gap capacitance dominating at very high temperatures (West, et al., 1997). With KNN thick films suffering a multitude of problems, with porosity thought to be prevalent i.e. the presence of numerous air gaps is thought to have a near similar detrimental effect to that seen in $BaTiO_3$.

Comparison of the KNN thick film relative permittivity values with those from literature showed some variance with Ryu *et al.* stating a relative permittivity for their KNN thick film

of 116 on a Si wafer (Ryu, et al., 2007), while Kosec *et al.* (textured KNN on alumina substrate) with a room temperature relative permittivity of 540 and a peak value of 6000 (Kosec, et al., 2010). The highest value for a doped thin film reported was 815 (Abazari & Safari, 2009). The KNN bulk sample tested showed a peak room temperature relative permittivity of 620.

While a decrease was seen in the observed *tanδ*, these were still very high when compared to PZT. The continuing high *tanδ* coupled with unstable and high ε^{T}_{33} highlighted the issue raised earlier that the high imaginary part of the permittivity (associated with the dielectric loss mechanism) was making a larger contribution to the overall relative permittivity than the real part of permittivity (related to AC capacitance) within these KNN samples, thus giving anomalously high capacitance readings.

The sol base-layer did not appear to have a large effect on the d_{33} as seen from *Figure 49*.

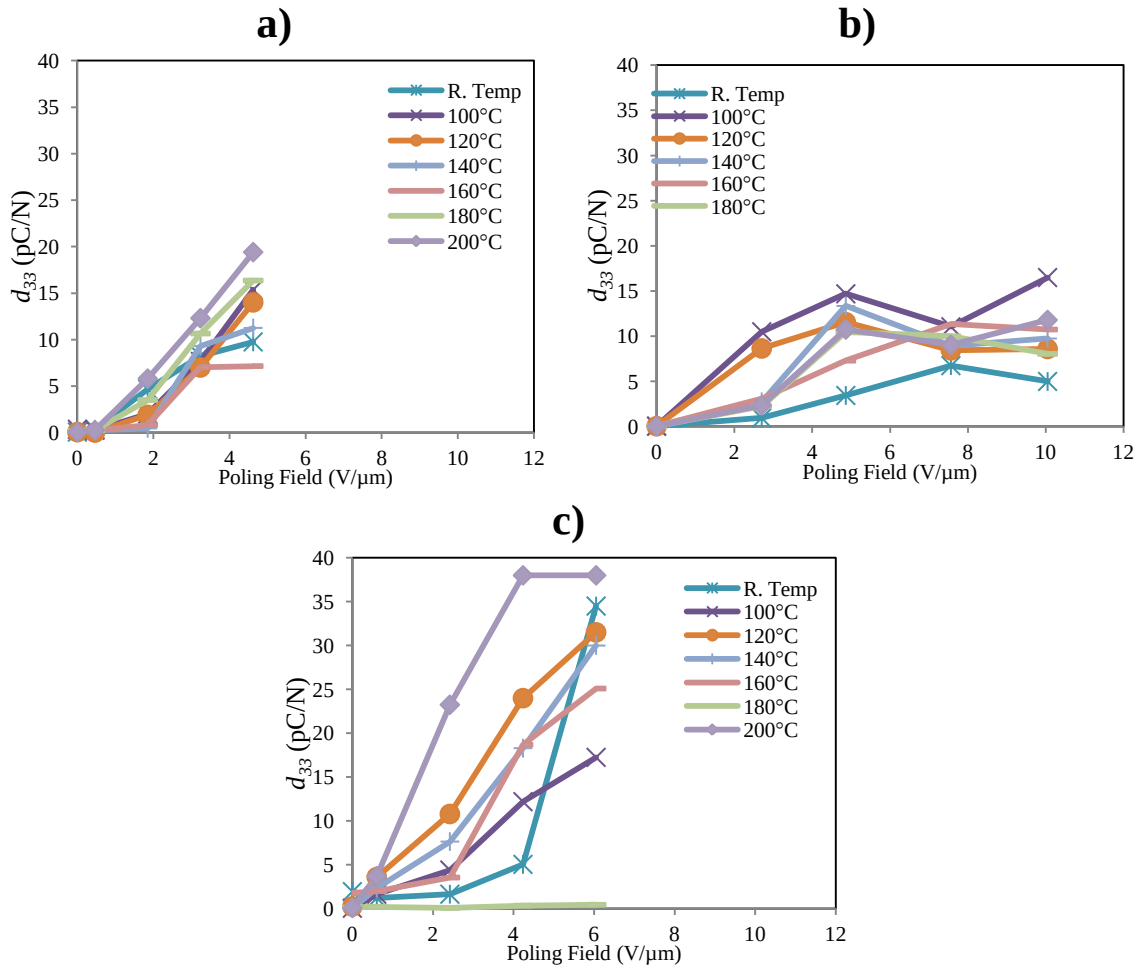

Figure 49 d_{33} as a function of poling voltage of two composite thick films tested at increasing poling voltages and a series of increasing temperatures. **a)** KNN **5S**[4(C+2S)] Thick Film; **b)** KNN **10S**[4(C+2S)]; **c)** PZT 4(C+2S) Thick Film (electrode failure occurred at 180°C hence poor reading)

Taking into account the different poling fields and thicknesses of each film tested, the KNN 5S[4(C+2S)] thick film has a peak d_{33} of 19pC/N at a poling field of 4.6 V/µm and the KNN 10S[4(C+2S)] thick film has a peak d_{33} of 13.35pC/N at a poling field of 4.9 V/µm, while the PZT thick film had higher d_{33} values with a high of 38pC/N at a poling field of 4.23 V/µm. These values are still a lot lower when compared to thin film and bulk KNN values that are reported; with lowest KNN thin film d_{33} reported with 46pC/N (Nakashima, et al., 2007); the highest for the KNN thin film of 450pC/N (Maiwa, et al., 2007). The highest recently

reported d_{33} figure for a doped KNN (KNN-LT) thick film has been reported by Hansen et al at 80pC/N (Hansen, et al., 2009).

Several authors have suggested that high *tanδ* would lead to a sample that is unable to store charge and therefore difficult to pole, leading to low d_{33} properties, which is true if the resistive element is the cause of high loss; the KNN samples, despite the high *tanδ* were able to exhibit reasonable d_{33} properties. This implies that while the resistive element within the KNN thick films appeared to be an issue, the effects were not so pervasive to affect the ability to polarise the domains to obtain reasonable d_{33}.

Bulk KNN exhibits acceptable d_{33}, *tanδ* and ε_r, but when deposited onto a Si-wafer in the thick film format, increased complexities resulting in more permutations of interactions such as the composite sol-gel, Si wafer interaction with the film, lower calcination temperatures etc. appeared to all have an effect on the piezoelectric and dielectric properties of the KNN thick films.

5.7. Impedance analysis of KNN thick films

The KNN thick films showed consistently high dielectric loss data with inconsistent relative permittivity properties indicating the detrimental effects the dielectric loss characteristics had on the KNN films overall dielectric properties. Within the film, a complex mechanism appeared to be in operation that may be caused by a number of competing factors i.e. alkali loss, porosity, extra-phases, impurities and a mutually destructive powder-sol interaction. Taking into account the limitations faced by the single frequency measurements of *tanδ* and ε_r, impedance measurements over a range of frequencies were performed. The impedance of

KNN films (0.005-13000kHz) is shown in *Figure 50* and compared to that of a PZT thick film.

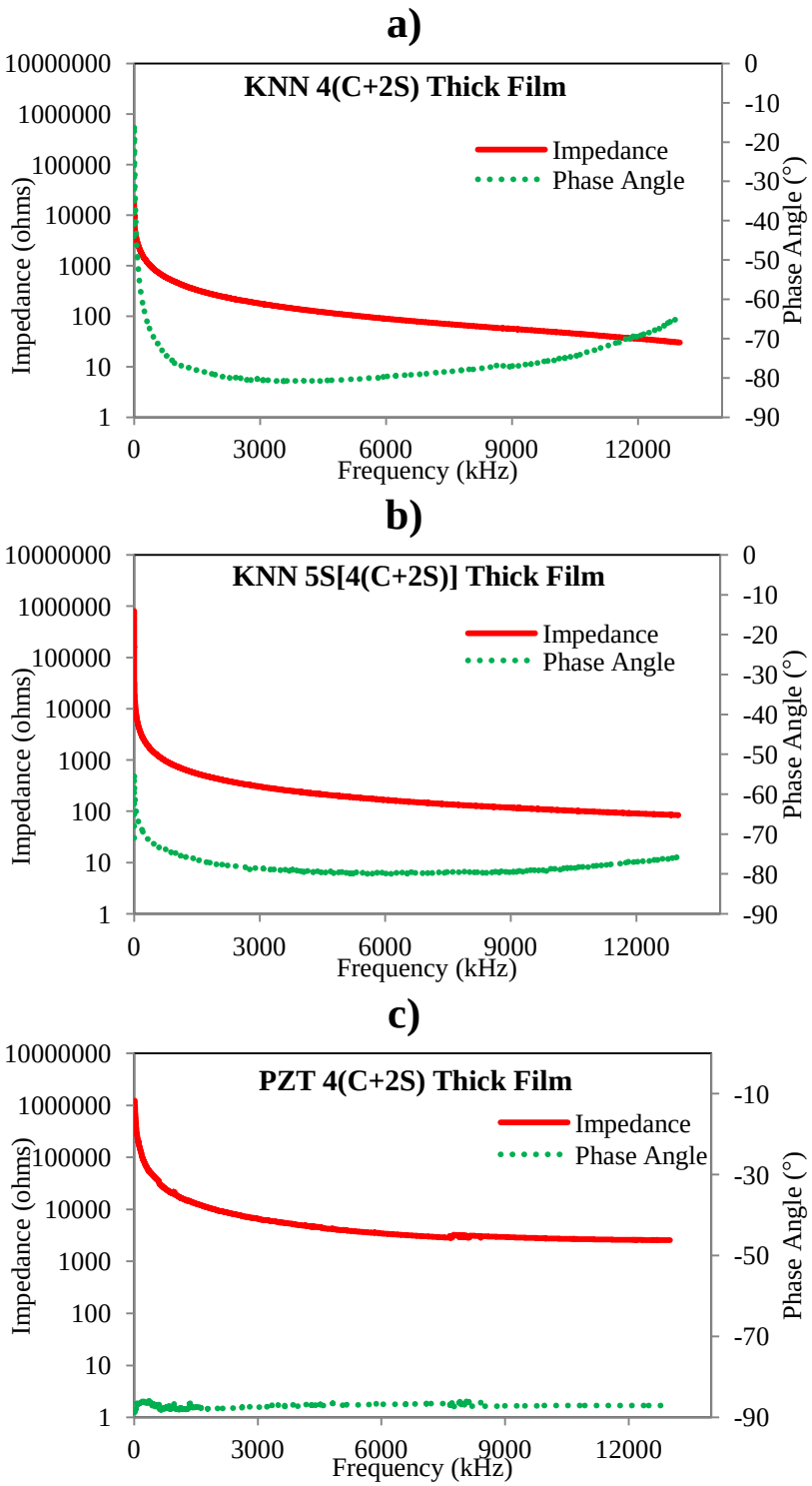

Figure 50 impedance measurement of thick films over a range of frequencies (10Hz-13MHz) **a)** MHS KNN 4(C+2S) thick film; **b)** MHS KNN 5S[4(C+2S)] thick film; **c)** PZT 4(C+2S) thick film

The PZT thick film sample showed a phase angle close to -90° which remained largely constant over the entire frequency range while the phase angle of the KNN samples changed with increasing frequency. The phase angles of the KNN thick films were quite similar, showing low values closer to 0° at low frequencies, increasing towards -90° midway and getting closer to 0° at higher frequencies with neither sample getting as close to -90° as the PZT sample.

As the capacitance and dielectric loss measurements on the Wayne-Kerr were undertaken at 1 kHz a comparison of the data from the Wayne Kerr and the Hewlett Packard LF Impedance Analyzer at 1 kHz is shown on *Table 15*, with the impedance phase angle converted to *tanδ*.

Table 15 showing inter-relationship between dielectric loss & impedance at 1kHz for KNN and PZT thick films

Impedance measurements at 1kHz					
	Phase Angle	*δ*	*tanδ*	*tanδ (%)*	*tanδ* (from Wayne Kerr) Un-Poled
KNN 4(C+2S)	-23.48°	-66.52°	2.302	230.2%	>100%
KNN 5S[4(C+2S)]	-57.78°	-32.22°	0.6302	63.02%	36%
KNN Bulk Disc	-85.85°	-4.15°	0.0726	7.26%	27%
PZT 4(C+2S)	-88.70°	-1.3°	0.0227	2.27%	6%

Taking into account that the data is taken from two different machines, the trend however is clear i.e. phase angles (*Table 15*) corroborated the *tanδ* results. The 4(C+2S) KNN thick film had very low impedance phase angle and very high dielectric loss, suggesting very poor capacitive ability; while the 5S[4(C+2S)] KNN thick film showed an improvement over the former, but was still poor when compared to the KNN bulk disc and the PZT sample as seen from *Figure 50*. Calculation of the *Q-factor* for each sample at 1 kHz further highlighted, the pervasive effects of the resistive element had on the overall impedance of the KNN thick films, with the 4(C+2S) KNN thick film displaying a *Q-factor* of 0.3; while the 5S[4(C+2S)] KNN thick film exhibited a *Q-factor* of 1.5. The bulk KNN sample displayed a *Q-factor* of 13.78 at 1 kHz; highlighting the huge difference in the characteristics of the resistive element

within the KNN thick films and the KNN bulk sample. Impedance analysis provided clarity in the electrical characterization of the thick films and so further analysis of the samples was carried out.

5.8. Summary

The initial issue with the Na ion-rich niobate powder was solved and KNN thick films were produced successfully. PZT thick films and bulk ceramic KNN discs were used as quantitative benchmarks and the KNN thick films were found to fall short of these benchmarks. The main differences between the KNN thick films and the KNN bulk samples i.e. processing, chemical and physical characteristics were investigated. These differences resulted in thick films with poor dielectric properties i.e. very high *tanδ*, inconsistent capacitance and relative permittivity properties and poor piezoelectric properties.

Evidence of imbalanced stoichiometry of the KNN powders was observed and further large scale alkali loss was noted to occur during calcination resulting in KNN thick films with highly imbalanced stoichiometries, that it was thought would result in highly porous films. It is worth noting that despite the large alkali losses that resulted in an imbalanced stoichiometry the material displayed a piezoelectric response as KNN is piezoelectric from a purely $KNbO_3$ sample to a sample containing 90% $NaNbO_3$. Substrate-film inter-diffusion was thought to occur and resulted in as yet unidentified extra-phases being produced. Comparison of S-FEG SEM micrographs of a KNN film to that of a PZT film showed no difference in density.

Increasing the amount of sol infiltrations proved detrimental to the dielectric properties of the film. That result combined with the result where a thick film, heat treated at 800°C, a

temperature that appeared to crystallise and densify the sol further, resulting in a film with low *tanδ* suggested the KNN sol may contribute to the poor and erratic dielectric properties.

A ZrO_2 buffer layer inserted onto the Si substrate to reduce inter-diffusion between the silicon and the KNN thick films, did not result in improvements to the key measured parameters and further investigation was abandoned. Introduction of a sol base-layer applied prior to the deposition of the main thick film resulted in the creation of a barrier layer that drastically improved the dielectric properties of the KNN thick films.

Chapter 6

6.Doped KNN thick films

6.1. Introduction

Doped KNN powders produced using the MHS and the ssMSS routes were used to produce KNN thick films. Un-doped KNN thick films were thought to suffer from high porosity due to alkali volatilisation, film-substrate inter-diffusion etc. and the sol acting as an impurity that was detrimental to the piezoelectric and dielectric properties of the KNN thick films. The use of dopants was generally expected to improve the piezoelectric and dielectric characteristics of the thick films, by improving densification and as a consequence their addition was expected to lead to a reduction in *tanδ*. It was envisaged that the introduction of the dopants would alter the concentration of oxygen vacancies and influence the structure and lattice energy of the eventual KNN thick film, since ionic sizes and charges of the dopants used, differ from those of the KNN constituents (Zhang & Whatmore, 2001). Oxygen vacancies in KNN films are said to be formed, because of the occurrence of alkali ion loss during the heat treatment process, leading to stoichiometric imbalances resulting in high *tanδ* (Wang, et al., 2010). Oxygen vacancies affect the structure of piezoelectric ceramics, causing the direction of spontaneous polarization to be affected within the crystal lattice, by either reducing or increasing the polarizability of the domains (Eichel, et al., 2009). Thus when comparing the mechanism of *tanδ* between PZT thick films and KNN thick films, a mechanism to mirror that of PZT was sought i.e. stability in *tanδ* prior to and after electrical poling at elevated temperatures. It was established that the presence of a sol base-layer improved the electrical properties of the KNN thick films and therefore was incorporated into the processing of the doped KNN thick films.

6.2. A-site doping

Lithium and Calcium doped KNN powders were used to make KNN thick films with the levels selected at 6% atomic mass of Li and Ca, by substitution at the A-site. Amongst the numerous benefits that may be accrued from the use of Li and Ca dopants, the most desired effects were improved density and as a consequence enhanced piezoelectric and dielectric results were envisaged. Films were tested for their piezoelectric and dielectric properties and compared to PZT and un-doped KNN thick films (*Figure 51*).

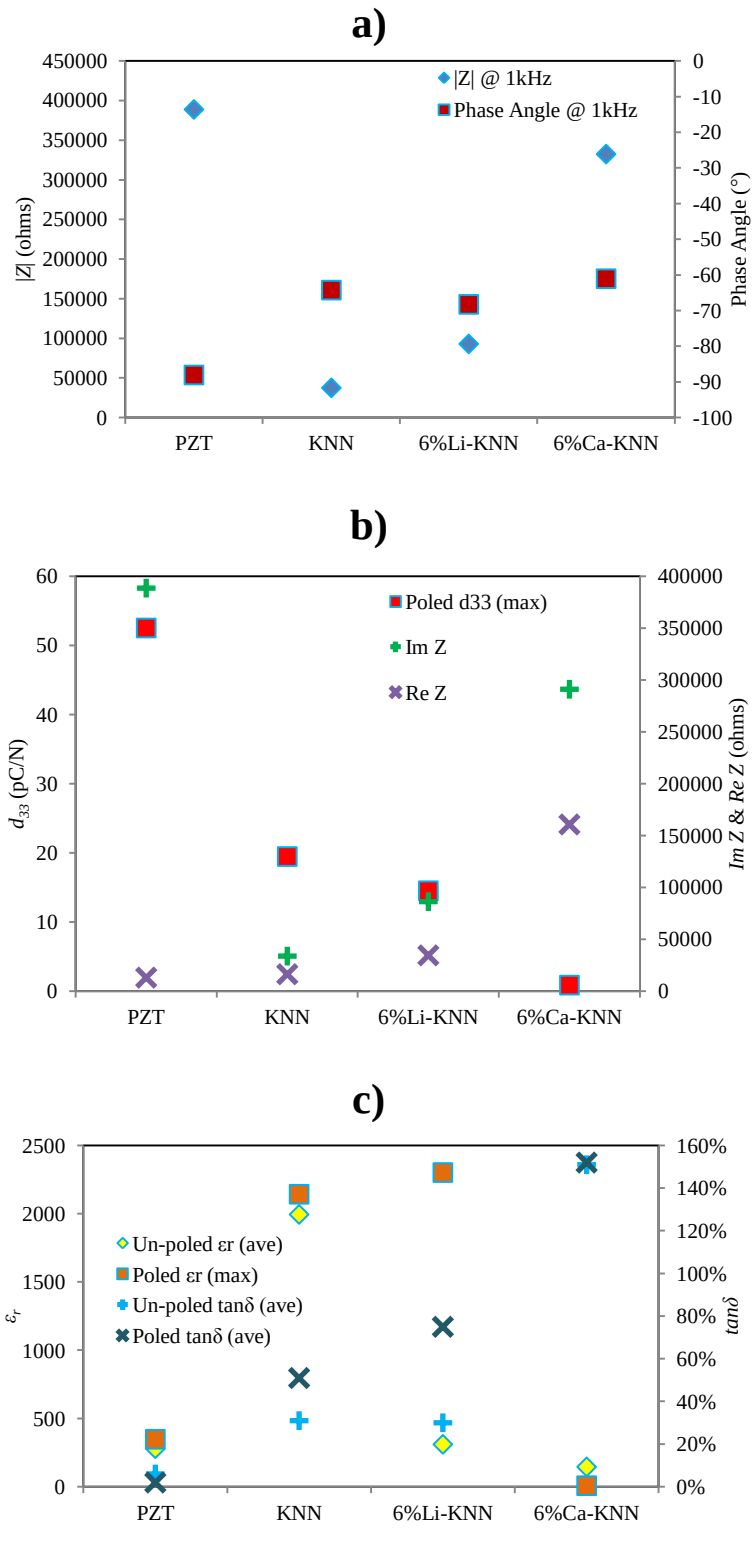

Figure 51 dielectric & piezoelectric properties of Li & Ca doped KNN thick films compared with those of PZT and un-doped KNN thick films; **a)** magnitude of impedance and phase angle, **b)** the real and imaginary parts of impedance and the piezoelectric coefficient results, **c)** relative permittivity and dielectric loss results measured prior to and after electric poling.

The piezoelectric and dielectric results shown in *Figure 51* of the two doped KNN thick films did not show the envisaged improvement in measured properties over an un-doped KNN thick film; and compared unfavourably to the PZT sample. The PZT sample displayed a phase angle of -88.1°; a large *Q-factor* of 30; very high d_{33} (when compared to KNN results) of 52.5pC/N with extremely low *tanδ* before and after electrical poling (6% & 2% respectively) with a ε^{T}_{33} of 348 after electrical poling.

The phase angles of the two doped KNN films were similar to that of the un-doped KNN sample; with the Li doped KNN film showing an improved phase angle of -68.3° (*Figure 51a*). The magnitude of impedance was very different between the three samples and was highest for the Ca doped film when compared to the un-doped KNN and the Li doped film. With all three KNN samples displaying near similar *Q-factors* i.e. un-doped KNN – 2.1, Li-KNN – 2.5 and Ca-KNN – 1.8; the large magnitude of impedance displayed by the Ca doped KNN sample (*Figure 51a*) was shown to be tempered by a very high resistive element present in that sample when compared to the other two (*Figure 51b*) resulting in a sample with much worse dielectric properties (*Figure 51c*). When compared to the PZT sample the resistive element of the KNN samples was much more prominent with respect to the capacitive reactance element which would result in dielectric results of lower quality when matched up to PZT.

The d_{33} displayed by these doped thick films was not much of an improvement on earlier un-doped KNN thick film samples produced, with the Ca doped film exhibiting a low d_{33} of 0.85pC/N (*Figure 51b*), indicating a poor polarizability. The Li doped thick film had a peak d_{33} of 14.5pC/N, which was lower than the un-doped KNN thick film.

The predicted *tanδ* reduction from the addition of A-site dopants was not achieved. The materials displayed high *tanδ* prior to electrical poling, with the Ca doped film being particularly poor (*tanδ* >100%) and the Li doped film matching the un-doped KNN thick film. After electrical poling the *tanδ* of the Li doped thick film (75%) worsened much more than the un-doped KNN film (51%) (*Figure 51c*) though both displayed the common KNN *tanδ* mechanism i.e. increasing after electrical poling at elevated temperatures. Considering the ε_r of KNN bulk sample and values seen in literature the results achieved with these doped thick film samples were not considered to be representative of the material, rather it was hypothesised that an already complex dielectric was further complicated by the addition of the dopants leading to such highly diverse results in relative permittivity. The A-site dopants did not produce the envisaged improvements in both piezoelectric and dielectric results.

The dopants were expected to occupy the A-site cation vacancies that result from alkali volatilisation (Fu, et al., 2011) and thus produce improved dielectric and piezoelectric characteristics. This goal was not achieved most likely due to the dominance of the porosity effects in the thick films relative to KNN bulk materials.

6.3. Transition metal doping

Transition metals were used to dope the KNN powders (all produced using ssMSS route) and these were processed into KNN thick films (using sol base-layer and 4(C+2S) deposition technique). An improvement in piezoelectric and dielectric characteristics was sought with the use of the transition metal dopants. Due to their multiple oxidation states they are able to occupy cation vacancies and absorb oxygen vacancies, and thus reduce the detrimental effects that accrue from these vacancies (Wang, et al., 2010).

Prior to electrical poling, impedance measurements were carried out on the samples followed by measurement of the d_{33}, $tan\delta$ and C to determine ε_r. After electrical poling at elevated temperatures the d_{33}, $tan\delta$ and C (to determine ε^{T}_{33}) measurements were carried out again at room temperature and results displayed in *Figure 52*.

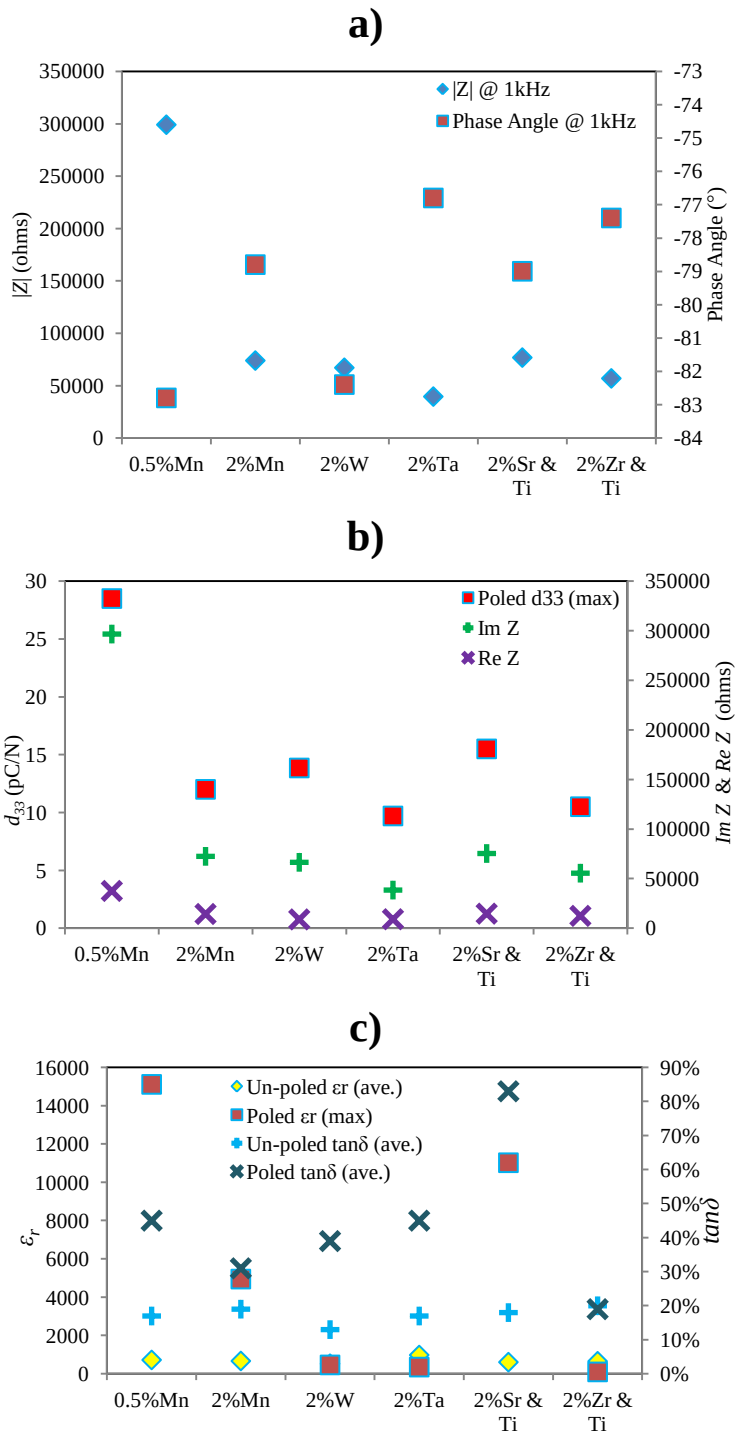

Figure 52 piezoelectric and dielectric properties of doped KNN thick films; **a)** magnitude of impedance and phase angle, **b)** the real and imaginary parts of impedance and the piezoelectric coefficient, **c)** relative permittivity and dielectric loss results measured prior to and after electric poling

The transition metal dopants considerably improved the KNN thick film phase angle properties from a previous peak of -68.3° realised with the A-site dopants; to producing several samples with beyond -76° phase angles, demonstrating a positive effect from transition metal dopants that dope both A- and B-sites. The preeminent results were achieved with the *0.5at.% Mn* and *2at.%W* doping which resulted in phase angles of -82.8° and -82.2°, respectively (*Figure 52a*), the highest achieved so far.

The *0.5at.% Mn-KNN* sample displayed a much higher magnitude of impedance (299,063 ohms) when compared to the other transition metal doped thick films (*Figure 52a*); which was due to a large increase in the capacitive reactance of this film with respect to the slight increase in the resistive element (*Figure 52b*). The other doped KNN thick films displayed lower levels of the resistive element when compared to the *0.5at.% Mn-KNN* sample, but with much lower reactive elements. All the samples displayed superior *Q-factors* at 1 kHz compared to earlier samples, which matched the un-doped KNN sample heat treated at 800°C, though not achieving PZT-like levels. The best doped KNN sample had an imaginary to real part of impedance ratio of 7.9 (*0.5at.% Mn-KNN sample*) (*Figure 52b*), when compared to previous samples (highest at 2.5).

Overall the impedance data indicated that the use of transition metal dopants affected the physical properties of the KNN thick films positively, by improving the phase angle data and the much improved *Q-factors*, achieved by larger increases in the reactive element of the materials when compared to the moderate increases seen in the resistive element. The impedance data further indicates that use of the transition metal dopants leads to an increase in the capacitive properties of the doped KNN thick films.

The d_{33} results were quite similar to results of previous un-doped KNN thick film samples which in several cases had d_{33} results that were higher than those of some of the doped KNN samples (*Figure 52b*). The *0.5at.% Mn-KNN* sample displayed one of the highest d_{33} results (28.5pC/N) of any KNN sample so far and coupled with the favourable impedance data may explain the higher d_{33}. Manganese is known to reduce domain size and hence increase the density of the ceramic's domains which in turn improves the piezoelectric characteristics (Lin, et al., 2010); though with the data matching those of earlier un-doped samples, it was established that the effect on the d_{33} of the transition metal dopants was negligible and the increase in the capacitive reactance element of the materials impedance did not translate into improved permanent polarization within the film that would lead to increased piezoelectric functionality. The dopants induce structural instabilities in the KNN leading to the enhancement of its electromechanical properties which may be induced by compositional instability (MPB), thermal instability (PPT), stress fields and in this case by the application of external electric fields (Rodel, et al., 2009).

Following the impedance result that predicted that these thick films would produce much improved capacitance characteristics, the ε_r prior to electrical poling a ε_r comparable to data from literature. The *0.5at.%-Mn KNN* thick film exhibited a recorded ε_r of 728 while the *2at.% Ta-KNN* sample had ε_r of 983 prior to electrical poling (*Figure 52c*).

The ε^T_{33} results after electrical poling at elevated temperature indicated the possibility that the films had broken down as the results were extremely inconsistent with some samples showing vastly increased ε^T_{33} while others showed dramatic drops in ε_r levels (*Figure 52c*).

Tanδ response followed a similar trend to earlier un-doped KNN samples that contained the sol base-layer. Prior to electrical poling the transition metal doped thick films displayed low

tanδ, with the *2at.% Zr & Ti-KNN* sample recording the highest *tanδ* (20%) and the *2at.% W-KNN* sample displaying a *tanδ* of 13%. After electrical poling the *tanδ* increased for all samples, with the exception of the *2at.% Zr & Ti-KNN* sample. The *tanδ* result for the *2at.% Zr & Ti-KNN* sample, remained largely unchanged after electrical poling at, with a *tanδ* of 19%. A thick film sample prepared from a KNN powder with *25at.% Zr-Ti* displayed similar *tanδ* behaviour, with a *tanδ* result prior to poling of 15% and after electrical poling of 16%. While the *tanδ* of the *2at.% Zr & Ti-KNN* sample did not match that of PZT the notable departure from the behaviour of other KNN thick films produced, was a promising development which suggests a positive line for future investigation. The Zr and Ti co-dopants are thought to have better control of the development of cation vacancies/holes and anion vacancies in the KNN thick films, leading to a reduction in *tanδ*. Ti has multiple oxidation states (Ti = +2, +3, +4) while Zr has a high oxidation state (+4) and thus may act together to neutralise different electric issues present in the electrically complex KNN thick film.

The higher *tanδ* results seen with most of the KNN thick films, reduced potential for the samples to be polarized completely as a large amount of electrical energy that drives polarisation was shielded thus resulting in d_{33} that may be lower than the materials real potential (Lin, et al., 2010). The complex microstructure found in thick films, results in material defects in the ceramic (e.g. porosity, dislocations, oxygen or cation vacancies, impurities) which are major source of *tanδ*. Each defect causes a correction in the surrounding ions relative to their state when the defect is absent and as a consequence induces screening charges which act against the polarization induced by the applied electric field (Dauchy, 2007). The envisaged overall improvements to the film by the use of dopants were not observed due to either one or more defects prevalent in the KNN thick films, though singular advances in various parameters i.e. *tanδ* control with the use of Zr and Ti doping and

superior measured impedance characteristics with the use of transition metal dopants were observed.

6.4. Summary

Numerous dopants were examined to observe the effect that they had on the piezoelectric and dielectric properties of KNN thick films which in the un-doped form suffered from extremely high *tanδ*, inconsistent *relative permittivity* and poor d_{33} data. No large scale improvement in these properties was observed with the use of most of the dopants with the exception of the Zr-Ti doped thick films that displayed stable *tanδ* results before and after elevated temperature electrical poling which was a departure from the observed behaviour of most other KNN samples i.e. much higher after electrical poling. This suggested the ability of doping to improve the KNN microstructure, leading it to adopt a different mechanism controlling *tanδ*; providing scope to improve this particular parameter with the use of this mix of dopants and possibly others, showing direction for future study.

Large improvements in the phase angles were noted with the use of aliovalent dopants; with several displaying phase angles above -76°, where previously with un-doped KNN thick films, all phase angles were between -20° to -65°. Some samples consistently displayed phase angles above -80° indicating a positive effect on the dielectric characteristics of the KNN thick films by some of the dopants. These improvements resulted in increases in the capacitive reactance of the doped KNN films that were much larger than the slight increases seen in the resistive element of the films. A hypothesis for this improvement is that the dopants control the negative effects of ion vacancies and improve film density.

The ε_r results were highly inconsistent showing huge differences prior to and after electrical poling when compared to those of the KNN bulk samples produced in this work and literature data for KNN bulk, thick and thin films and the in-house processed PZT samples. The consistently high dielectric losses and poor impedance relative to a similar PZT sample that the KNN thick film samples were exhibiting were thought to be responsible. This suggests a need for further investigation of the intricacies of interactions within the KNN thick films, in order to reduce the pervasive effect that the resistive element within the films have and increase the reactive element, to improve KNN thick film capacitance and in turn the piezoelectric and dielectric properties of the films.

Chapter 7

7.Effect of heat treatment & sol base-layers on KNN thick films

7.1. Introduction

With the underlying issues of extremely high levels of *tanδ*, erratic relative permittivity, d_{33} levels not displaying materials potential all highlighted by the poor impedance properties; a better understanding of the effects that physical and processing changes have on these parameters was sought. An investigation of the effect of calcination temperatures was carried out, as it plays an important role in helping to achieve the optimal structure and electrical properties of the ceramic. A study into the effect of sol base-layers, on piezoelectric and dielectric properties of un-doped KNN thick films, was also carried out to assess the overall impact the high density interface had on the measured properties.

The heat treatment temperatures selected were from 650°C, increasing at each step by 50°C to a maximum of 800°C. The samples investigated varied from those without a sol base-layer deposited i.e. 4(C+2S), to a maximum of 3 sol base-layers deposited as shown in *Table 16*. All the powders were made by the MHS method and all samples had 4(C+2S) composite sol-gel deposition as standard applied after the sol base-layer was applied. *Z*, d_{33}, ε_r and *tanδ* measurements were made prior to each sample being electrically poled at elevated temperatures and the d_{33}, ε^T_{33} and *tanδ* measured after poling and once cooled to room temperature.

Table 16 the sol base-layers deposited and the heat treatment temperatures utilised for each sample

Sample Reference	No. of Sol base-layers	Heat Treatment Temperature
PZT	3S	700°C
0S-650°C	0S	650°C
1S-650°C	1S	
2S-650°C	2S	
3S-650°C	3S	
0S-700°C	0S	700°C
1S-700°C	1S	
2S-700°C	2S	
3S-700°C	3S	
0S-750°C	0S	750°C
1S-750°C	1S	
2S-750°C	2S	
3S-750°C	3S	
0S-800°C	0S	800°C
1S-800°C	1S	
2S-800°C	2S	
3S-800°C	3S	

7.2. Effect of heat treatment and sol base-layers on the dielectric properties prior to electrical poling

The effect that increasing sintering and various sol base-layers had on the dielectric properties prior to the application of an electric field on the KNN thick films was investigated. Because of the random distribution of the domain orientations within the thick film there is an almost uniform distribution of spontaneous polarization directions among the domains and therefore no macroscopic piezoelectric behaviour is present at this stage and the material is isotropic.

7.2.1. *Z* prior to electrical poling

The effect of the sintering temperature and the sol base layer had on the magnitude of impedance of KNN thick films is shown in *Figure 53*.

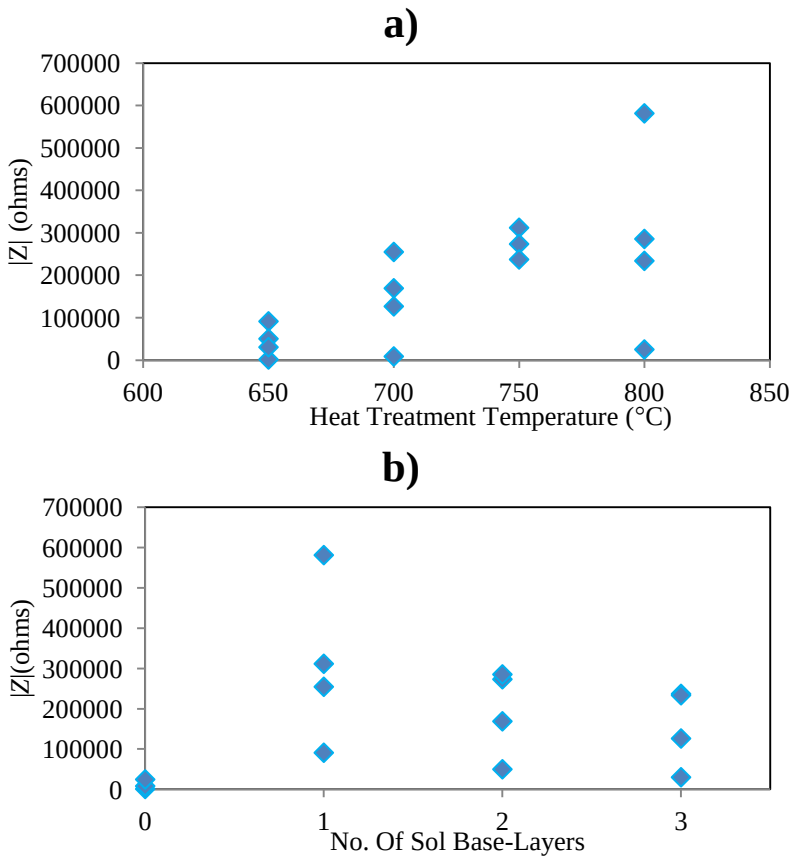

Figure 53 the magnitude of impedance of KNN thick film samples as a function of **a)** heat treatment temperature; **b)** sol base-layers

As the sintering temperature is increased the magnitude of impedance generally increases (*Figure 53a*). This suggests increased crystallisation and lower porosity. *Figure 53b* shows the lower magnitude of impedance displayed by the four samples lacking the sol base-layer with a low of 1,148 ohms and a high of 24,737 ohms; when compared to samples with this layer present which exhibited a low of 30,167 ohms displayed by the sample heat treated at 650°C and a range from 126,367 ohms to 581,333 ohms for samples with the base layer heat treated at above 700°C.

The effect that increasing heat treatment temperature and sol base-layers had on the phase angle prior to electrical poling of the KNN thick films was investigated (*Figure 54*).

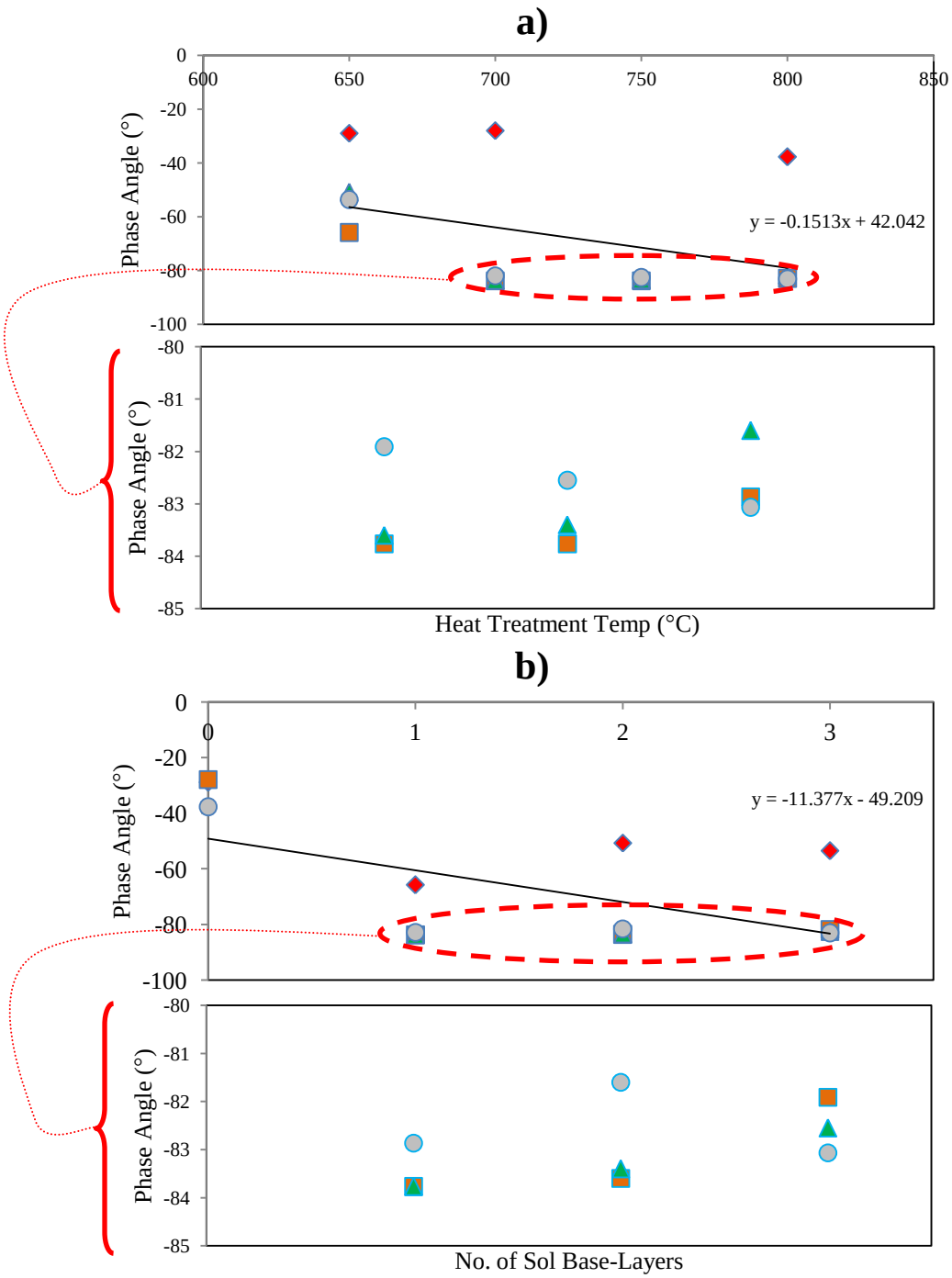

Figure 54 trend of the phase angle of KNN thick film samples as a function of **a)** heat treatment temperature; **b)** the number of sol base-layers deposited.

a) Sol base-layers ◆ – 0 sol layers; ■ – 1 sol layer; ▲ – 2 sol layers; ● – 3 sol layers.
b) Heat treatment temp. ◆ – 650°C; ■ – 700°C; ▲ – 750°C; ● – 800°C.

As with the magnitude of impedance data an improvement in the phase angle as the sintering temperature is increased is observed. At 650°C the phase angle results range from a low of -28.9° peaking at -65.8°; whereas the samples heat treated at between 700°C and 800°C exhibited a phase angle range beyond -81° when samples without a base layer are excluded. Increasing the sol base-layers leads to an improvement in the phase angle of samples measured prior to electrical poling. The samples without a sol base-layer had low phase angles (*Figure 54a*) with samples displaying phase angles between -28° to -38°. These results highlighted the significance of the sol base-layer, as it improves the phase angle of the thick films to similar levels seen with doped KNN thick films i.e. beyond -50°. *Figure 54a* & *b* also show a closer observation of the congested phase angle results of samples with sol base-layers heat treated at 700°C and above which displayed phase angle data beyond -80°. Little change is observed in the phase angle as the amount of sol base-layers is increased from 1 to 3. The thick films heat treated at 650°C clearly exhibited the worst phase angles across the board, indicating this temperature does not realise the full potential of the material (*Figure 54a*).

The *Q-factor* highlights in a simplified manner what conclusions may be drawn from the impedance data. The significance of the sintering temperature range of 700°C – 800°C and the use of the sol base-layers are shown by the impedance data to produce the optimal results. The KNN thick films within these bands displayed a range of *Q-factors* between 6.8 and 9.2. Samples heat treated at 650°C and without the sol base layer had low *Q-factor* data ranging from a low of 0.4 to a high of 2.2 indicating a much lower ratio of the energy stored to the energy dissipated per A.C. cycle. Noting the results achieved throughout the research of KNN thick films, it was understood that the impedance data was a good predictor of samples that would exhibit high $tan\delta$ and erratic ε_r.

7.2.2. *Tanδ* prior to electrical poling

Knowing that *tanδ* is equal to the tangent of the angle between a capacitor's impedance vector and the negative reactive axis, similarity with the results was expected and observed. Thus samples with low *tanδ* displayed phase angles beyond -80° while those with poor phase angles exhibited high levels of *tanδ*. It has been established from the impedance data that samples heat treated at 650°C and samples without the sol base-layer exhibited poor impedance data overall. *Figure 55a* & *b* show the *tanδ* results of the KNN thick films, with samples heat treated at 650°C and without the sol base layer removed.

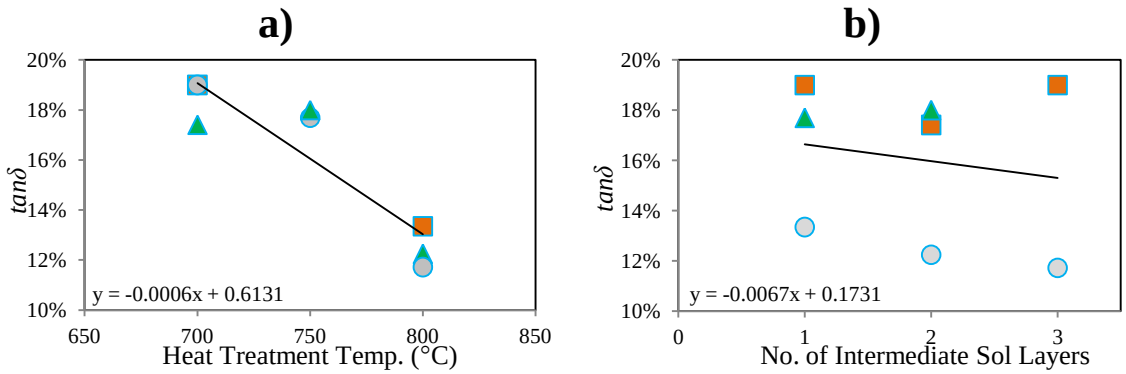

Figure 55 trend of *tanδ* of un-poled KNN thick film as a function of **a)** heat treatment temperature and **b)** the number of sol base-layers

a) Sol base-layers – 1 sol layer; ▲ – 2 sol layers; ● – 3 sol layers.
b) Heat treatment temp. – 700°C; ▲ – 750°C; ● – 800°C.
Note – *Sample 3S750°C* was an outlier and ended up facing similar exclusion as other excluded data.

There is a slight decrease in the *tanδ* as the sintering temperature increases (*Figure 55a*). The effect of heat treatment temperature at both 700°C – 750°C appears to be similar. Samples treated at 800°C with the sol base-layer display the lowest *tanδ*, indicating the higher sintering temperature is a beneficial aid to reducing the dielectric loss of the KNN thick films.

Increasing the number of sol base-layers reduces the *tanδ* of the KNN thick films thus indicating the sol base-layer technique is a beneficial method that may be utilised to decrease the *tanδ* of KNN thick films (*Figure 55b*), as in its absence the *tanδ* is very high.

7.2.3. ε_r prior to electrical poling

Figure 56 shows the effect of sintering and sol base-layers on ε_r. Due to the high dielectric losses and the direct relation this has with relative permittivity, only measurements from samples with *tanδ* of <20% were considered. Samples heat treated at 650°C and those without the sol base-layer were the samples with >20% *tanδ* and the ε_r results of these sample were highly erratic ranging from lows of 1.7 to highs beyond 5000, thus justifying the exclusion. The ε_r data used is the average collected over each entire thick film.

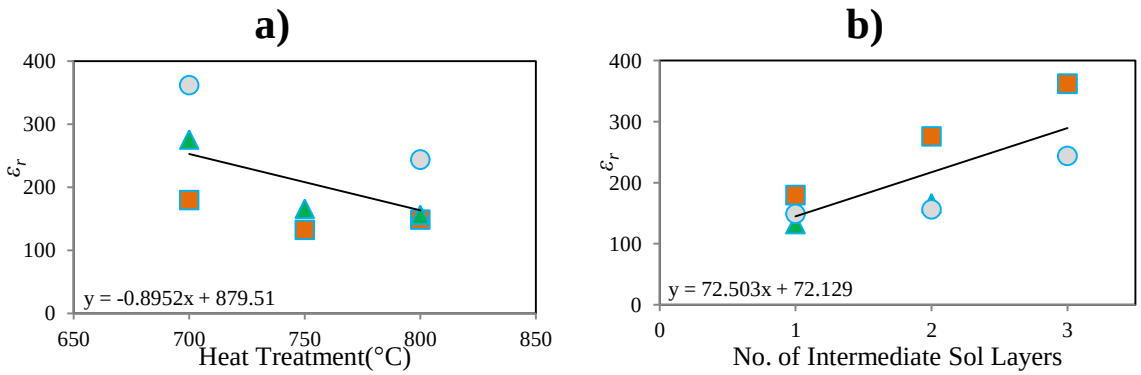

Figure 56 showing trend of ε_r of KNN thick films prior to electrical poling as a function of **a)** heat treatment temperature and **b)** the number of sol base-layers deposited

a) Sol base-layers ■ – 1 sol layer; ▲ – 2 sol layers; ● – 3 sol layers.
b) Heat treatment temp. ■ – 700°C; ▲ – 750°C; ● – 800°C.
Note – *Sample 3S750°C* was an outlier and ended up facing similar exclusion as other excluded data.

There does not appear to be a determinable trend in the ε_r as the temperature at which the KNN thick films are heat treated is increased as the results are near similar. Increasing the sol base-layers has the clear effect of increasing the ε_r; this indicates that the sol base-layer enhances the ferroelectric properties and adds more capacitive capacity to the thick films. The increases are especially pronounced with samples heat treated at 700°C.

Noting the overall dielectric results obtained throughout the research it was noted that a vast improvement in the impedance and *tanδ* data occurred during this section of the research, when compared to previous un-doped KNN thick films. The data largely matched that of the doped KNN thick films (***Chapter 6***); where it was stated the use of dopants resulted in

improved dielectric properties. This may be explained by the differences in the size of substrate used for deposition as the samples used in this chapter were diced after composite slurry deposition while samples in previous chapters were diced prior to deposition.

The composite slurry was deposited onto the centre of the silicon wafer which was then spun at high angular velocities and as the spin speed increases from zero to the maximum spin speed, centrifugal forces, drive of the slurry radially outward. Any excess slurry flows to the perimeter of the substrate and evaporates. As the viscosity of the slurry increases the effect of the centrifugal forces decreases, which results in a decrease in the amount of excess slurry that is lost. In the final stage of spin coating, evaporation of excess slurry is prominent, resulting in a reduction in the thickness of the deposited film. As a result of the equilibrium of the forces i.e. the outward flow of the slurry due the rotating forces and viscosity increases in the slurry, the uniformity of the film increases. Evaporation also tends to occur uniformly across the film assuming the film distribution is initially uniform (Tillman, 2012). Thus the deposition of the thick films in this instance on whole wafers diced after deposition, as opposed to the small sections diced from wafers prior to deposition used previously (***Chapter 5*** & ***Chapter 6***) indicated the difference in forces faced during film deposition resulting in increased performance from films deposited over larger surfaces (in this chapter) was due to increased uniformity which was the hypothesis for the vast differences observed. It was also noted that samples heat treated at 800°C did not suffer similar particle adhesion issues as an earlier sample (***section 5.4.5***) which was attributed to the use of larger substrates.

Ideally the optimal sintering temperature would promote the development of the crystal structure and aid micro-structural densification, leading to improvements in dielectric and piezoelectric properties. All the samples heat treated at 650°C, displayed higher levels of dielectric loss, poor impedance and erratic relative permittivity, whereas with the samples

heat treated at between 700°C – 800°C, the dielectric results were near similar over a range of sol base-layers. Samples heat treated at 650°C, also displayed the highest *tanδ*, worst impedance and most erratic ε_r levels of all samples with or without the sol base-layers. Thus at 650°C the results suggest the structure may not be fully developed. *Figure 57* & *Figure 58* show SEM & XRD evidence respectively, of differences in films heat treated at 650°C and 700°C.

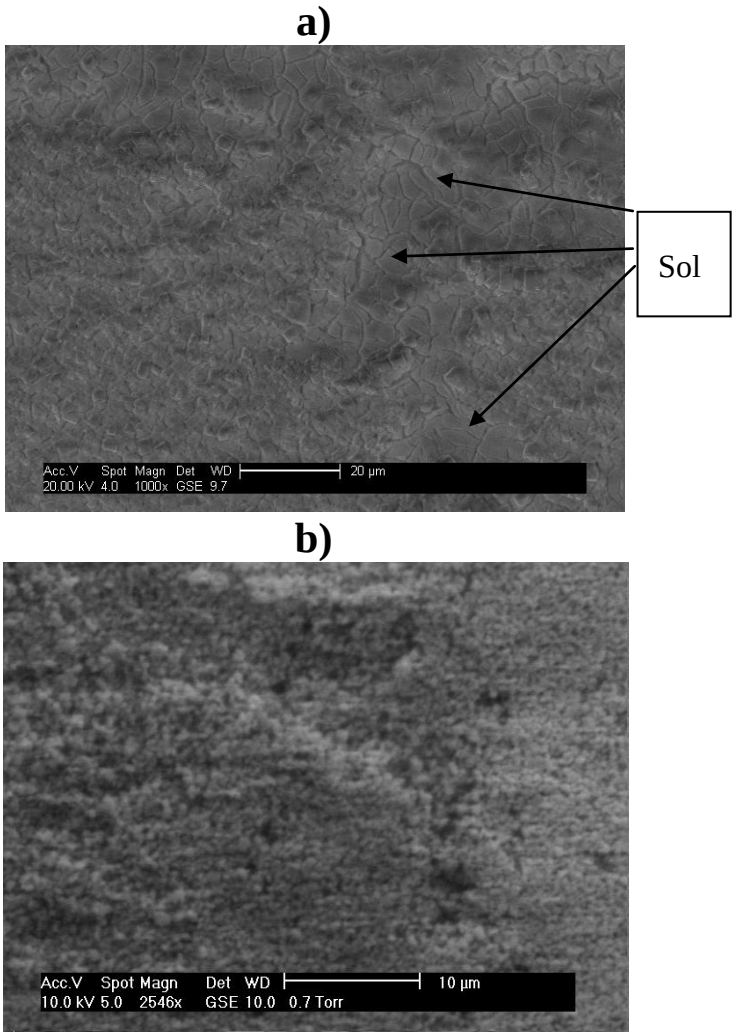

Figure 57 SEM micrographs of KNN thick films **a)** heat treated at 650°C **b)** heat treated at 700°C

Figure 57a shows areas where elements of the sol are still present as separate phases; while *Figure 57b* shows a KNN thick film sample that shows no evidence of this solidified liquid.

The solidified sol was expected to be seen in XRD analysis as an amorphous phase as a broad peak.

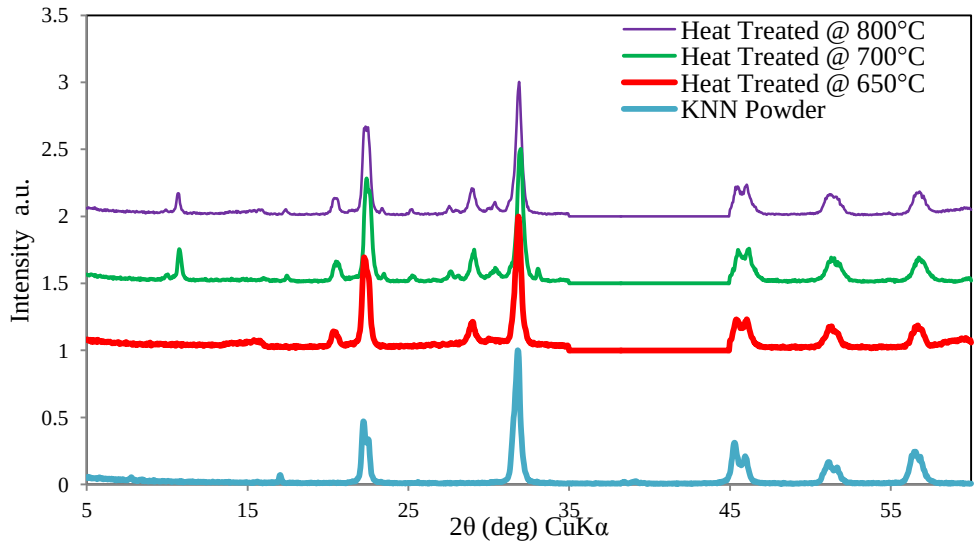

Figure 58 XRD of KNN thick films heat treated at 650°C, 700°C and 800°C with reference KNN powder.
Section 35°-44° removed as it contains Pt electrode peak

The XRD pattern (*Figure 58*) shows that KNN thick films heat treated at 650°C displayed a crystal phase structure different to that of the samples heat treated at 700°C and 800°C, with slight evidence of an amorphous phase at 15° observed. The samples heat treated at higher temperatures posses extra phases (normally leads to detrimental effects), which indicates more energy was present in the system leading to more reaction activity. The higher activity may have resulted in higher levels of KNN sol crystallisation, as well as side reactions that resulted in extra-phases. The lack of a similar phase structure in the sample heat treated at 650°C may indicate less energy present to drive the reaction resulting in a lower level of sol crystallisation. From the results two hypothesis were developed, the first being that poor crystallisation of the sol was a significant factor in the poor characteristics exhibited. The second hypothesis was that high levels of porosity within the KNN thick films heat treated at 650°C, due to the lower amount of energy present to drive the densification, was the reason for the poor properties displayed by these films.

The complex microstructure of the thick film, results in material defects in the ceramic (e.g. porosity, dislocations, ion vacancies, impurities) which are said to be a source of dielectric loss (Dauchy, 2007) and thus defects in the form of discrete amorphous KNN sol, results in the reduced functionality of the film.

The large contrast in dielectric results between samples with the sol base-layer and those without it highlight the importance of this processing step to the improvement of the dielectric properties of the films prior to electrical poling. The sol base-layer lowers the resistive component by reducing the continuous path through the system that is present in the samples that did not have the sol base-layer deposited. The sol base-layer does this by creating a layer of high resistance to the passage of current. The relative consistency of the observed ε_r results combined with the impedance and the low $tan\delta$ results serve to indicate the actual level of KNN thick films' relative permittivity.

7.3. Effect of heat treatment temperatures and sol base-layers on dielectric properties after electrical poling

The effect that increasing sintering and the deposition of the sol base-layers had on the dielectric properties after the application of an electric poling field (8-10V/μm) on the KNN thick films at elevated temperatures was investigated. The poling of the material results in the growth and alignment of domains whereby polarity of whole regions is reversed to match the electric field resulting in the irreversible displacement of the domain walls. This gives rise to the KNN thick films being polarized in the direction parallel to the applied field, and the materials are now anisotropic, i.e. piezoelectric.

7.3.1. Effect on *tanδ* after electrical poling

Figure 59 shows the effects of heat treatment and sol base-layers on *tanδ* after electrical poling of the KNN thick films at elevated temperatures. *Figure 59a* & *b* show the results of all the samples with *tanδ*, with the enlargement of congested areas with *tanδ* below 100%. The trend of *tanδ* is calculated using samples with *tanδ* below 100% as samples with *tanδ* beyond 100% are considered to be unrepresentative of the material.

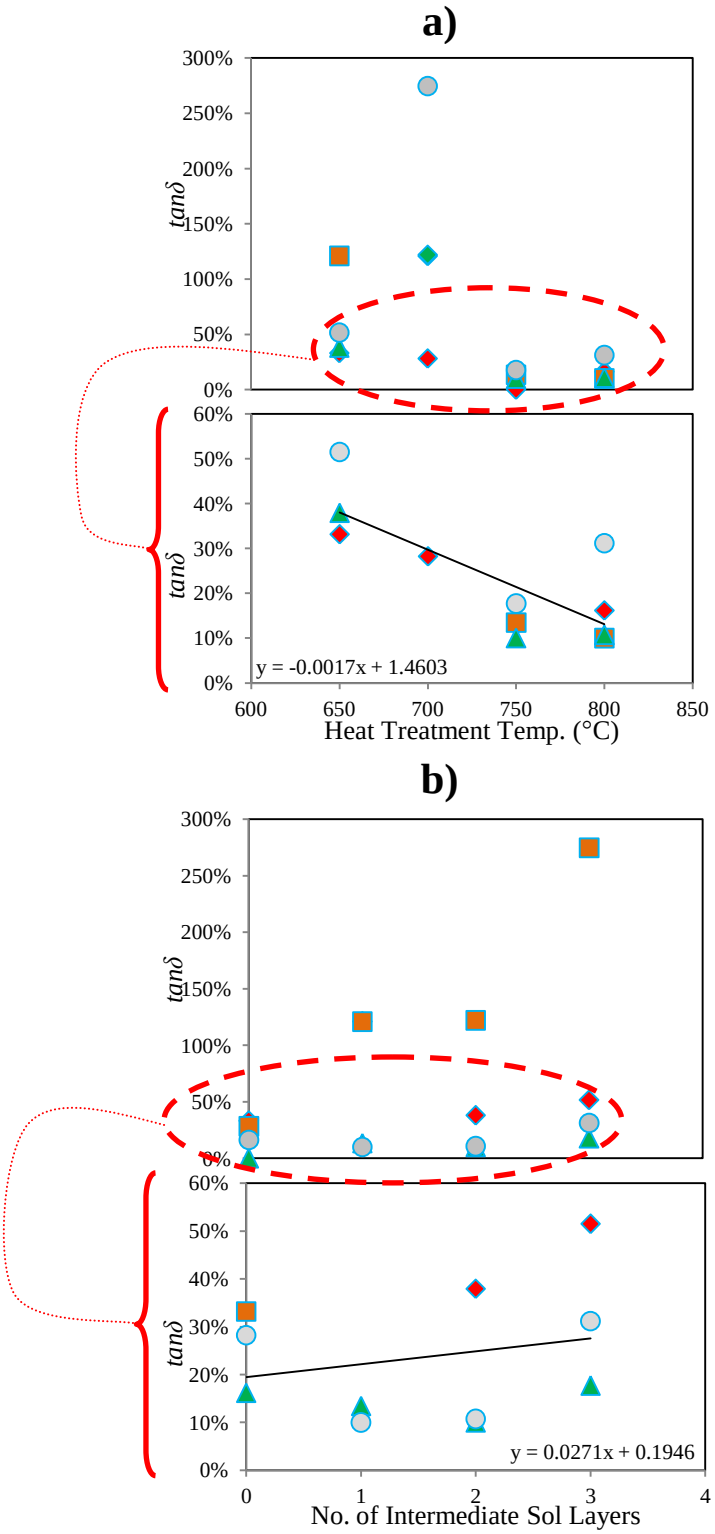

Figure 59 *tanδ* results after electrical poling as a function of **a)** heat treatment temperature; **b)** sol base-layers; enlarged areas focussing on results below 100%

a) Sol base-layers ◆ – 0 sol layers; ■ – 1 sol layer; ▲ – 2 sol layers; ● – 3 sol layers.

b) Heat treatment temp. ◆ – 650°C; ■ – 700°C; ▲ – 750°C; ● – 800°C.

Note – *Sample 0S750°C* was not included as it was a poor sample and could not be poled as its electrodes all failed.

The first thing to notice is the samples heat treated at 650°C and those without the sol base-layer performed much better after electrical poling at elevated temperatures than they did prior to this procedure. A hypothesis may be that the combined energy put into the system during this procedure i.e. electrical and heat energy, may have forced out absorbed atmospheric moisture in the thick films heat treated at 650°C. In the case of samples without the sol base-layer the KNN thick film is considered to be porous and thus absorbs atmospheric moisture prior to poling at elevated temperatures; once poling commences this is driven off resulting in improved results.

There is a decrease in the *tanδ* as the sintering temperature is increased (*Figure 59a*). Samples heat treated at 700°C (i.e. *1S700°C, 2S700°C, 3S700°C*) exhibited poor *tanδ* in some cases much higher than those of samples calcined at 650°C. It was considered that these samples may be outliers as the trend did not follow what was happening with the other samples tested, or it may be an actual effect whereby at this temperature various crystallisation effects occur that are detrimental to the material's dielectric properties which are not present at 650°C and disappear at high temperatures.

High sintering temperatures aid the reaction of the KNN sol to form the desired phase composition and remove any organic materials, water or other volatile materials left after mixing and therefore permit better homogeneity after the heat treatment.

Due to the higher levels of crystallisation of the film, this facilitates the removal of any organic materials, water or other volatile material left and thus allows for better film homogeneity with good dielectric properties. As a consequence of these facts the samples heat treated at 750°C and 800°C generally exhibited the lowest *tanδ* results ranging from lows of 10% to 31%. The level of *tanδ* also decreased drastically after electrical poling with

all samples calcined at 750°and 800°C (with the exception of *0S750°C* which suffered electrode failure and *3S800°C*) displaying *tanδ* between 10 – 18%, which was unprecedented for KNN thick films, in this research. Three samples displayed *tanδ* of 10% and 11% which matched those of the KNN bulk sample.

Tanδ as a function of the sol base-layers is quite stable with a slight increase in *tanδ*, as more sol base-layers are applied. On the whole the samples with a sol base-layer and those without a sol base-layer, registered near similar levels of dielectric loss. This implies that the electrical poling at high temperatures reduces the barrier layer effect provided by the sol base-layer, leaving the main part of the thick film (i.e. composite slurry) to dictate the properties of the entire film. This similarity in *tanδ* between the samples with a sol base-layer and those without one suggests in earlier testing prior to electrical poling, the sol base-layer was dictating the measured property characteristics or reduced the negative response witnessed in samples without the barrier layer.

A general examination of the results shows several samples that possessed high levels of *tanδ* prior to electrical poling and after this process exhibited reductions in the level of dielectric loss; which was a characteristic contrary to that previously displayed by KNN samples. This phenomenon never observed before with KNN thick films in this research, was displayed by low heat treatment temperature samples and high heat treated temperature samples; as well as samples with and without the sol base-layers. This further highlights the hypothesis that porosity within the films is exploited by atmospheric moisture which affects the measured dielectric properties prior to electrical poling. After electrical poling the moisture evaporates allowing for more representative measurement of the dielectric characteristics across all the samples.

Since the sol base-layer acts as a good barrier at 700°C and beyond, prior to electrical poling, this implies that at these sintering temperatures a full crystallisation of the sol throughout the thick film occurs. Therefore it is not incomplete crystallisation of sol present in both the sol base-layer and the main composite thick film that is responsible for poor properties seen with samples heat treated at 650°C; rather it must be the porosity of the thick film that is responsible for the poor impedance and dielectric loss results overall, as shown by the eventual reduction in the high electrical resistance provided by the sol base-layer. With the reduction of the barrier resistance of the sol base-layer following electrical poling at high temperatures the porosity of the KNN thick films dictates the dielectric properties of the entire film.

7.3.2. Effect on ε^{T}_{33} after electrical poling

Figure 60 shows the effect that increasing the temperature at which the KNN thick films are treated and varying the levels of sol base-layers has on ε^{T}_{33} after the electrical poling of the thick films at elevated temperatures. As explained in ***section 7.2.3*** due to the high dielectric losses and the direct relation this has with relative permittivity, only measurements from samples with *tanδ* of <20% were considered to determine the trend and considered to more accurately define the material properties. Thus in *Figure 60a* & *b* all the data is represented i.e. including results of samples with dielectric losses beyond 20% and a closer observation of the congested area between a relative permittivity of 0 – 900 is carried out. In *Figure 60c* & *d* the samples with *tanδ* below 20% are examined, with only 6 samples making the cut.

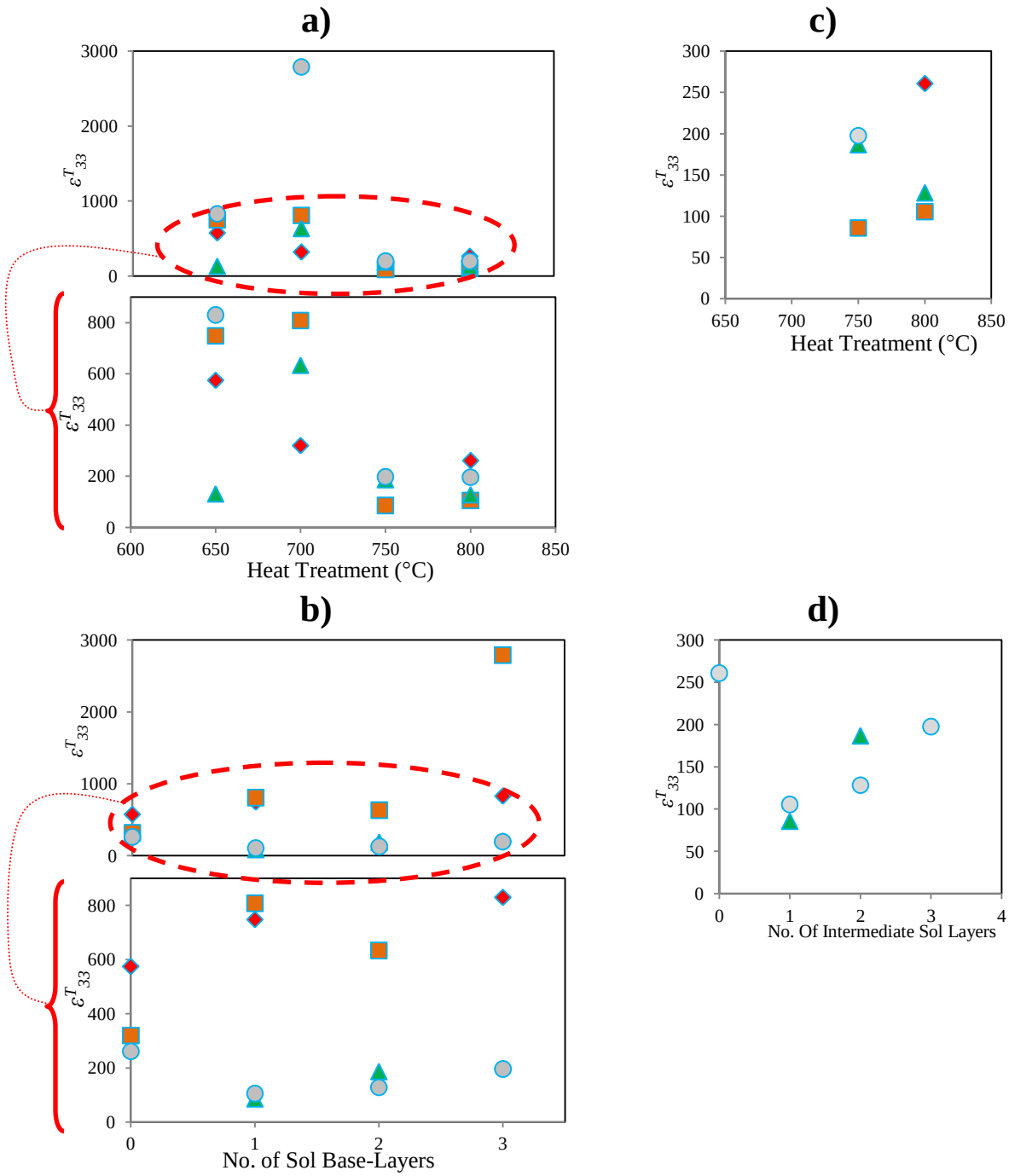

Figure 60 ε^T_{33} of KNN thick film samples as a function of **a)** heat treatment temperature; **b)** the number of sol base-layers deposited; **c)** focusing closer on heat treatment temperature results of samples with *tanδ* >20%; **d)** focusing closer sol base-layers of samples with *tanδ* >20%

a) Sol base-layers ◆ – 0 sol layers; ■ – 1 sol layer; ▲ – 2 sol layers; ● – 3 sol layers.
b) Heat treatment temp. ◆ – 650°C; ■ – 700°C; ▲ – 750°C; ● – 800°C.

Note – *Sample 0S750°C* was not included as it was a poor sample and could not be poled as its electrodes all failed.

The ε^{T}_{33} results after electrical poling at elevated temperatures were mostly below 900, except for one result (*3S-700°C* = 2791), thus showing more consistency of the samples when compared to the results prior to electrical poling. This further highlights the effects of moisture prior to the poling at high temperature which were reduced producing less erratic results, though taking into account the high levels of dielectric loss displayed by the KNN thick films, the relative permittivity was expected to be affected. A decrease in the ε^{T}_{33} as the heat treatment temperature is increased (*Figure 60a*) is observed. Samples heat treated at 750°C and 800°C had near similar relative permittivity and combined with their lower *tanδ* results, these samples more accurately reflected the level of ε^{T}_{33} of KNN thick films.

The sol base-layers did not appear to have much effect on the ε^{T}_{33} of the KNN thick films after electrical poling (*Figure 60b*) as sample with this layer and without it displayed near similar levels of relative permittivity.

The KNN thick film relative permittivity results do not show much of a trend after electrical poling. The KNN thick films displayed huge variance before and after electrical poling indicating the instability of the dielectric properties of these films that was related to the high dielectric loss results that are consistently exhibited by the KNN thick films throughout this study. The high *tanδ* is directly related to the imaginary part of the relative permittivity, indicating that more energy is dissipated through dipole motion (Bishop, 2001).

7.4. Effect of heat treatment and sol base-layers on d_{33}

Figure 61 shows the general trend of the effect of sintering and sol base-layers on the d_{33} of un-doped KNN thick films. Taking into account the fact that, high levels of dielectric loss can reduce the ability of a material to realise its full polarizability potential, if electrical

conduction occurs during DC poling, the d_{33} results were not considered as absolute definitions of this materials piezoelectric potential. The d_{33} data used was the maximum level displayed by each thick film after electrical poling.

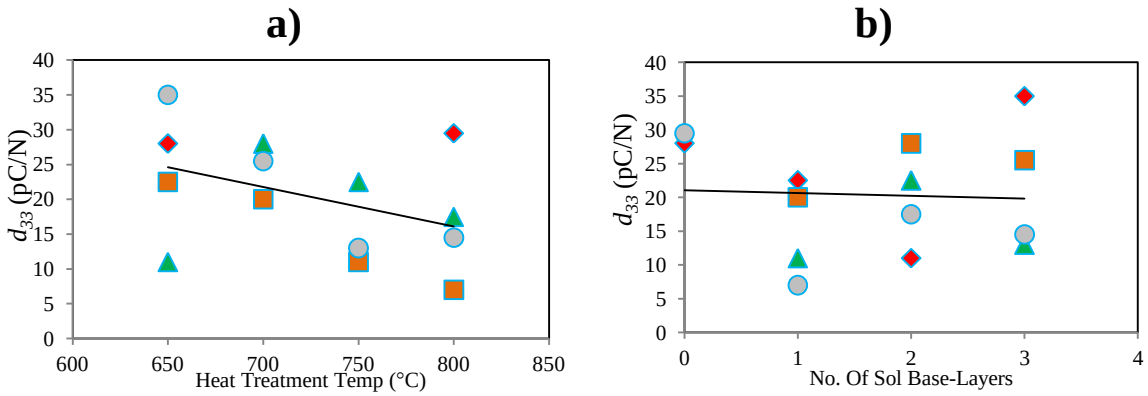

Figure 61 d_{33} of KNN thick films as a function of **a)** heat treatment temperature and **b)** sol base-layers

a) Sol base-layers – 0 sol layers; – 1 sol layer; – 2 sol layers; – 3 sol layers.
b) Heat treatment temp. – 650°C; – 700°C; – 750°C; – 800°C.

Two samples i.e. *samples 0S-700°C* & *0S-750°C*) did not produce d_{33} readings, the first gave uncharacteristically low levels of d_{33} while the second suffered from electrode failure. The trend observed in *Figure 61a* is a gradual decrease in the d_{33} as the heat treatment temperature is increased. Overall, increasing sol layers prior to the deposition of the composite sol-gel appeared to have little effect on the d_{33} (*Figure 61b*) as samples without the sol base-layer gave equally high d_{33} results.

A previous KNN sample that had the 4(C+2S) composite slurry deposited displayed a peak d_{33} of 34pC/N; while the highest d_{33} displayed by a KNN thick film doped with 0.5% Mn was 28.5pC/N. The result from these un-doped KNN thick films saw a peak d_{33} result of 35pC/N with several other samples with results above 20pC/N.

It is worth noting the effects of depositing the thick films on larger substrates when compared to earlier samples. From an initial dicing into quarters which was used with earlier samples including the sample that returned the peak d_{33} of 34pC/N, experiments carried out on the

doped KNN were carried out on smaller wafer sections, whereby wafers were divided into 10 pieces. With this matrix investigation the KNN film samples were applied to full wafers which were later divided and heat treated at different temperatures. Visual examination indicated deposition on a larger wafer resulted in superior samples and thus may explain the superior piezoelectric and dielectric results displayed.

7.5. Summary

Samples heat treated at 650°C were more susceptible to the absorption of atmospheric moisture which affected the dielectric properties prior to heat treatment. The results suggested that at 650°C the films were not fully crystallised resulting in poor results across all parameters measured. Poor crystallisation results in the continued presence of water secondary phases, all of which are a hindrance to the functionality of the thick films. This also leads to higher levels of porosity in these films as a lower volume of KNN crystals are formed within the film, thus contributing to the lower functionality of the film.

At 700°C and above, there was considerable improvement in the results, suggesting full crystallisation of the sol with better film homogeneity and thus lower dielectric loss, more stable relative permittivity and impedance results were observed. This showed that the sol proved to be a significant factor in producing the lower $tan\delta$ and high impedance. The overall dielectric results of the KNN thick films in this chapter were poor when compared to those of PZT thick films, though when reflected against previous results, with more research to develop a better understanding of the internal structure improved results are envisaged.

The sol base-layers acted as layer that enhanced the properties of the KNN thick films prior to electrical poling at elevated temperatures which was displayed by low $tan\delta$, stable ε_r and

good impedance properties when compared to samples without the sol base-layer. After poling at elevated temperatures the shielding qualities of the sol base-layer were not as effective and the KNN thick films' dielectric properties deteriorated as several samples with dielectric losses below 20% prior to electrical poling, faced increases in the losses after electrical poling. The sol base-layer had little effect on the piezoelectric properties of the KNN films. The dielectric property results served to highlight the hypothesis that the porosity of the KNN films may be the source of the poor properties.

Chapter 8

8.1.Conclusion

The aim of this thesis was to develop a process of making Pb-free thick films that can be used in micro-systems for medical applications and a range of Micro-Electro-Mechanical Systems (MEMS) devices. It was thought that this would allow the processing of Pb-free KNN thick films that matched PZT's dielectric and piezoelectric properties, thus making KNN a suitable candidate to replace PZT.

The Molten Salt Synthesis (MSS) method was initially selected as the desired powder synthesis route due to advantages over other methods of KNN powder synthesis. KNN powder synthesis by the MSS route was found to favour the incorporation of Na ions at the expense of the K ions, resulting in a Na ion-rich alkali niobate, due to the detrimental reaction of the molten salt (NaCl) with the K_2CO_3 reactant leading to the formation of KCl and K substitution from the carbonate by Na. This generated more Na ions that reacted with the niobium oxide to produce the K ion-deficient niobate, leading to the search for alternative MSS related KNN powder synthesis routes.

A new contribution to KNN powder synthesis, the two step Molten Hydroxide Synthesis (MHS) method was subsequently developed. Here K_2CO_3, KOH and Nb_2O_5 were reacted to produce potassium niobate derivatives and in a second stage Na ions were introduced to produce KNN. The successful development of this method allowed the mid-range temperature production of highly reactive, small particle size KNN powders. A second novel KNN powder production method i.e. the MSS method utilising KCl as the single solvent in the absence of NaCl, was also successfully developed to produce KNN. Each of the three KNN powder processing routes appeared to suffer from alkali loss, especially sodium leading

to powders that had a stoichiometric imbalance. KNN powders were successfully doped with transition metals, an alkali metal and alkaline earth metal dopants.

The KNN thick films in this research have shown great promise, returning decent piezoelectric results and dielectric results. Initial KNN thick films suffered from very high dielectric losses with highly variable dielectric properties. Alkali loss in both the KNN powder and during the sintering of the KNN thick films, leading to an imbalanced stoichiometry and porosity may be responsible for the high dielectric loss and unstable relative permittivity. Despite the shift from the ideal alkali stoichiometry (that produces the highest piezoelectric response) and the problematic dielectric characteristics, many of the KNN thick films tested displayed good d_{33} piezoelectric activity peaking at 35pC/N.

The introduction of a sol base-layer reduced the measured dielectric losses (lowest measured - 10%) and stabilised the relative permittivity and this was a third novel contribution to aid further research into a process of making KNN thick films. The sol base-layer had little effect on the piezoelectric properties of the KNN thick films (highest measured - 35pC/N). The levels of the three main parameters used to characterise the KNN thick films did not quite match those of PZT, but with future research to better understand the effect of microstructure on the materials piezoelectric and dielectric properties, this material appears to be a credible Pb-free candidate to replace PZT in various thick film applications. Non-modified PZT compositions are known to exhibit piezoelectric properties much lower than when the material is modified. The initial studies into the piezoelectric properties of unmodified PZT ceramics in 1950s reported a d_{33} of about 160pC/N; a level similar to current unmodified KNN materials. With numerous researchers dedicated to PZT research over more than six decades, better processing methods, extensive chemical modifications of pure PZT by well researched targeted doping, gave rise to the unrivalled success of PZT. With this in mind

KNN and other Pb-free candidates may still exhibit better properties than those reported currently when given similar attention (Damjanovic, et al., 2010).

8.2.Further work

There are several directions the quest for Pb-free piezoelectric materials may go. The search may look into new untested novel materials as wide range replacements for PZT or application specific replacements. Other materials such as electro-restrictive materials or flexo-electric materials may also offer Pb-free solutions to various piezoelectric applications. By carrying out practical research and focussing on structure to property relationships and also by computational methods better understanding of Pb-free candidates such as KNN may lead to greater improvements in the properties of these materials.

The direction that the research of this particular subject ought to take would involve improving the existing Pb-free candidates, including KNN based materials by chemical doping, controlling structural instabilities and understanding the extrinsic contributions such as domain wall contributions. The research into Pb-free materials is at an early stage and it has been suggested that the piezoelectric characteristics displayed by these materials currently may not yet be optimised. This may be done by:

- **More research into the material**

  Little evidence exists of research into the domain wall activity/contribution within KNN materials and as has been suggested earlier, in PZT, domain walls have been

found to account for as much as 70% of the piezoelectric response. Thus a first step would be an investigation into the domain wall activity present in KNN.

From the work in this project the complexity of the KNN thick film's dielectric properties indicates a large subject area for research with a better understanding of the microstructure which may help control these properties.

- **Improved processing**

  KNN exhibits an extensive concentration of A-site and oxygen vacancies which also contributes to the lack of control on the structural characteristics of the material (Damjanovic, et al., 2010).

  Improvements to processing may include improving the control of the stoichiometry of the material during processing, as has been shown heat treatment of thick films leads to alkali metal losses that affect the piezoelectric properties of the finished KNN thick films. The introduction of the sol base-layer resulted in vastly reduced dielectric loss and more stable relative permittivity prior to electrical poling. That result suggests further research into new novel processing ideas may bring desired improvements in the material properties.

  Several other methods of thick film processing exist which may be utilised to produce KNN thick films avoiding the composite sol-gel deposition method. The pulsed laser deposition method has been recommended to produce thin films of KNN with near stoichiometric composition (Rodel, et al., 2009) and may be thus adopted as a method to produce KNN thick films. Electrohydrodynamic atomisation (EHDA) is another processing direction that may be utilised to deposit KNN and reduce the stoichiometric imbalances. Aerosol deposition of KNN thick has been successfully used to produce KNN thick films of Si substrates.

- **Extensive research on the chemical doping of pure KNN**

  No research has been carried out on acceptor and donor doping in KNN to produce soft and hard versions as is the case with PZT (Damjanovic, et al., 2010), indicating a large field of study awaiting future researchers. From the work in this project chemical modifications were found to improve impedance characteristics and reduce the dielectric losses. As a consequence, with the vast array of elements available for use as piezoelectric dopants as well and the numerous combination possibilities of co-doping, a large field of research exists for the research of Pb-free materials.

Bibliography

Abazari, M. & Safari, A., 2009. Effects of doping on ferroelectric properties and leakage current behavior of KNN-LT-LS thin films on SrTiO3 substrate. *Journal of Aplied Physics,* Volume 105, p. 094101.

Acmite Market Intelligence, 2011. *World Piezoelectric Device Market.* [Online]
Available at: http://www.acmite.com/brochure/Brochure-Piezoelectric-Device-Market-Report.pdf
[Accessed 23 April 2012].

Agilent

Technologies, 2009. *Agilent Impedance Measurement Handbook.* [Online]
Available at: http://cp.literature.agilent.com/litweb/pdf/5950-3000.pdf
[Accessed 26 April 2012].

Aksel, E. & Jones, J. L., 2010. Advances in Lead-Free Piezoelectric Materials for Sensors and Actuators. *Sensors,* Volume 10, pp. 1935-1954.

APC International Ltd., 2012. *APPLICATIONS OF PIEZOELECTRIC CERAMICS.* [Online]
Available at: http://www.americanpiezo.com/knowledge-center/piezo-theory/applications.html
[Accessed 02 October 2012].

APC International, 2002. *Piezoelectric Ceramics: Principles and Applications.* Mackeyville(Pennsylvania): APC International.

Atomistic Simulation Group, 2012. *Database of Ionic Radii.* [Online]
Available at: http://abulafia.mt.ic.ac.uk/shannon/ptable.php
[Accessed 25 July 2012].

Aurelienr.com, 2001. *The Piezoelectric Effect.* [Online]
Available at: http://www.aurelienr.com/electronique/piezo/piezo.pdf
[Accessed 17 April 2012].

Barbara Malic, J. B. J. H. D. J. M. K., 2005. Alkaline-earth doping in (K,Na)NbO3 based piezoceramics. *Journal of the European Ceramic Society,* Volume 25, pp. 2707-2711.

Barrow, D., Petroff, T. & Sayer, M., 1995. Thick ceramic coatings using a sol gel based ceramic-ceramic 0–3 composite. *Surface and Coatings Technology,* November, Volume 76-77, pp. 113-118.

Birol, H., Damjanovic, D. & Setter, N., 2005. Preparation and characterization of KNbO3 ceramics. *Journal of the American Ceramic Society,* 88(7), pp. 1754-1759.

Bishop, C., 2001. *The Relationship Between Loss, Conductivity, and Dielectric Constant.* [Online] Available at: http://www.electromagnetics.biz/The%20Relationship%20Between%20Loss.pdf [Accessed 20 April 2012].

Bobnar, V., Malic, B., Holc, J. & Kosec, M., 2005. Electrostrictive effect in lead-free relaxor K0.5Na0.5NbO3–SrTiO3 ceramic system. *Journal of Applied Physics,* Volume 98, p. 024113.

Bortolani, F., 2010. *Synthesis and Development of Lead Zirconate Titanate Inks for Direct Writing.* Cranfiled(Bedfordshire): Cranfield University.

Cakare-Samardzija, L., Malic, B. & Kosec, M., 2008. K0.5Na0.5NbO3 Thin films prepared by Chemical Solution Deposition. *Ferroelectrics,* Volume 370, pp. 113-118.

Centre Interdisciplinaire de Microscopie Electronique, 2009. [Online]
Available at:
http://cime.epfl.ch/files/content/sites/cime2/files/shared/Files/Teaching/MSE_603_2011_spring/Chapter%2013%20-%20EDX.pdf
[Accessed 01 February 2012].

Chang, Y. et al., 2007. Dielectric and piezoelectric properties of alkaline-earth titanate doped (K0.5Na0.5)NbO3 ceramics. *Materials Letters,* Volume 61, pp. 785-789.

Chowdhury, A., Bould, J., Londesborough, M. G. & J.Milne, S., 2011. The effect of refluxing on the alkoxide-based sodium potassium niobate sol–gel system: Thermal and spectroscopic studies. *Journal of Solid State Chemistry,* February, 184(2), p. 317–324.

Chowdhury, A. et al., 2010. Nano-powders of Na0.5K0.5NbO3 made by a sol–gel method. *JOURNAL OF NANOPARTICLE RESEARCH,* 12(1), pp. 209-215.

Cooper, V. R., Grinberg, I., Martin, N. R. & Rappe, A. M., 2002. Local Structure of PZT. *American Institute of Physics* , 629(1), pp. 26-35.

Coté, G. L., Lec, R. M. & Pishko, M. V., 2003. *Emerging Biomedical Sensing Technologies and Their Applications.* s.l., IEEE SENSORS JOURNAL, pp. 251-266.

Cross, L. E. & Newham, R. E., 1987. History of Ferroelectrics. In: *Ceramics and Civilization, Volume 111. High-Technology Ceramics - Past, Present and Future.* s.l.:s.n., pp. 289-291.

Damjanovic, D., Klein, N., Li, J. & Porokhonskyy, V., 2010. What can be expected from lead-free piezoelectric materials?. *Functional Materials Letters,* 3(1), pp. 5-13.

Dauchy, F., 2007. *Stress Analysis, Dielectric, Piezoelectric, and Ferroelectric Properties of PZT Thick Films. Fabrication of a 50MHz Tm-pMUT Annular Array.* [Online]

Available at: https://dspace.lib.cranfield.ac.uk/handle/1826/2464?mode=simple
[Accessed 25 July 2012].

Demartin Maeder, M., Damjanovic, D. & Setter, N., 2004. Lead Free Piezielectric Materials. *Journal of Electroceramics*, Volume 13, pp. 385-392.

Don Whitley Scientific Limited, 1999. *INTRODUCTION TO PRINCIPLES OF IMPEDANCE.* [Online]
Available at:
ftp://ftp.ksph.kz/Food%20Microbiology1/File%20da%20prendere/New%20methods/Impedance.pdf
[Accessed 24 April 2012].

Dorey, R. A., 2010. *Low temperature production of lead-free piezoelectric thick films.* Trondheim, Piezo Institute.

Dorey, R. A., Haigh, R., S.B., S. & Whatmore, R. W., 2002. Effect of sol infiltrations on electrical properties of PZT. *British Ceramic Transactions,* 101(4), pp. 146-148.

Dorey, R. A. et al., 2008. Integrating functional ceramics into microsystems. *Journal of the European Ceramic Society*, 28(7), pp. 1397-1403.

Dorey, R. A., Stringfellow, S. & Whatmore, R. W., 2002. Effect of sintering aid and repeated sol infiltrations on the dielectric and piezoelectric properties of a PZT composite thick film. *Journal of the European Ceramic Society,* 12 April, 22(16), p. 2921–2926.

Dorey, R. A. & Whatmore, R., 2004. Electroceramic Thick Film Fabrication for MEMS. *Journal of Electroceramics,* 12(1-2), pp. 19-32.

Educational Innovations, Inc., 2012. *Piezo Popper Kit.* [Online]
Available at: http://cdn.teachersource.com/downloads/lesson_pdf/HS-2A.pdf
[Accessed 27 April 2012].

Egerton, L. a. D. D., 1959. Piezoelectric and dielectric properties of ceramics in the system potassium-sodium niobate.. *Journal of th American Ceramic Society,* 42(9), pp. 438-442.

Eichel, R.-A.et al., 2009. Local variations in defect polarization and covalent bonding in ferroelectric Cu at the morphotropic phase boundary. *Physical Chemistry Chemical Physics*, Volume 11, pp. 8698-8705.

Encyclopædia Britannica, 2012. *dielectric.* [Online]
Available at: http://www.britannica.com/EBchecked/topic/162630/dielectric
[Accessed 20 April 2012].

Environment Agency, 2012. *Waste electrical and electronic equipment (WEEE).* [Online]
Available at: http://www.environment-agency.gov.uk/business/topics/waste/32084.aspx
[Accessed 27 April 2012].

Environment and Heritage Service, 2005. *Waste Electrical and Electronic Equipment,* s.l.: Environment and Heritage Service.

ETH Zurich, 2003. *Electrochemical Impedance Spectroscopy.* [Online]
Available at:
http://www.google.co.uk/url?sa=t&rct=j&q=&esrc=s&source=web&cd=1&ved=0CCcQFjAA&url=http%3A%2F%2Fwww.nonmet.mat.ethz.ch%2Feducation%2Fcourses%2Fceramic2%2FEIS.ppt&ei=liyZT5DOJJC18QPszaitBg&usg=AFQjCNGKr8qqIi488iF-iSPvgPY_ARzolw
[Accessed 26 April 2012].

EUROPEAN PARLIAMENT AND OF THE COUNCIL, 2007. *THE REVIEW OF DIRECTIVE 2002/95/EC,* Brussels: s.n.

Fan, Z. et al., 2008. Hydrothermal Synthesis of (K,Na)NbO3 Particles. *Japanese Journal of Applied Physics,* 47(9), pp. 7685-7688.

Frubing, P., 2001. *Dielectric Spectroscopy.* [Online]
Available at: http://polymerscience.physik.hu-berlin.de/anleitg/dielectric.pdf
[Accessed 26 April 2012].

Fu, F. et al., 2011. Electrical properties of Li doped sodium potassium niobate thick films prepared by a tape casting process. *Journal of Alloys and Compounds,* Volume 509, pp. 7130-7133.

Fukada, E., 1983. Piezoelectric properties of biological polymers. *Quarterly Reviews of Biophysics,* Volume 16, pp. 59-87.

Gong, W. P. a. J., 2012. Influence of Ta5+ Doping on the Piezoelectric Properties of KNN Ceramics. *Key Engineering Materials,* Volume 512 - 515, pp. 1399-1402.

Gonzalez, U. F. & Moussa, W. A., 2002. *SIMULATION OF MEMS PIEZOELECTRIC MICROPUMP FOR BIOMEDICAL APPLICATIONS.* [Online]
Available at: http://www.algor.com/news_pub/tech_white_papers/mems_micropump/default.asp
[Accessed 29 June 2011].

Guo, Y., Kakimoto, K.-i. & Ohsato, H., 2004. Dielectric and piezoelectric properties of lead-free (Na0.5K0.5)NbO3–SrTiO3 ceramics. 129(5), pp. 279-284.

Guo, Y., Kakimoto, K.-i. & Ohsato, H., 2004. Phase transitional behavior and piezoelectric properties of (Na0.5K0.5)NbO3–LiNbO3 ceramics. *Applied Physics Letters,* 85(18), pp. 4121-4123.

Hansen, K., Astafiev, K. & Zawada, T., 2009. *Lead-free piezoelectric thick films based on potassium sodium.* Rome, s.n., pp. 1738 - 1741.

Harris, N. et al., 2006. A multilayer thick-film PZT actuator for MEMs applications. *Sensors and Actuators A,* 17 July, Volume 132, p. 311–316.

High Voltage Incorporated, 2007. *TAN δ (DELTA) CABLE TESTING.* [Online]
Available at: http://www.hvinc.com/downloads/Tan_Delta_FAQ.pdf
[Accessed 26 July 2010].

Hollenstein, E., Davis, M., Damjanovic, D. & Setter, N., 2005. Piezoelectric Properties of Li- and Ta-Modified (K0.5Na0.5)NbO3 Ceramics. *Applied Physics Letters,* 87(18), pp. 182905-182905.

Huang, Z. et al., 2006. Piezoelectric PZT films for MEMS and their characterization by interferometry. *Journal of Electroceramics,* 20(1), pp. 11-16.

Huidong, L., 2008. *Li Huidong.* [Online]
Available at: http://dspace.library.drexel.edu/bitstream/1860/2799/1/Li_Huidong.pdf
[Accessed 11 May 2012].

Ichiki, M., Zhang, L., Tanaka, M. & Maeda, R., 2004. Electrical Properties of Piezoelectric Sodium-Potassium Niobate. *Journal of the European Ceramic Society,* Volume 24, pp. 1693-1697.

Illinois Capacitor Inc., 2012. *Impedance, Dissipation Factor and ESR.* [Online]
Available at: http://www.illinoiscapacitor.com/pdf/papers/impendance_dissipation_factor_esr.pdf
[Accessed 28 May 2012].

Jarupoom, P. et al., 2008. Structures and Properties of Lead-Free NKN Piezoelectric Ceramics. *Ferroelectric Letters,* Volume 35, pp. 119-127.

Johnson, G. L., 2001. Lossy Capacitors. In: *Solid State Tesla Coil.* Manhattan(Kansas): Prentice-Hall Englewood Cliffs (NJ).

Jordan, T. & Ounaies, Z., 2001. *Piezoelectric Ceramics Characterization,* Hampton: International Council of Associations for Science Education.

Kalantari, K. et al., 2011. Ti-doping to reduce conductivity in Bi 0.85Nd 0.15FeO 3 ceramics. *Advanced Functional Materials,* 21(19), pp. 3737-3743.

Kalinin, S., Rodriguez, B. J. & Gruverman, A., 2007. *Electromechanical Behavior in Biological Systems at the Nanoscale.* New York(New York): Springer Science+Business Media.

Kim, E., 2000. *Dielectric materials and polarization.* [Online]
Available at: http://home.sandiego.edu/~ekim/e171f00/lectures/dielectrics.pdf
[Accessed 20 April 2012].

Kistler, 2007. *New Piezoelectric Materials Improve Sensor Performance.* [Online]
Available at: http://www.sem.org/PDF/kistler_PiezoStar.pdf
[Accessed 17 April 2012].

Kosec, M. et al., 2001. Interface reactions among electrodes, substrates and Pb(Zr,Ti)O3-based films. *Acta Chimica Slovenica,* Volume 48, pp. 51-62.

Kosec, M., Rojac, T., Holc, J. & Malic, B., 2010. *K0.5Na0.5NbO3 (KNN) based thick films.* Trondheim, electroceramics 12.

Kugler, V. M. et al., 2004. Microstructure/dielectric property relationship of low temperature synthesised (Na,K)NbOx thin films. *Journal of Crystal Growth,* Volume 262, pp. 322-326.

Kuščer, D., Skalar, M., Holc, J. & Kosec, M., 2009. Processing and properties of 0.65Pb(Mg1/3Nb2/3)O3–0.35PbTiO3 thick films. *Journal of the European Ceramic Society,* Volume 29, pp. 105-113.

Lai, F. & Li, J.-F., 2007. Sol-Gel Processing and Characterization of (Na,K)NbO3 Lead-Free Ferroelectric Films. *Ferrroelectrics,* 358(1), pp. 181-187.

Lau, S. T. et al., 2011. *KNN/BNT composite lead-free films for high-frequency ultrasonic transducer applications.* s.l., s.n., pp. 249-254.

Li, J. & Sun, Q., 2009. Characterization of (Na0:47K0:47Li0:06)(SbxNb1-x)O3 ceramics prepared by molten salt synthesis method. *Solid State Communications,* Volume 149, pp. 581-584.

Li, M. et al., 2010. Influence of nonstoichiometry on extrinsic electrical conduction and microwave dielectric loss of BaCo 1/3Nb 2/3O 3 ceramics. *Journal of the American Ceramic Society,* 93(12), pp. 4087-4095.

Lin, D. et al., 2010. Influence of MnO2 Doping on the Dielectric and Piezoelectric Properties and the Domain Structure in (K0.5Na0.5)NbO3 Single Crystals. *Journal of the American Ceramic Society,* 93(4), pp. 941-944.

Lin, P. et al., 2007. Effect of polyvinyl acetate on structures and properties of PbZr0.52Ti0.48O3 thick films. *JOURNAL OF APPLIED PHYSICS,* Volume 102, p. 084109.

Li, Q., Zhang, L. & Zhao, T., 2009. Definition of Instantaneous Dielectric Loss Factor and Digital Algorithm for Online Monitoring. *IEEE TRANSACTIONS ON INSTRUMENTATION AND MEASUREMENT,* March, 58(3), pp. 666-673.

Li, Y. et al., 2010. Synthesis and piezoelectric properties of KxNa1-xNbO3 ceramic. *Journal of Alloys and Compounds,* Volume 496, pp. 282-286.

López-Juárez, R., González, F. & Villafuerte-Castrejón, M.-E., 2011. Lead-Free Ferroelectric Ceramics with Perovskite Structure. In: M. Lallart, ed. *Ferroelectrics - Material Aspects.* s.l.:InTech, pp. 305-330.

Lüker, A., 2011. *A Short History of Ferroelectricity.* [Online]
Available at:
http://groups.ist.utl.pt/rschwarz/rschwarzgroup_files/Ferroelectrics_files/A%20Short%20History%20of%20Ferroelectricity.pdf
[Accessed 16 April 2012].

Macdonald, J. R., 1992. Impedance Spectroscopy. *Annals of Biomedical Engineering,* Volume 20, pp. 289-305.

Madaro, F. et al., 2010. Molten salt synthesis of K4Nb6O17, K2Nb4O11 and KNb3O8 crystals with needle- or plate-like morphology. *CrystEngComm,* 01 November, 13(5), pp. 1304-1313.

Maiwa, H., Kogure, T., Ishizaka, K. & Hayashi, T., 2007. *Preparation and Properties of Lithium-doped K0.5Na0.5NbO3 Thin Films by Chemical Solution Deposition.* s.l., s.n., pp. 110-111.

Malic, B. et al., 2008. Synthesis of Sodium Potassium Niobate: A Diffusion Couples Study. *Journal of the American Ceramic Society,* 91(6), pp. 1916-1922.

Massachusetts Institute of Technology, 2005. *Capacitance and Dielectrics.* [Online]
Available at: http://web.mit.edu/8.02t/www/materials/StudyGuide/guide05.pdf
[Accessed 23 April 2012].

Mazurek, B. & Moron, L., 2007. Polarization spectra analysis for the investigation of space charge in dielectric nanocomposites. *Materials Science-Poland,* 25(3), pp. 899-911.

Measurement Specialities Inc., 1999. *Piezo Film Sensors Technical Manual,* Norristown: Measurement Specialities Inc.

Meng, C., Wei, W., Shieh, J. & Chen, C., 2006. Colloidal processing of Pb(Zr,Ti)O3 targets Part II – Effect of NbO2.5 additive. *Journal of Ceramic Processing Research,* 7(4), pp. 281-287.

Mishra, S. K., Mittal, R., Pomjakushin, V. Y. & Chaplot, S., 2011. Phase stability and structural temperature dependence in sodium niobate: A high resolution powder neutron diffraction study. *Physical Review B,* 7 April, 83(13), p. 134105.

Morgan Technical Ceramics, 2009. *Markets.* [Online]
Available at: http://www.morganelectroceramics.com/markets/
[Accessed 19 January 2012].

Murata Manufacturing Company, 1997. *www.murata.com.* [Online]
Available at: http://www.symmetron.ru/suppliers/murata/sensors/p19e6.pdf
[Accessed 12 June 2010].

Murata Manufacturing Company, 1997. *www.murata.com.* [Online]
Available at: http://www.symmetron.ru/suppliers/murata/sensors/p19e6.pdf
[Accessed 12 June 2010].

Nakashima, Y., Sakamoto, W., Shimura, T. & Yogo, T., 2007. Chemical Processing and Characterization of Ferroelectric (K,Na)NbO3 Thin Films. *Japanese Journal of Applied Physics,* 46(10B), pp. 6971-6975.

NEC-Tokin, 2010. *Piezoelectric Ceramics.* [Online]
Available at: http://www.nec-tokin.com/english/product/pdf_dl/piezoelectricceramics.pdf
[Accessed 10 June 2010].

Nobre, M. & Lanfredi, S., 2003. Dielectric loss and phase transition of sodium potassium niobate ceramic investigated by impedance spectroscopy. *Catalysis Today,* Volume 78, pp. 529-538.

Nuffer, J. & Bein, T., 2006. *Application of Piezoelectric Materials in Transportation Industry.* San Sebastian, s.n.

Okada, K. & Sekino, T., 2003. *Agilent Technologies Impedance Measurement Handbook.* Santa Clara: Agilent Technologies Co. Ltd.

Park, J. H. et al., 2006. Resonance properties and mass sensitivity of monolithic microcantilever sensors actuated by piezoelectric PZT thick film. *Journal of Electroceramics,* 17(2-4), pp. 565-572.

Pérez de la Cruz, J., 2012. Piezoelectric Thick Films: Preparation and Characterization. In: N. Islam, ed. *Microelectromechanical Systems and Devices.* s.l.:InTech.

Piezo Systems Incorporated, 2012. *History of Piezoelectricity.* [Online]
Available at: http://www.piezo.com/tech4history.html
[Accessed 10 April 2012].

PRIME Faraday Partnership, 2002. *An Introduction to MEMS (Micro-electromechanical Systems),* s.l.: Prime Faraday Technology Watch.

Pulvari, C. F., 1960. Ferroelectricity. *Physics Review,* 120(5), p. 1670–1673.

Raju, G. G. .., 2003. Space Charge in Solid Dielectrics. In: *Dielectrics in Electric Fields.* s.l.:CRC Press, pp. 515-570.

Ringgaard, E. & Wurlitzer, T., 2005. Lead-Free piezoceramics based on alkali niobates. *Journal of the European Ceramic Society,* Volume 25, pp. 2701-2706.

Robert, G., Damjanovic, D. & Setter, N., 2001. Piezoelectric hysteresis analysis and loss separation. *JOURNAL OF APPLIED PHYSICS,* 01 November, 90(9), pp. 4668-4675.

Rodel, J. et al., 2009. Perspective on the Development of Lead-free Piezoceramics. 92(6), pp. 1153-1177.

Ryu, J. et al., 2007. Fabrication and ferroelectric properties of highly dense lead-free piezoelectric (K0.5Na0.5)NbO3 thick films by aerosol deposition. *Applied Physics Letters,* 90(15), pp. 152901-1-152901-3.

Saito, T., Adachi, H. & Wada, T., 2005. Pulsed Laser Deposition of Ferroelectric (Na0.5K0.5)NbO3-Based Thin Films. *Japanese Journal of Applied Physics,* 44(19), pp. L573-L575.

Saito, Y. et al., 2004. Lead-free piezoceramics. *Nature,* 432(7013), pp. 84-87.

Santos, I., Loureiro, L., Silva, M. & Cavaleiro, A., 2002. Studies of hydrothermal synthesis of niobium oxides. *Polyhedron,* Volume 21, pp. 2009-2015.

Schwartz, R. W., 1997. Chemical Solution Deposition of Perovskite Thin Films. *Chemistry of Materials,* Volume 9, pp. 2325-2340.

Shannon, R. D., 1976. Revised effective ionic radii and systematic studies of interatomic distances in halides and chalcogenides. *Acta Crystallographica Section A,* September, A32(5), pp. 751-767.

Shibata, K. a. O. F., 2011. *Piezoelectric element.* USA, Patent No. US 7,901,800 B2.

Shimamura, K., Takeda, H., Kohno, T. & Fukuda, T., 1996. Growth and characterization of lanthanum gallium silicate La3Ga5SiO14 single crystals for piezoelectric applications. *Journal of Crystal Growth,* Volume 163, pp. 388-392.

Signorelli, R., Ku, D. C., Kassakian, J. G. & Schindall, J. E., 2009. *Electrochemical Double-Layer Capacitors Using Carbon Nanotube Electrode Structures.* s.l., s.n., pp. 1837-1847.

Smeltere, I. et al., 2011. The Effect of Dopants on Sintering and Microstructure of Lead-free KNN Ceramics. *MATERIALS SCIENCE,* 17(1), pp. 62 - 64.

Stewart, M., Cain, M. G. & Hall, D. A., 1999. *Ferroelectric Hysteresis Measurement & Analysis.* [Online]
Available at: http://interactive.npl.co.uk/multiferroics/images/7/7a/CMMT_A(152).pdf
[Accessed 28 May 2012].

Su, B. & Button, T., 2001. Journal of the European Ceramic Society. Volume 21, pp. 2777-2781.

Tech-FAQ, 2012. *The Piezoelectric Effect.* [Online]
Available at: http://www.tech-faq.com/piezoelectric-effect.html
[Accessed 10 April 2012].

Tillman, M., 2012. *Effect of constrained sintering on the piezoelectric properties of PZT thick films.* [Online]
Available at: https://dspace.lib.cranfield.ac.uk/bitstream/1826/7321/1/Mark_Tillman_Thesis_2012.pdf
[Accessed 15 July 2012].

Torah, R., Beeby, S. & White, N., 2004. Improving the piezoelectric properties of thick-film PZT: the influence of paste composition, powder milling process and electrode material. *Sensors and Actuators A,* Volume 110, p. 378–384.

UK Centre for Materials Education, 2008-2010. *Piezoelectric Materials and Applications.* [Online]
Available at: http://www.whystudymaterials.ac.uk/casestudies/piezo.asp
[Accessed 19 January 2012].

Wang, L. et al., 2010. Enhanced ferroelectric properties in Mn-doped K0.5Na0.5NbO3 thin films derived from chemical solution deposition. *Applied Physics Letters,* Volume 97, p. 072902.

Wang, L., Yao, K. & Ren, W., 2008. Piezoelectric K0.5Na0.5NbO3 thick films derived from polyvinylpyrrolidone-modified chemical solution deposition. *APPLIED PHYSICS LETTERS,* Volume 93, p. 092903.

Wang, Y. et al., 2007. Hydrothermal Synthesis of Potassium Niobate Powders. *Ceramics International,* Volume 33, pp. 1611-1615.

West, A. R., Sinclair, D. C. & Hirose, N., 1997. Characterization of Electrical Materials, Especially Ferroelectrics by Impedance Spectroscopy. *Journal of Electroceramics,* 1(1), pp. 65-71.

Yang, H., Lin, Y., Wang, F. & Luo, H., 2008. Chemical Synthesis of K0.5Na0.5NbO3 Ceramics and Their Electrical Properties. *Materials & Manufacturing Processes,* 23(5), pp. 489-493.

Yang, Z., Chang, Y., Zong, X. & Zhu, J., 2005. Preparation and properties of PZT-PMN-PMS ceramics by molten salt synthesis. *Materials Letters,* Volume 59, pp. 2790-2793.

Yoon, H. K., Cho, Y. S. & Kang, D. H., 1998. Molten Salt Synthesis of Lead Based Relaxors. *Journal of Materials Science,* Volume 33, pp. 2977-2984.

Zeng, J., Kwok, K. & Chan, H., 2007. KxNa1−x NbO3 powder synthesized by molten-salt process. *Materials Letters,* Volume 61, pp. 409-411.

Zhang, F. et al., 2008. Hydrothermal Synthesis of (K,Na)NbO3 Particles. *Japanese Journal of Applied Physics,* 47(9), pp. 7685-7688.

Zhang, Q. & Whatmore, R. W., 2001. Sol–gel PZT and Mn-doped PZT thin films for pyroelectric applications. *Journal Of Physics D: Applied Physics,* Volume 34, p. 2296–2301.

Zhao, H.-J.et al., 2003. *Fabrication of High Quality PZT Thick Film Using Lift-Off Technique.* s.l., s.n., pp. 502 - 505.

Zhihong, W. et al., 2005. Characterization of Composite Piezoelectric Thick Film for MEMS Application. *Surface and Coatings Technology,* 198(1-3), pp. 384-388.

Zhou, Q. F., Shung, K. K. & Huang, Y., 2004. *Fabrication of Sol-gel modified piezoelectric thick films for high frequency ultrasonic applications.* s.l., IEEE, pp. 1958 - 1961.

Zhou, Q. F., Shung, K. K. & Huang, Y., 2007. Improvement Electrical Properties of Sol–Gel Derived Lead Zirconate Titanate Thick Films for Ultrasonic Transducer Application. *Journal of Materials Science,* 42(12), pp. 4480-4484.

Zhu, C., 2008. *Dielectric Loss.* [Online]
Available at: http://faculty.kfupm.edu.sa/EE/zhamouz/051/EE620-051/others/2_Dielectric_loss.pdf
[Accessed 20 April 2012].